DEVELOPMENT AND ANALYSIS OF THREE APPROACHES FOR GCL DESICCATION CYCLING

By

FAITH M. ZANGL

A Thesis submitted in partial fulfillment of

the requirements for the degree of

MASTER OF SCIENCE

(Geological Engineering)

at the

UNIVERSITY OF WISCONSIN-MADISON

2014

DEVELOPMENT AND ANALYSIS OF THREE APPROACHES FOR GCL DESICCATION CYCLING

Approved by:

William J. Likos, PhD

ABSTRACT

Geosynthetic clay liners (GCLs) are hydraulic barriers that contain of a thin layer of Na-bentonite clay encased by two geotextiles and are held together by needle-punching fibers or glue. Na-bentonite, mainly comprised of the smectite mineral montmorillonite, has characteristically high swell and low hydraulic conductivity (i.e 10^{-11} m/s), making Na-bentonite an ideal material for use in landfill covers to decrease the influx of water into a landfill.

There is the potential for cation exchange of divalent cations for bound monovalent sodium during GCL permeation. When cation exchange is coupled with desiccation, the hydraulic performance of a Na-bentonite GCL can be affected over time. While previous laboratory wet-dry cycling studies have explored the importance of applied stress and environmental controls during testing, they have generally required a large amount of specimen handling that can result in non-representative deformations in the form of GCL curling. Experiments conducted in this study have been designed to examine more representative methods of GCL desiccation during wet-dry cycling (Chapter 1).

Conventional Na-bentonite specimens were initially permeated with either deionized water or a pore water prepared to simulate typical landfill cover soils. Specimens were then subjected to one of three cyclic desiccation techniques that were designed for a greater degree of environmental control. Unconfined desiccation is the method previously used in literature that represents the least environmental control and consists of drying in a controlled-humidity environment without applied overburden stress. GCLs subjected to perforated plate desiccation were dried in a controlled-humidity environment under an applied overburden stress of 20 kPa. In-permeameter drying represents the greatest degree of environmental control and consists of the GCL being flushed with controlled-humidity gas while maintained under isotropic stress conditions.

Various aspects such as the testing duration, hydraulic conductivity as a function of wet-dry cycles, and drying uniformity were compared between the three desiccation techniques. In addition, images of the desiccation cracking patterns were taken and quantitatively compared using a novel image analysis algorithm (Appendix C).

Although the unconfined method results in an unnatural degree of GCL deformation in the form of curling, the hydraulic conductivity as a function of wet-dry cycles was unaffected when bentonite paste is added to the sidewalls. Therefore, the results of previous wet-dry cycling studies utilizing this technique are valid. The testing duration of a GCL subjected to perforated plate desiccation is significantly longer than the other methods. As a result, perforated plate desiccation is not recommended for future GCL wet-dry cycling studies. Even though in-permeameter desiccation requires additional equipment and can artificially accelerate the desiccation process, the method is recommended with a reduced air flow rate.

A study was undertaken to verify the GCL image processing and analysis techniques (Chapter 2). Validation of the image analysis method is provided by observation of small error values in comparisons made between simulated crack geometries of known dimensions and those quantified using the analysis.

In addition, polymer modifications of bentonite focused on activating and maintaining osmotic swell in adverse conditions. Experiments conducted in this study have focused on the effect of wet-dry cycling on the hydraulic performance of polymer-modified GCLs (Appendix A). Three GCL products were tested and include a bentonite polymer composite (BPC) GCL, a dry polymer- bentonite mix GCL, and a conventional untreated Na-bentonite GCL.

ACKNOWLEDGEMENTS

The UW-Madison Geological Engineering Department has helped me on my path to discovery both in my undergraduate career and in my Master's studies. The wonderful professors and graduate students of Geological Engineering have taught me engineering fundamentals, critical thinking skills, writing techniques, and presentation proficiency. The geological engineering department has been both extremely challenging and supportive.

First and foremost, I need to thank my advisor, Professor Bill Likos, who taught me about creative thinking, methodical research, and clay science fundamentals. This document would not exist without him. I would also like to thank Professor Tuncer Edil for helping me to make continual progress on my research through his participation in weekly research meetings. Thank you to Professor Craig Benson for agreeing to be a member of my defense committee and for sharing his unique insights on my research topic during research meetings. Many thanks are also due to Xiaodong 'Buff' Wang for his time and expertise during my endless hours in the laboratory both as a research assistant and as a teaching assistant.

Financial support for this study is from the University of Wisconsin – Madison and Colloid Environmental Technologies Co. (CETCO). I would also like to thank CETCO for providing the geosynthetic clay liners used in my research projects. This support is gratefully acknowledged. The findings and recommendations that have been presented are solely those of the author, and do not necessarily represent the policies or opinions of the sponsors.

Thank you also to my friends and family for their positive affirmations and motivation. I would like to extend a special thank you to the GCL research group, particularly Jiannan 'Nick' Chen, Missy Setz, Hülya Salihoğlu, Kuo Tian, and Weijuan Geng. These people helped me prepare for research presentations, solve problems, and generate ideas that helped me on my research path. I would also like to thank Joe Scalia and Sabrina Bradshaw for their patience and mentorship that encouraged me to work hard and learn. Much of this work also could not have

been accomplished without the assistance of Bennett Hasseldeck, Sam Wilson, and Michael Zimmerman, my undergraduate research assistants. Thank you for your time and commitment to my projects and ideas.

Thanks to the whole GLE family, particularly Brigitte Brown, Idil Akin, Yang Li, and Dante Fratta. Endless thanks are extended to my parents, Joe and Linda Zangl, and to the encouragement of my sisters, Mary Zangl, Michelle Gruenberger, Rose Zangl, Anna Pranskunas, and Betsy Grahl. Finally, special thanks to the love of my life, Mitchel Wiese, who helped me so much beyond building lab equipment, discussing idea practicality, and providing emotional support.

TABLE OF CONTENTS

LIST OF TABLES

LIST OF FIGURES

CHAPTER 1

DESICCATION TECHNIQUES FOR WET-DRY CYCLING OF GEOSYNTHETIC CLAY LINERS

1.1 ABSTRACT

Recent landfill cover field studies have confirmed that osmotic swelling can be inhibited and hydraulic conductivity can be three to four orders of magnitude higher than desired if the bentonite in a GCL is subjected to wet-dry cycles. While a significant amount of past research has been directed toward understanding controls on hydraulic performance of GCLs subject to desiccation cycling, most previous studies have focused predominantly on the degree of cation exchange within the bentonite and not on the desiccation method or apparatus. Previous laboratory studies have explored the importance of applied stress and environmental controls during GCL desiccation, but have generally required a large amount of specimen handling (e.g., removal from the permeameter) and non-representative deformations in the form of extensive specimen curling. Associated impacts to hydraulic conductivity measured in such experiments, therefore, may not be representative of field applications where cover soils apply overburden stress and such deformation is inhibited.

Experiments have been conducted in this study to examine more representative laboratory methods of GCL desiccation during wet-dry cycling. Conventional Na-bentonite specimens were initially permeated using either deionized water (control) or pore water prepared to simulate typical landfill cover soils. GCLs were then subjected to one of three cyclic desiccation techniques: (i) unconfined desiccation, where the GCL was subject to ambient air-drying with no overburden stress applied; (ii) perforated plate desiccation, where the GCL was subject to ambient air-drying under a vertical total stress simulating ~1 m of overlying cover soil; or (iii) in-permeameter drying, where the GCL was flushed with controlled-humidity gas while

maintained under isotropic stress conditions. To compare the different desiccation techniques, a novel image analysis algorithm was developed and used to quantitatively compare the GCL desiccation cracking patterns.

Hydraulic conductivity upon rehydration after two wet-dry cycles ranges from 7.88×10^{-12} m/s to 1.21×10^{-10} m/s (1.5 orders of magnitude) in each case and does not appear to be affected by the desiccation method. The unconfined desiccation method might not be preferred due to extensive GCL curling and the subsequent addition of bentonite paste to prevent sidewall leakage. However, since hydraulic conductivity was unaffected when bentonite paste was added to the sidewall, the results of previous wet-dry cycling studies using unconfined desiccation appear to be valid. The long testing duration prevents perforated plate desiccation from being a practical method to simulate wet-dry cycling. The active drying nature of in-permeameter drying influences the desiccation cracking pattern in a way that may not be representative of the crack patterns found in landfill covers. Based on all observations of testing duration, hydraulic conductivity, and desiccation cracking patterns, either unconfined or in-permeameter desiccation with a modified air flow rate is recommended.

1.2 BACKGROUND

Geosynthetic clay liners (GCLs) contain a thin layer of bentonite clay sandwiched between two geotextiles. The most significant component of the Na-bentonite in GCLs is sodium montmorillonite, a member of the smectite family. When exposed to deionized water (DW), sodium montmorillonite is capable of a high degree of osmotic interlayer swelling and correspondingly low hydraulic conductivity (i.e. 10^{-11} m/s) during hydration and permeation. However, recent field studies have confirmed that osmotic swelling is inhibited and hydraulic conductivity can be three to four orders of magnitude higher than desired if the bentonite in a GCL is not fully hydrated and if cation exchange has resulted in a predominantly polyvalent

cation exchange complex (Egloffstein 2001; Melchior 2002; Benson et al. 2007; Meer and Benson 2007).

1.2.1 Field Studies

Exhumed GCLs from several studies (James et al. 1997; Melchior 1997, 2002; Egloffstein 2001, 2002; Benson et al. 2007; Meer and Benson 2007) contained zones of extensive cracks as wide as two mm that have been attributed to concurrent desiccation and cation exchange.

James et al. (1997) exhumed an adhesive-bonded GCL containing Na-bentonite to determine why a cover with a GCL was leaking excessively. The GCL was placed on compacted clay and was overlain by a 150-mm-thick layer of gravel and a 300-mm-thick surface layer. The exhumed GCL contained finely cracked zones, had an average gravimetric water content of 116%, and Na in the original bentonite was extensively replaced by Ca. Multiple sources of the Ca involved in exchange were suggested, including calcite in the bentonite (2%), rainfall percolating through overlying calcareous soil, and the water used to initially hydrate the GCL (Ca concentration ≈ 0.003 M). Hydraulic conductivity (k) tests were not conducted on the exhumed GCL.

Melchior (1997, 2002) studied five GCLs containing Na-bentonite that were installed in a landfill cover near Hamburg, Germany. All GCLs were covered with 150 mm of sandy gravel overlain by a 300-mm thick surface layer of topsoil. Root penetration of the GCL occurred within 5 months of installation, and extensive cracking (cracks as wide as two mm) of the bentonite was observed in slightly more than one year. Moreover, complete exchange of Ca for Na occurred and the free swell index (ASTM D5890) of the bentonite was comparable to that of Ca-bentonite. Hydraulic conductivities ranged between 1×10^{-7} and 3×10^{-6} m/s and water contents ranged between 55 and 100% (average = 60%). Desiccation cracks were observed in GCLs having water content near 100%.

Egloffstein (2001, 2002) summarized the properties of GCLs exhumed from landfill covers in Germany. Gravimetric water contents of the GCLs ranged from 40 to 120% and complete exchange of Ca for Na occurred in as little as 2 years. Egloffstein (2002) reported a k of approximately 10^{-9} m/s for exhumed GCLs under an applied effective stress of 20 kPa. No information was provided regarding the permeant liquid. Egloffstein (2001) also conducted a long-term k test on a new GCL specimen that was initially permeated with DW, then a $CaCl_2$ solution. Permeation with the Ca solution caused the k to increase to 3×10^{-10} m/s, which was considerably lower than the k of the exhumed specimens. Based on this observation, Egloffstein (2001) concluded that the higher k of the exhumed GCLs were due to ion exchange combined with desiccation cracks that did not seal during rehydration.

Mansour (2001) exhumed GCLs from a test section consisting of a 660-mm-thick surface layer of well-graded sandy soil with fines overlying a conventional GCL located in a semiarid area of California. The exhumation was conducted five years after the test section was constructed. Tests conducted on the exhumed GCL using DW as the permeant liquid at a confining stress of 35 kPa yielded a k of 1.9×10^{-11} m/s. Analysis of soluble salts in the surface layer and the GCL indicated that the pore water in both materials was dominated by Na. The sodium rich condition of the surface layer likely prevented cation exchange in the GCL.

Henken-Mellies et al. (2002) conducted a 3-year field test of a GCL containing Ca-bentonite in a landfill cover system underlain by a pan lysimeter. A geocomposite drainage layer was placed directly above the GCL and was overlain by a 1-m-thick surface layer. The average leakage rate for the 3-year observation period was 1.7×10^{-10} m/s, although daily percolation rates as high as 2.0×10^{-8} m/s were recorded. Higher water contents generally were observed in the spring and early summer, whereas lower water contents were observed over the rest of the year.

Mackey and Olsta (2004) exhumed GCLs from two landfills (A and B) on the coast of Florida, where the final cover consisted of a surface layer overlying a needle-punched GCL. Both systems had been in service for more than five years. The cover soil for Landfill A consisted of clean sand that was 610 to 810 mm thick. The cover soil for Landfill B consisted of silty sand that was 460 to 860 mm thick. The bentonite from both sites was observed to be moist (water contents were not reported) and to have a Ca-dominated cation exchange complex. The k of the GCL exhumed from Landfill A ranged between 8.5×10^{-11} and 6.4×10^{-8} m/s. Lower k was reported for the GCL exhumed from Landfill B (3.5×10^{-11} to 2.3×10^{-10} m/s).

Benson et al. (2007) measured the percolation from a landfill final cover containing a GCL as the primary hydraulic barrier. The GCL was covered with 760 mm of vegetated silty sand and underlain with two gravel-filled lysimeters to monitor percolation from the base of the cover. Within four to 15 months after GCL installation, higher than anticipated percolation rates were recorded in both lysimeters. Samples of the conventional GCL that were exhumed from the cover ultimately had hydraulic conductivities on the order of 5×10^{-7} m/s. These high hydraulic conductivities were theorized to be caused by polyvalent for monovalent cation exchange coupled with desiccation. In addition, Benson et al. (2007) measured the k of a Na-bentonite GCL specimen with a 0.0125 M $CaCl_2$ solution. The k remained steady at 2.3×10^{-10} m/s after 1,599 days. The specimen was then removed from the permeameter and dried to a water content of 50%, then permeated again with the $CaCl_2$ solution for 30 days. This single cycle of desiccation caused the hydraulic conductivity of the GCL to increase to 4.7×10^{-8} m/s. Benson et al. (2007) concluded that dehydration after cation exchange had a dramatic effect on the hydraulic performance of GCLs.

Meer and Benson (2007) measured the k of GCLs exhumed from four landfills that had been in service between 4.1 and 11 years. They found that divalent cations (primarily Ca) had replaced most of the native Na in the exchange complex of the bentonite. Hydraulic

conductivities of the exhumed GCLs fell in a broad range (5.2 x 10^{-11} to 1.6 x 10^{-6} m/s). Comparison of these data with other data from the United States and Europe indicated that exchange of Ca and/or Mg for Na is likely to occur in the field unless the overlying cover soil is sodic. The comparison also showed that hydraulic conductivities on the order of 10^{-8} to 10^{-6} m/s should be expected if exchange occurs coincidently with dehydration, and that the effects of dehydration are permanent once the water content of the GCL drops below approximately 100%.

These observations indicate that desiccation and wet-dry cycling do occur in near-surface GCL applications and that the practical implications on barrier performance are considerable.

1.2.2 Previous Laboratory Studies on Wet-Dry Cycling of Clay Barrier Systems

A large number of laboratory studies (Shan and Daniel 1991; Daniel et al. 1993; Boardman and Daniel 1996; Lin and Benson 2000; Benson and Meer 2009; Mazzieri 2011) have been conducted to examine the coupled effect of cation exchange and desiccation of GCLs. In the past, focus was placed on the hydration phase of wet-dry cycling because the degree of swell at the onset of each wet-dry cycle is controlled by the ionic strength (I) and the relative abundance of monovalent and divalent cations (RMD) in the hydrating liquid (Jo et al. 2001; Kolstad et al. 2004). RMD is defined as

$$RMD = \frac{M_M}{\sqrt{\mathrm{M}_D}} \qquad (1)$$

where M_M = total molarity of monovalent cations; and M_D = total molarity of divalent cations in the solution (Kolstad et al. 2004). Both ionic strength and RMD will affect the distribution and composition of cations adsorbed on the clay surface.

Shan and Daniel (1991) assessed how desiccation affected the k of adhesive-bonded GCLs by subjecting a GCL specimen to wet-dry cycling in a laboratory permeameter apparatus. Tap water from Austin, TX was used as the permeant liquid and an effective stress of 14 kPa was used during permeation. Specimens were removed from the permeameter and desiccated via air-drying under an applied vertical stress of approximately 1 kPa. After four wetting cycles, the GCL retained low k (1.83×10^{-11} m/s).

Daniel et al. (1993) evaluated how wet-dry cycling affected the permeability of adhesive-bonded GCLs when exposed to hydrocarbons. Specimens were permeated under an average effective stress of 14 kPa, then desiccated in sealed vessels of known relative humidity (RH) and unknown (uncontrolled) vertical total stress. Specimens that were hydrated to greater than 100% retained low permeability.

Boardman and Daniel (1996) evaluated the effect of desiccation on the k of GCLs by conducting wet-dry cycling tests in large tanks. The specimens were hydrated under an average effective stress of 7.7 kPa for three weeks. The tanks were then drained and hot-air ventilation was used to dry the GCLs under an applied total vertical stress of 9.6 kPa. Care was taken to ensure that the temperature of the test did not exceed 27 to 32 °C. A clamp along the sidewalls of the tank restrained the GCL during drying. Desiccation was considered complete when the 50-mm thick, 75 mm wide bentonite edge seal was desiccated. The cracks that formed during desiccation swelled and healed on rewetting, and the GCLs maintained low k (1.31×10^{-11} m/s) after rehydration.

Lin and Benson (2000) studied the effects of wet–dry cycling on the k of a needle-punched GCL hydrated with DI water and a 0.0125 M $CaCl_2$ solution prepared to represent the pore water of vegetated surface layers in Wisconsin. Hydraulic conductivity tests were conducted on GCL specimens that were repeatedly permeated and then allowed to air dry

under zero applied vertical stress until the mass ceased to change (gravimetric water content ≈ 15% to 20%). All specimens retained low k (10^{-11} m/s) through four wet–dry cycles.

Benson and Meer (2009) conducted wet-dry cycling on needle-punched GCLs hydrated with a range of soil pore waters representative of landfill cover pore waters throughout the United States. The wet-dry cycling procedure from Benson and Meer (2009) was similar to that carried out by Lin and Benson (2000) with the exception of the applied 20 kPa vertical effective stress in the form of lead weights. The chemistry of the soil pore water solution was found to control the final k of bentonite exposed to several wet-dry cycles. For instance, wet-dry cycling with solutions with an RMD lower than 0.07 resulted in reduced swell and k in the range of 7.1 x 10^{-8} m/s to 2.5 x 10^{-6} m/s after rehydration.

Mazzieri (2011) performed wet-dry cycling testing on a dense-prehydrated (DPH) GCL using deionized water (DW) and a 0.0125 M $CaCl_2$ solution. DPH-GCLs are polymer-modified GCLs produced through the uniform prehydration of a dilute aqueous solution containing Na-carboxylmethyl cellulose and methanol to a water content of approximately 43%, then densification by calendaring (first described in Kolstad et al. 2004). Hydration was performed in an oedometer cell at vertical stress of 12.5 kPa. Severe desiccation was achieved in a thermostatic chamber at a constant temperature of 35 °C, RH ranging between 20 and 40%, and under a vertical stress of 6 kPa. The drying phase was considered complete when mass loss of the GCL ceased. The water content, after dehydration, w_{dry}, was estimated gravimetrically by assuming that the initial solid mass (soils, adsorbed polymers and geotextiles) had remained constant. After rehydration, the specimens were transferred to a permeameter for hydraulic conductivity testing. An average effective stress of 12.5 kPa was applied during permeation. The impact of wet-dry cycles on k was found to be limited when DW was used as hydrating liquid. Conversely, the k permanently increased to 5.5 x 10^{-7} m/s after the third cycle of severe desiccation using the $CaCl_2$ solution.

A summary of the field and laboratory studies cited in the literature review is included in Table 1.1.

1.2.3 Objectives of Current Study

While such lab wet-dry cycling studies have explored the importance of applied stress and environmental controls during testing, they have generally required a large amount of specimen handling and in some cases, can result in non-representative deformations in the form of extensive specimen curling if stress is not applied during drying. Associated impacts to k measured in such experiments, therefore, may not be representative of field applications where cover soils apply overburden stress and such deformation is inhibited. These impacts, however, remain largely untested and therefore unknown.

Experiments conducted in this study have been designed to examine more representative methods of GCL desiccation during wet-dry cycling. Results are compared among three laboratory methods developed to examine cyclic desiccation of conventional Na-bentonite GCLs. Specimens were initially permeated for one month using either deionized water (control) or pore water prepared to simulate typical landfill cover soils. GCLs were then subjected to one of three cyclic desiccation techniques: (i) unconfined desiccation, where the GCL was subject to ambient air-drying with no overburden stress applied; (ii) perforated plate desiccation, where the GCL was subject to ambient air-drying under a vertical total stress simulating ~1 m of overlying cover soil; or (iii) in-permeameter drying, where the GCL was flushed with controlled-humidity gas while maintained under isotropic stress conditions. The ambient air-drying methods (i and ii) require removing the GCL from the permeameter after hydration and permeability testing, thus causing a stress change that can result in disturbance. The in-permeameter method (iii) precludes the need to remove the GCL and thus eliminates potential influences of this disturbance. Analyses conducted to examine differences among the

three test approaches include quantitative imaging of desiccation crack patterns and corresponding measurements of GCL k upon rehydration.

1.3 MATERIALS

1.3.1 GCL

The GCL product used in this study is a conventional Na-bentonite (Na-B) GCL, provided by Colloid Environmental Technologies Company (CETCO) under the name Bentomat ST (Hoffman Estates, IL). The free swell index (SI) of the bentonite in DW was 26.0 mL/2 g (per ASTM D5890) and the cation exchange capacity (CEC) was 81.0 cmol+/kg (per ASTM D7503). The liquid limit was determined to be 481% and the plasticity index was determined to be 451% (per ASTM D4318). X-ray diffraction (XRD) analysis indicated that the bentonite contains 84% montmorillonite, 9% quartz, 3% plagioclase, and ≤ 2% of clinoptilolite, illite, mica, orthoclase, and calcite. A summary of the bentonite mineralogy, cation exchange capacity, and swell index is provided in Table 1.2.

1.3.2 Permeant Liquids

Scalia and Benson (2010) collected soil cover layers from various landfills around the United States, performed column elution tests (via Benson and Meer 2009) to collect soil pore water, analyzed the resultant eluate, and compiled this data in addition to data from similar studies (Meer and Benson 2007; Bradshaw 2008) (Fig. 1.1). Results were considered to represent typical pore fluid chemistries for landfills where GCLs may be used in barrier applications. Based on this data, two permeant solutions were chosen for this study: (i) DW, used as the control and (ii) a predominantly divalent synthetic solution considered to yield a conservative estimate of GCL k for MSW landfill cover applications, termed Conservative Water (CW). Refer to Table 1.3 for chemistries of the permeant solutions.

1.4 METHODS

GCL specimens were subjected to wet-dry cycling involving repeated permeation followed by desiccation. These cycles were repeated up to five times and GCLs were disassembled periodically for image and solids analysis via spatially distributed water content samples.

1.4.1 Permeation

GCL specimens were tested for k in flexible-wall permeameters according to ASTM D 5084 Method B (falling headwater-constant tail water) to simulate a wet spring scenario for a near-surface GCL application (e.g., landfill cover). In-cell hydration with the permeant solution of interest was conducted for 48 hours prior to flow. After the permeameter was assembled and connected to the falling headwater apparatus, cell pressure was applied and all tubing was saturated with the permeant liquid. The inflow line of the permeameter was left open to allow the specimen to hydrate while the effluent line remained closed. An average hydraulic gradient of 30 was chosen to simulate conditions experienced by GCLs in typical landfill cover applications (Lin and Benson 2000). The effective stress, 20 kPa, was chosen to simulate approximately one meter of cover soil. Hydraulic conductivity tests were continued until at least the following criteria were met: no systematic trend in k over time, (per ASTM D5084); at least four consecutive k readings within ± 25% of the mean (per ASTM D5084); at least four consecutive outflow-to-inflow ratios within 1.0 ± 0.25 (per ASTM D 5084); and the tests were permeated for four weeks.

1.4.2 Desiccation Techniques

Three desiccation techniques were used to assess the effects of wet-dry cycling on GCL k. The methods consisted of (i) ambient air drying under zero applied confining stress, which will be termed “unconfined desiccation” (Fig. 1.2a), (ii) ambient air-drying under an applied vertical stress of 20 kPa simulating ~1 m of overlying cover soil (Fig. 1.2b), or (iii) a novel in-permeameter drying technique where gas of known relative humidity (RH) is circulated through

the endcaps of the permeameter while the GCL is maintained under 26.5 kPa of isotropic stress in the confining cell (Fig. 1.2c). The former two approaches are intended to replicate similar previous studies (Shan and Daniel 1991, Daniel et al 1993, Lin and Benson 2000, Benson and Meer 2009), whereas the latter approach is intended to isolate the potential effects of reduced specimen disturbance by better simulating field conditions. The methods are qualitatively compared in Table 1.4. The unconfined and perforated plate methods rely on passive drying in a controlled RH environment. The in-permeameter method is an active drying method due to control over the air flowrate. The unconfined and perforated plate methods require removing the GCL from the permeameter after hydration and permeability testing, thus causing a stress change that can result in disturbance. The in-permeameter method precludes the need for GCL removal from the permeameter and thus eliminates potential influences of this disturbance.

GCL specimens in each case were desiccated to extreme lows of gravimetric water content (w = 12.5%). The soil water characteristic curve (SWCC) (Likos 2004) was determined for the Na-bentonite contained within the GCL (Fig. 1.3). The wetting and drying curves represent the maximum and minimum water contents experienced by soil at each RH value. Based on the SWCC, an equilibrium RH of 70% was determined to correspond to the average relative humidity between the wetting and drying curves at a gravimetric water content of 12.5%. Thus, all specimens were desiccated in environments where the RH was kept constant at 70%. The RH of the environment was continuously monitored with a capacitance-film humidity/temperature probe. The probe measured humidity between 0% RH and 99% RH at 0.01% RH resolution.

1.4.2.1 Unconfined Desiccation Method

The unconfined desiccation approach (Fig. 1.2a) is similar to that employed in several previous wet-dry experiments (Shan and Daniel 1991, Daniel et al 1993, Lin and Benson 2000). After hydration and permeation, the GCL was removed from the permeameter for air-drying.

Specimens were desiccated in a controlled RH environment (RH = 70%) without applied vertical stress. The RH of a small room was controlled using a residential room humidifier system (Honeywell model HCM-6009, Palatine, Illinois, USA) and monitored using a humidity probe. If the RH deviated from the target of 70% RH by 5%, the controls on a humidifier were manually adjusted. In general, the RH was maintained at 73.7% +/- 4.3% with a maximum RH of 86.5% and a minimum RH of 57.4% using this approach. Specimens were periodically weighed and desiccation was considered complete when the specimen mass ceased changing. An important consideration when using the unconfined method is that there is the potential for much disturbance caused by removing the GCL from the permeameter without any protective plate and no stress application during drying. In addition, the desiccation rate may affect the severity of desiccation, the cracking pattern, and the corresponding efficacy with which desiccation cracks heal upon rehydration. Overall, the approach is considered to represent a worst case scenario in terms of deviation from representative field conditions.

1.4.2.2 Ambient Air-Drying Method

The ambient air-drying method adopted here (Fig. 1.2b) was designed to include two rigid perforated PVC plates placed above and below the GCL. The purpose of these plates was to limit disturbance due to physical movement of the GCL during removal from the permeameter, as noted above for the unconfined desiccation method. On the other hand, the method does require removing the GCL from the permeameter after hydration, thus causing a change in stress. This stress change is not representative of typical field applications and can result in disturbance. Specimens were desiccated in the same controlled RH environment (RH ≈ 70%) under an applied vertical stress of 20 kPa selected to simulate ~ 1 m of overlying cover soil in a typical surface cover application. As previously stated, the RH of a small room was controlled through humidity probe monitoring. If the RH changed, the controls on a humidifier were

manually adjusted. Specimens were periodically weighed and desiccation was considered complete when the specimen mass ceased changing.

1.4.2.3 In-permeameter Drying Method

A novel in-permeameter method was developed as part of the effort to minimize specimen disturbance inherent to the previous two techniques. This approach utilized an automatic RH control system (Likos and Lu 2003) and precluded the need to remove the GCL from the permeameter for cyclic drying-wetting, thus eliminating any change in total stress and the associated potential for disturbance. The Auto RH Control System (Fig. 1.2c) as described by Likos and Lu (2003) and Nishimura and Fredlund (2003) was initially developed to develop total suction characteristic curves in the high suction range and to perform unsaturated triaxial tests for unsaturated clayey soils. Pressurized ambient air was introduced to the system at a specified flow rate and divided amongst two gas streams. The first gas stream is bubbled through a DW-filled bottle, resulting in vapor-saturated (relative humidity ~ 100%; “wet”) air. The second gas stream is routed through a column filled with $CaSO_4$ desiccant, resulting in desiccated (relative humidity ~ 2%; “dry”) air. The “wet” and “dry” gas streams are then reintroduced at the initial flow rate. The resulting “humid” gas stream, having a RH that is a direct function of the “wet” to “dry” gas flow maintained by the control computer, is routed through the top and bottom end caps and porous plate on either side of the GCL specimen. A net water exchange between the liquid and vapor phases occurred in the GCL headspace until equilibrium between the air and water phases was achieved. Signals from the humidity probe formed a feedback loop with the control computer for automated regulation of the “wet” to “dry” gas flow ratio using the two mass-flow controllers. This technique was employed until the effluent RH came to equilibrium with the influent RH of 70%.

1.4.3 Image Processing and Analysis

To compare the different desiccation techniques, image analysis was employed. Image analysis was used to compare the desiccation cracking patterns of the GCL permeated with DW that was subjected to one wet-dry cycle.

1.4.3.1 Disassembly and Image Acquisition

After one wet-dry cycle, the permeameter was disassembled. A sharp scalpel was used to cut the needle stitching fibers and remove the woven geotextile from the GCL.

The level of success in any image processing work is dependent on the quality of captured images. Images of GCLs sans woven geotextiles were taken by an Epson B11B198011 Perfection V600 Photo Scanner 1200 dots per inch (dpi) image scanner (Long Beach, California, USA). The scanner was placed on the GCL at the center of the 215.9 by 297.2 mm scanning board. Images were taken at a measurement angle of 90° from the GCL.

The resultant full-color images were 10,281 by 13,305 pixels. Each image was 215.9 by 279.4 mm in size, which resulted in a pixel size of 0.021 mm (Fig. 1.4).

1.4.3.2 Image Processing

The full-color GCL images were imported into Adobe Photoshop (San Jose, California, USA). A square image of 2400 by 2400 pixels was cropped from the center of the GCL image to eliminate edge effects (Fig. 1.6a).

The cropped images were then imported into Matlab (Matrix Laboratory) where a custom code (Appendix C) was written for processing and analysis (Mathworks, Natick, Massachusetts, USA). A flow chart of image processing is shown in Fig. 1.5.

The full-color images were converted to 8 bit images (Fig. 1.6b). An example of a gray-scale histogram is shown in Fig. 1.6c. The two ends of a gray-scale histogram vary between 0

(pure black) and 255 (pure white). Because the cracks were darker than the bentonite cells (solid material among the cracks), the cracks were assigned a lower value. Next, the images were morphologically closed (Fig 1.6d and Fig. 1.6e). Closing is an operation that reduces dark features while not affecting the background and consists of dilation followed by erosion using the same structuring element. Dilation expands the light colors in a grayscale image, while erosion expands the dark colors in a grayscale image. The resulting image was then thresholded using an adaptive mean threshold on 300 pixel by 300 pixel squares.

After thresholding, binary images were obtained in which white regions (bentonite) were assigned a value of 1 and black regions (cracks) 0 (Fig 1.6f).

The basic idea in binary morphology is to probe an image with a simple, pre-defined binary structuring element and draw conclusions on how this shape fits or misses the shapes in the image. The binary image was morphologically opened, an operation that removes small dark pixels from the foreground and places them in the image background (Fig 1.6g). Opening consists of erosion followed by dilation using the same binary structuring element.

Next, all white pixel areas smaller than 1000 square pixels were removed from within the crack area (Fig 1.6h). The complement, or inverse, of the image was obtained (Fig 1.6i). Again, all white pixel areas smaller than 1000 square pixels were removed from within the bentonite cells (Fig 1.6j). The image complement was obtained (Fig. 1.6k). The image was thinned, where selected white foreground pixels were removed until lines of 1 pixel thickness remained (Fig 1.8a). Pixels were removed so that a white object without enclosed black pixels shrunk to a minimally connected stroke, and a white object with enclosed black pixels shrunk to a connected ring halfway between each black object and the outer boundary. The thinned image was then pruned (Fig. 1.8b). Pruning is a binary subtractive operation that erases black pixels

surrounded by eight white pixel neighbors. The resultant image was a skeletonized version of the cracks.

1.4.3.3 Image Analysis

Several parameters were obtained to characterize the geometrical properties of the crack pattern. These include the crack intensity factor (CIF, Eqn. 2), average bentonite cell area (A_A), maximum bentonite cell area (A_M), average crack width (W_A), maximum crack thickness (W_M), and the frequency histogram of bentonite cell area, crack thickness, and crack orientation.

Miller et al. (1998) introduced the CIF when investigating the cracking behavior of compacted clay liners as a descriptor of the extent of surficial cracking (Eqn. 1). CIF is defined as

$$CIF = \frac{A_C}{A_T} \qquad (2)$$

where A_c = the surface area of the cracks (white area); and A_T = the total surface area of the image.

The Roberts Operator (Roberts 1963) was used to detect crack edges using an intensity gradient analysis of the pruned image. The intensity gradient analysis moves through the image with the Roberts morphological operator and detects edges based on the rate of pixel value change. The direction of smallest change gives the orientation of cracks whereas the direction of largest change gives the edge of the crack.

Images subjected to edge detection were fused with the pruned image to form a new image (Fig. 1.8g). The full color fused image was then converted to binary using Otsu's method (Otsu 1979). Small holes were removed from within the black pixels. The Cartesian coordinates of the detected edges were then converted to polar coordinates using the Hough Transform.

The line length and orientation with respect to horizontal were extracted from the polar coordinates to form the frequency histogram of crack orientation (Fig. 1.14).

The process of determining crack width began by removing the crack interior of the image before morphological thinning (Fig. 1.8b). The edges of the crack exterior were extracted using the Roberts Operator (Roberts 1963) (Fig. 1.8d). The image subjected to edge detection was fused with the crack exterior image to form a new image (Fig. 1.8f). The full color fused image was then converted to binary using Otsu's method (Otsu 1979). Small holes were removed from within the black pixels. As a result of crack interior removal, all pixels surrounded by four white pixels were black, distinguishing the boundary pixels as white. An Euclidean distance transform was performed on the resultant image. The Euclidean distance formula is defined as

$$distance = \sqrt{(x_2 - x_1)^2 + (y_2 - y_1)^2} \quad (3)$$

where (x_1, y_1) and (x_2, y_2) are the Cartesian coordinates of two selected points. The distance transform assigned a number for each image pixel that is the distance between that pixel and the nearest white pixel in the image.

The resultant distance matrix was the same size as the original image. The value corresponding to each point in the distance matrix defines the shortest distance between each point and the nearest white border. However, the matrix also includes the distance from within the bentonite cells to the nearest crack border. To eliminate the effects of the bentonite cells, the distance matrix was compared to a skeletonized version of the cracks (Fig. 1.8g). In this final crack thickness matrix, all values in the distance matrix that did not correspond to the crack skeleton were assigned a value of zero. The crack skeleton was assumed to be located in the exact middle of the crack and the cracks were assumed to be symmetrical, meaning that the crack width is two times the value given in the distance matrix. The crack thickness matrix was

compared to the original image. The mean crack thickness, maximum crack thickness, and frequency histogram of crack thickness were extracted from the crack thickness matrix.

The number and size of bentonite cells were measured while analyzing the binary images. The fused binary image was used to extract the number, size, and centroid of the clay cells. A bentonite cell was defined as a black region bounded by white cracks on all sides. The frequency histogram of bentonite cell area was also obtained.

1.4.4 Solids Analysis

Spatially distributed samples of the GCL after the one wet-dry cycle were collected (locations depicted in Fig. 1.12). Water content was measured in accordance with ASTM D2216. The water content mean and standard deviation were calculated (Fig. 1.12). The water content coefficient of variation was determined for each desiccation method.

1.5 RESULTS

1.5.1 Qualitative Observations

Regardless of the desiccation method, cracks appeared to originate from needle-stitching fibers or flaws contained within the GCL bentonite. However, the presence of needle-stitching fibers did not guarantee the formation of cracks. This is consistent with observations made by Costa et al. (2013). When comparing the desiccation cracking patterns of clay, potato starch and milled quartz sand, Costa et al. (2013) discovered that the exact positions of crack initiations are controlled by flaws or pores contained within the material. However, not all flaws were activated because the activation of one flaw would generate a zone of low stress, and the nearby flaws may not receive sufficient stress to initiate or propagate.

The GCL subjected to unconfined desiccation became distorted from a circular shape to an oval shape after desiccation (Fig. 1.9). In order to prevent preferential flow along the sidewalls during permeation, fresh bentonite was hydrated and added to the GCL edge.

1.5.2 Cycle Duration

In general, the wet-dry cycling duration is shorter for a GCL permeated with CW than with DW. When DW is used as a permeant liquid, little cation exchange occurs between the bentonite contained within a GCL and the permeant liquid. Since CW contains divalent cations (Table 1.3), a greater degree of monovalent for divalent cation exchange will occur. Water is more weakly bound in the interlayer space of a bentonite with a greater degree of cation exchange The weakly bound water requires a lower soil suction and therefore a shorter time duration for removal from the interlayer space.

A GCL desiccated in 15 days and reached hydraulic equilibrium in 15 days when permeated with DW and desiccated using the unconfined method (Fig. 1.10a). The desiccation time (13 days) and time to hydraulic equilibrium (19 days) were slightly shorter when CW was used as the permeant liquid (Table 1.5).

The perforated plate desiccation method required the longest time duration for completion. A GCL permeated with DW required 115 days for desiccation and 33 days to reach hydraulic equilibrium while a GCL permeated with CW required 100 days for desiccation and 26 days to reach hydraulic equilibrium (Table 1.5). The perforated plate method is impractical due to the long drying time and resultant extensive testing duration for multiple wet-dry cycles.

The in-permeameter method required the least time for desiccation due to the active flow of dry air. A GCL desiccated in 11 days and reached hydraulic equilibrium in 30 days when permeated with DW while a GCL permeated with CW reached hydraulic equilibrium in 10 days and desiccated in 10.5 days (Fig. 1.10b). The flow rate of dry air over the GCL specimen also affects drying time. When dry air was introduced at a flow rate of 200 cc/min, the specimen dried in 15 days. The drying time decreased to 11 days when dry air was introduced at 500 cc/min (Fig. 1.11).

1.5.3 Uniformity

The location and values of spatially distributed water content samples for the desiccation methods are shown in Fig. 1.12. The perforated plate method has the lowest coefficient of variation; therefore, the perforated plate desiccation method results in the most uniform desiccation. This is likely due to the long drying duration, which allows water enough time to migrate and come to steady state. However, all three desiccation methods have a coefficient of variation of less than 5%, a strong indication of a high degree of drying uniformity.

1.5.4 Hydraulic Conductivity

Hydraulic conductivity values of GCL specimens subjected to repeated permeation followed by desiccation are shown in Fig. 1.13. Hydraulic conductivity upon rehydration after two wet-dry cycles ranges from 7.88×10^{-12} m/s to 1.21×10^{-10} m/s (1.5 orders of magnitude) in each case and does not appear to be affected by the desiccation method.

1.5.5 Image Analysis

1.5.5.1 Crack Index Factor (CIF)

The measured CIF for the unconfined, perforated plate, and in-permeameter desiccation methods was 31.8%, 32.7%, and 32.8%. There does not appear to be a large deviation in CIF for GCLs subjected to different desiccation methods. Any differences in the CIF could be explained by differences in the mean final water content. A lower water content is indicative of a greater degree of cracking. The lowest mean water content (10.7%) was found for the in-permeameter method (CIF = 32.8%) whereas the highest mean water content (14.9%) was found for the unconfined method (CIF = 31.8%). Therefore, the degree of cracking is similar for all three methods.

1.5.5.2 Cell Area and Crack Thickness

The measured mean cell areas for the unconfined, perforated plate, and in-permeameter desiccation methods were 9.5 mm^2, 10.5 mm^2, and 9.1 mm^2. The p-value for all tests was less than 0.005, meaning that the cell area distributions for all methods are statistically different from each other (Table 1.6). The measured mean crack thickness for the unconfined, perforated plate, and in-permeameter desiccation methods were 0.52 mm, 0.59 mm, and 0.50 mm. The p-value for all tests was less than 0.005, meaning that the crack thickness distributions for all methods are statistically different from each other (Table 1.6).

The in-permeameter method dried GCLs at a higher rate than the unconfined method and perforated plate method. The in-permeameter method exhibited the smallest clay cells and the thinnest cracks, followed by the unconfined method and the perforated plate method. Cracks form when tensile stress and strain energy due to increased soil suction exceed the bonding strength of grains. At a higher desiccation rate, more cracks were needed to release the rapid tensile stress increase in the specimen, which subsequently reduced the crack spacing and size of the clay cells.

The results are consistent with literature findings. Costa et al. (2008) qualitatively discovered that a higher desiccation rate resulted in smaller clay cells for fat clay. Costa et al. (2013) quantitatively investigated the effect of desiccation rate on the desiccation crack pattern of clay, potato starch, and milled quartz sand, all of which had similar fracture energy. The mean cell area decreased with increased desiccation rates.

The maximum crack thicknesses found for all three desiccation methods are consistent with the literature value of maximum crack thickness. Melchior (2002) exhumed GCLs in a landfill cover near Hamburg, Germany and discovered cracks as wide as two mm. The

maximum crack thickness was 2.11 mm for the unconfined method, 2.24 mm for the perforated plate method, and 1.78 mm for the in-permeameter method.

1.5.5.3 Crack Orientation

The desiccation crack orientation histograms of the various methods with respect to horizontal obtained from image analysis are shown in Fig. 1.14. The desiccation cracks as formed by the unconfined method appear to have a preferred orientation. The unconfined desiccation method result in a large degree of GCL curling (Fig. 1.9). The preferred crack orientation for the unconfined method is likely due to the flattening of the GCL for image acquisition. Neither the perforated plate nor the in-permeameter desiccation methods appear to have a preferred orientation.

1.6 PRACTICAL IMPLICATIONS

All desiccation methods are valid ways to desiccate GCLs during wet-dry cycling. The hydraulic conductivity after repeated wet-dry cycles does not appear to be affected to a great degree regardless of the desiccation method (Fig. 1.13). Although the unconfined desiccation method required GCL modification between cycles through the addition of bentonite paste to the GCL sides, hydraulic conductivity as a function of wet-dry cycles was unaffected with the addition of bentonite paste. Therefore, the results of previous studies using unconfined desiccation are valid. The long desiccation duration prevents perforated plate desiccation from being a practical method of simulating wet-dry cycling. To perform in-permeameter desiccation, additional equipment is required that can be expensive. Furthermore, active drying influences the desiccation cracking pattern in such a way that may not be representative of the crack patterns of landfill covers. However, the flow rate of dry air over the specimen could be altered to lengthen the desiccation time and potentially prevent desiccation cracking pattern differences.

Based on all observations of testing duration, hydraulic conductivity, and desiccation cracking patterns, either unconfined or in-permeameter desiccation are recommended. The perforated plate method is not recommended due to the long testing duration. The in-permeameter air flow rate should be modified from 500 cc/min to 200 cc/min to decrease the desiccation rate. Further studies could be performed to determine realistic desiccation durations for GCLs in landfill cover scenarios and to obtain high-resolution photos of exhumed GCL cracking patterns.

1.7 SUMMARY AND CONCLUSIONS

Experiments conducted in this study have been designed to examine more representative methods of GCL desiccation during wet-dry cycling. Conventional Na-bentonite specimens were initially permeated, subjected to one of three cyclic desiccation techniques: (i) unconfined desiccation; (ii) perforated plate desiccation; or (iii) in-permeameter drying, and disassembled. To compare the different desiccation techniques, image analysis was used to compare the desiccation cracking patterns of the GCL permeated with DW and subjected to one wet-dry cycle. In addition, dry time, time to hydraulic equilibrium, drying uniformity, and hydraulic conductivity with respect to wet-dry cycles were compared. The hydraulic conductivity after repeated wet-dry cycles does not appear to be affected to a great degree regardless of the desiccation method. Although the unconfined desiccation method resulted in extensive GCL curling and required the addition of bentonite paste to prevent sidewall leakage, the hydraulic conductivity as a function of wet-dry cycles is unaffected when bentonite paste was added. Therefore, the results of previous studies using unconfined desiccation are valid. The long desiccation duration of perforated plate desiccation prevents the method from being a practical method of simulating wet-dry cycling. The active nature of in-permeameter drying influences the desiccation cracking pattern in a way that may not be representative of the crack pattern in landfill covers. However, the flow rate of dry air over the specimen could be altered to lengthen

the desiccation time and potentially prevent desiccation cracking pattern differences. Unconfined desiccation or in-permeameter desiccation with a modified air flow rate is recommended.

1.8 REFERENCES

ASTM D4318, 2010, "Standard Test Methods for Liquid Limit, Plastic Limit, and Plasticity Index of Soils," *Annual Book of ASTM Standards*, ASTM International, West Conshohocken, PA.

ASTM D4373, 2007, “Standard Test Method for Rapid Determination of Carbonate Content of Soils,” *Annual Book of ASTM Standards*, ASTM International, West Conshohocken, PA.

ASTM D5084, 2003, “Standard Test Method for Measurement of Hydraulic Conductivity of Saturated Porous Materials Using a Flexible Wall Permeameter,” *Annual Book of ASTM Standards*, ASTM International, West Conshohocken, PA.

ASTM D5890, 2006, “Standard Test Method for Swell Index of Clay Mineral Component of Geosynthetic Clay Liner,” *Annual Book of ASTM Standards*, ASTM International, West Conshohocken, PA.

ASTM D7503, 2010, “Standard Test Method for Measuring Exchange Complex and Cation Exchange Capacity of Inorganic Fine-Grained Soils”, *Annual Book of ASTM Standards*, ASTM International, West Conshohocken, PA.

Benson, C. and Meer, S., 2009, “Relative Abundance of Monovalent and Divalent Cations and the Impact of Desiccation on Geosynthetic Clay Liner,” *J. Geotech. Geoenviron. Eng.*, Vol. 135(3), pp. 349–358.

Benson, C., Thorstad, P., Jo, H., and Rock, S., 2007, "Hydraulic performance of geosynthetic clay liners in a landfill final cover," *Journal of Geotech. and Geoenviron. Engineering*, Vol.133(7), pp.814-827.

Boardman, T., and Daniel, D., 1996, "Hydraulic conductivity of desiccated geosynthetic clay liners," *Journal of Geotech. Engineering*, Vol.122(3), pp.204-208.

Bradshaw, S., 2008, “Effect of Cation Exchange During Subgrade Hydration and Leachate Permeation,” M.S. thesis, University of Wisconsin—Madison, WI, USA.

Costa, S., Kodikara, J., and Shannon, B., 2013, “Salient factors controlling desiccation cracking of clay in laboratory experiments,” *Géotechnique*, Vol.63(1), pp.18-29.

Costa, S., Kodikara, J., and Thusyanthan, N., 2008, “Study of desiccation crack evolution using image analysis,” *Unsaturated Soils Advances in Geo-Engineering Proc. of the 1st European Conference*, Durham, United Kingdom.

Daniel D., Shan., H., and Anderson, J., 1993, "Effects of partial wetting on the performance of the bentonite component of a geosynthetic clay liner," *Geosynthetics '93*, Vol. 1, Vancouver, Canada, pp. 1483-1496.

Egloffstein, T., 2001, “Natural bentonites – Influence of the ion exchange and partial desiccation on permeability and self-healing capacity of bentonites used in GCLs,” *Geotextiles and Geomembranes*, Vol.19(7), pp.427-444.

Egloffstein, T., 2002, “Bentonite as sealing material in geosynthetic clay liners – Influence of the electrolytic concentration, the ion exchange and exchange with simultaneous partial desiccation on permeability,” *Clay Geosynthetic Barriers*, H. Zanzinger,R. M. Koerner, and E. Gartung, (eds.), pp. 141-153.

Henken-Mellies, W., Zanzinger, H., and Gartung, E., 2002, "Long-term field test of a geosyntheticl barrier in a landfill cover system," *Clay Geosynthetic Barriers*, H. Zanzinger, R. Koerner, and E. Gartung, eds., pp.303-309.

James, A., Fullerton, D., and Drake, R., 1997, "Field performance of GCL under ion exchange conditions," *Journal of Geotech. and Geoenviron. Engineering*, Vol.123(10), pp.897-901.

Jo, H., Katsumi, T., Benson, C., and Edil, T., 2001, Hydraulic conductivity and swelling of non-prehydrated GCLs permeated with single species salt solutions, *J. Geotech. Geoenvironmental Eng.*, 127(7), 557-567.

Kolstad, D., Benson, C., and Edil, T., 2004, “Hydraulic Conductivity and Swell of Nonprehydrated GCLs Permeated with Multi- Species Inorganic Solutions,” *J. Geotech. Geoenviron. Eng.*, Vol. 130(12), pp. 1236–1249.

Kolstad, D., Benson, C., Edil, T., and Jo. H., 2004, “Hydraulic conductivity of a dense prehydrated GCL permeated with aggressive inorganic solutions,” *Geosynthetics International*, Vol.11(3), 233-241.

Likos, W., 2004, “Measurement of Crystalline Swelling in Expansive Clay,” *Geotech. Testing Journal*, Vol. 27(6), pp. 540–546.

Likos, W., and Lu, N., 2003, "Automated humidity system for measuring total suction characteristics of clay," *J. Geotechnical Testing*, Vol. 26(2), pp. 1-12.

Lin, L. and Benson, C., 2000, “Effect of Wet-Dry Cycling on Swelling and Hydraulic Conductivity of GCLs,” *J. Geotech. Geoenviron. Eng.*, Vol. 126(1), pp. 40–49.

Mackey, R., and Olsta, J., 2004, "Performance of geosynthetic clay liners used in two landfill closures in a coastal area of Florida," *Advances in Geosynthetic Clay Liners Technology:*

2nd Symp., STP 1456, R. Mackey and K. von Maugeuge, eds., ASTM, West Conshohocken, Pa., pp. 53-71.

Mansour, R., 2001, "GCL perforance in semi-arid climate conditions," *Proc., Sardinia 2001, 8th Int. Waste Management and Landfill Symp.*, T. Christensen, R. Cossu, and R. Stegmann, eds., CISA, Cagliari, Italy, pp.219-226.

Mazzieri, F., 2011, “Impact of desiccation and cation exchange on the hydraulic conductivity of factory-prehydrated GCLs,” *Geo-Frontiers*, pp. 976-985.

Meer, S., and Benson, C., 2007, "Hydraulic conductivity of geosynthetic clay liners exhumed from landfill final covers," *Journal of Geotech. and Geoenviron. Engineering*, Vol.133(5), pp.550-563.

Melchior, S., 1997, "In situ studies on the performance of landfill caps," *Proc., Int. Containment Technology Conf.*, Florida State University, Tallahassee, Florida, pp. 365-373.

Melchior, S., 2002, "Field studies and excavations of geosynthetic clay barriers in landfill covers," *Proc., Int. Geosynthetic Clay Barriers Symp.*, H. Zanzinger, R. M. Koerner, and E. Gartung, Eds., Swets and Zeitlinger, Lisse, Netherlands, pp.321-330.

Miller, C., Mi, H., and Yesiller, N., 1998, “Experimental analysis of desiccation crack propagation in clay layers,” *Journal Of The American Water Resources Association*, Vol.34(3), pp.677-686.

Nishimura, T., and Fredlund, D., 2003, "A new triaxial apparatus for high total suction using relative humidity control," *Proceedings of the 12th Asian Regional Converence on Soil Mechanics and Geotechnical Engineering*, Vol. 1, Singapore, pp. 65-68.

Otsu, N., 1979, "A threshold selection method from gray-level histograms," *EEE Transactions on Systems, Man, and Cybernetics*, Vol. SMC-9(1), pp. 62-66.

Roberts, L., “Machine perception of three dimensional solids”, PhD Dissertation, Massachusetts Institute of Technology, Cambridge, Massachusetts, 1963.

Scalia, J., and Benson, C., 2010, "Hydraulic conductivity of geosynthetic clay liners exhumed from landfill final covers with composite barriers," *Journal of Geotech. and Geoenviron. Engineering*, Vol.137(1), pp.1-13.

Scalia, J., and Benson, C., 2010, “Effect of Permeant Water on the Hydraulic Conductivity of Exhumed GCLs," *Geotechnical Testing Journal*, 1-11.

Shan, H., and Daniel, D., 1991, "Results of laboratory tests on a geotextile/bentonite liner material," *Geosynthetics '91*, Vol. 1, Atlanta, GA, USA, pp.517-535.

1.9 TABLES

Table 1.1 Summary of field and laboratory studies cited in the literature review.

Field Studies	Laboratory Studies
James et al. (1997)	Shan and Daniel (1991)
Melchior (1997)	Daniel et al. (1993)
Mansour (2001)	Boardman and Daniel (1996)
Melchior (2002)	Lin and Benson (2000)
Egloffstein (2002)	Egloffstein (2001)
Henken-Mellies et al. (2002)	Benson et al. (2007)
Mackey and Olsta (2004)	Benson and Meer (2009)
Benson et al. (2007)	Mazzieri (2011)
Meer and Benson (2007)	

Table 1.2 Mineralogy, cation exchange capacity, swell index, mass per unit area, water content, loss on ignition, and bound cations in the exchange complex of fresh bentonite from the GCL used in this study.

	Properties	Na-B GCL	Determination Method
Index Properties	Swell Index (mL/2 g)	29.5	ASTM D5890
	Mass per Unit Area (kg/m^2)	5.7	
	Water Content (%)	4.7	ASTM D2216
	Loss on Ignition (%)	2.06	Scalia 2012
	Liquid Limit (%)	481	ASTM D4318
	Plastic Limit (%)	451	
Mineralogy	Montmorillonite (%)	84	X-Ray Diffraction
	Quartz(%)	9	
	Plagioclase(%)	3	
	Clinoptilolite (%)	2	
	Illite, Mica, Orthoclase (%)	1	
	Average calcite by mass (%)	1.03	ASTM D4373
Bound Cations (cmol+/kg)	Na	30.5	ASTM D7503
	Ca	28.8	
	Mg	8.4	
	K	2.2	
	CEC ($cmol^+/kg$)	81.0	

Table 1.3 Na and Ca concentrations and chemical properties of permeant waters used in GCL testing.

Permeant Solution	**Abbreviation**	**[NaCl] (M)**	**[$CaCl_2$] (M)**	**I (M)**	**RMD ($M^{1/2}$)**	**pH**	**Electrical Conductivity**
Deionized Water	DW	<0.005	<0.005	$<1.3x10^{-7}$	undefined	6.5	18.9
Conservative Water	CW	0.0003	0.0019	0.004	0.006	6.0	442

Table 1.4 Relative comparison of desiccation methods.

	Unconfined	Perforated Plate	In-permeameter
Drying Control?	Passive	Passive	Active
Specimen Disturbance?	Major	Minor	None
Relative Drying Time	Rapid	Slow	Flow rate dependent

Table 1.5 Summary table that compares the unconfined, perforated plate, and in-permeameter desiccation methods.

		Unconfined	Perforated Plate	In-permeameter
Dry Time (days)	DW	15	115	11
	CW	13	100	10.5
Time to Hydraulic Equilibrium (days)	DW	19	33	30
	CW	15	26.3	10
Mean Water Content		14.9%	12.2%	10.7%
Drying Uniformity CV		3.86%	2.39%	2.83%
CIF		31.8%	32.7%	32.8%
Number of Cells		182	166	190
Cell Area (mm^2)	Average	9.5	10.5	9.1
	Maximum	57.4	43.3	41.8
Crack Width (mm)	Average	0.52	0.59	0.5
	Maximum	2.11	2.24	1.78

Table 1.6 Paired t-test results comparing the cell size and crack thickness frequency distributions of the desiccation methods.

		Comparison of		
		Perforated Plate and In-Permeameter Desiccation	In-Permeameter and Unconfined Desiccation	Unconfined and Perforated Plate Desiccation
Cell Area	t-value	36.9	-8.6	-23.3
	Degrees of Freedom	356	372	348
	p-value	< 0.005	< 0.005	< 0.005
Crack Thickness	t-value	71.0	-17.6	-50.0
	Degrees of Freedom	222492	223558	216322
	p-value	< 0.005	< 0.005	< 0.005

1.10 FIGURES

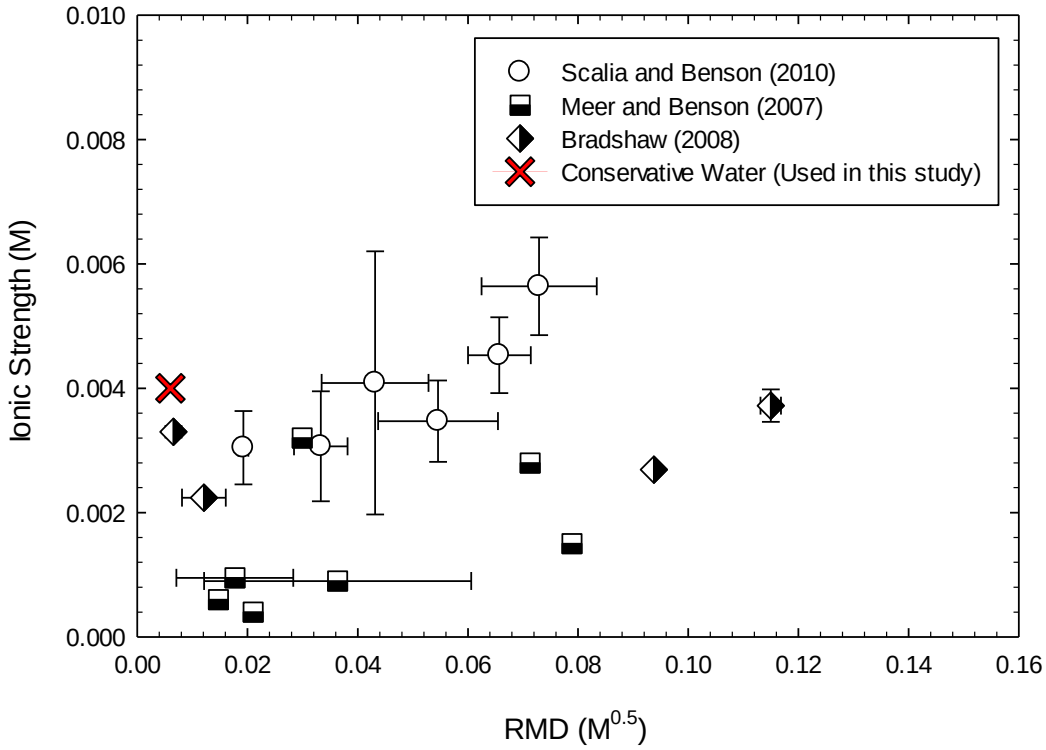

Fig. 1.1. Ionic strength versus RMD of pore water eluent solutions from batch test procedure ASTM D6141. Error bars correspond to one standard deviation from the mean. Conservative water (CW), the permeant water used for laboratory testing, is also shown. Modified from Scalia and Benson (2010).

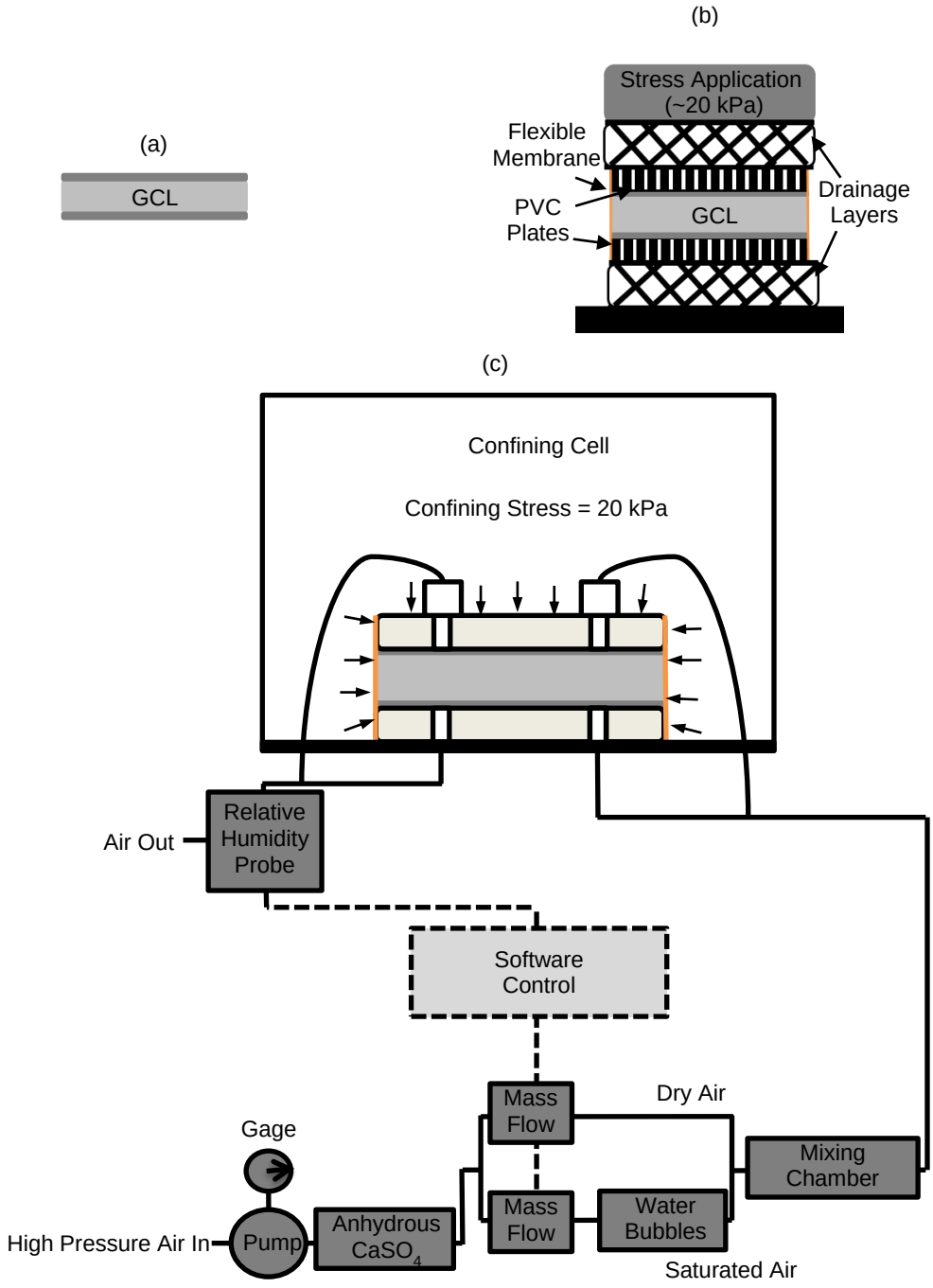

Fig. 1.2. Schematic drawings of the experimental GCL desiccation systems (a) unconfined desiccation (b) perforated plate desiccation employs rigid perforated PVC plates placed above and below the GCL to limit physical disturbance (c) in-permeameter drying eliminates both stress changes and the potential for physical disturbance.

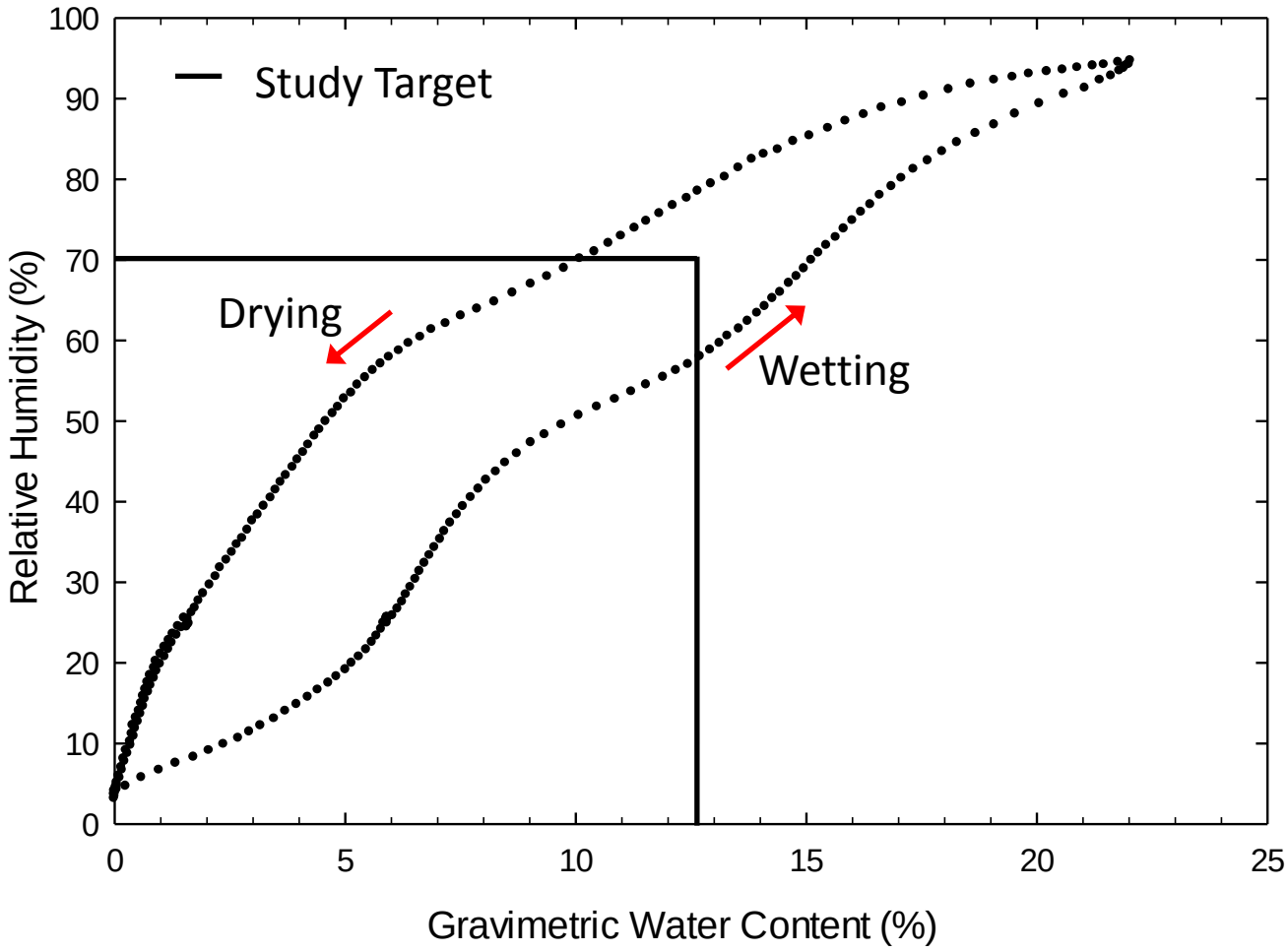

Fig. 1.3. Na-bentonite soil water characteristic curve (via Likos 2004). Based on the SWCC, an equilibrium RH of 70% was determined that was the average of the wetting and drying curves at the approximate air-dried gravimetric water content of 12.5%. Courtesy of Idil Akin.

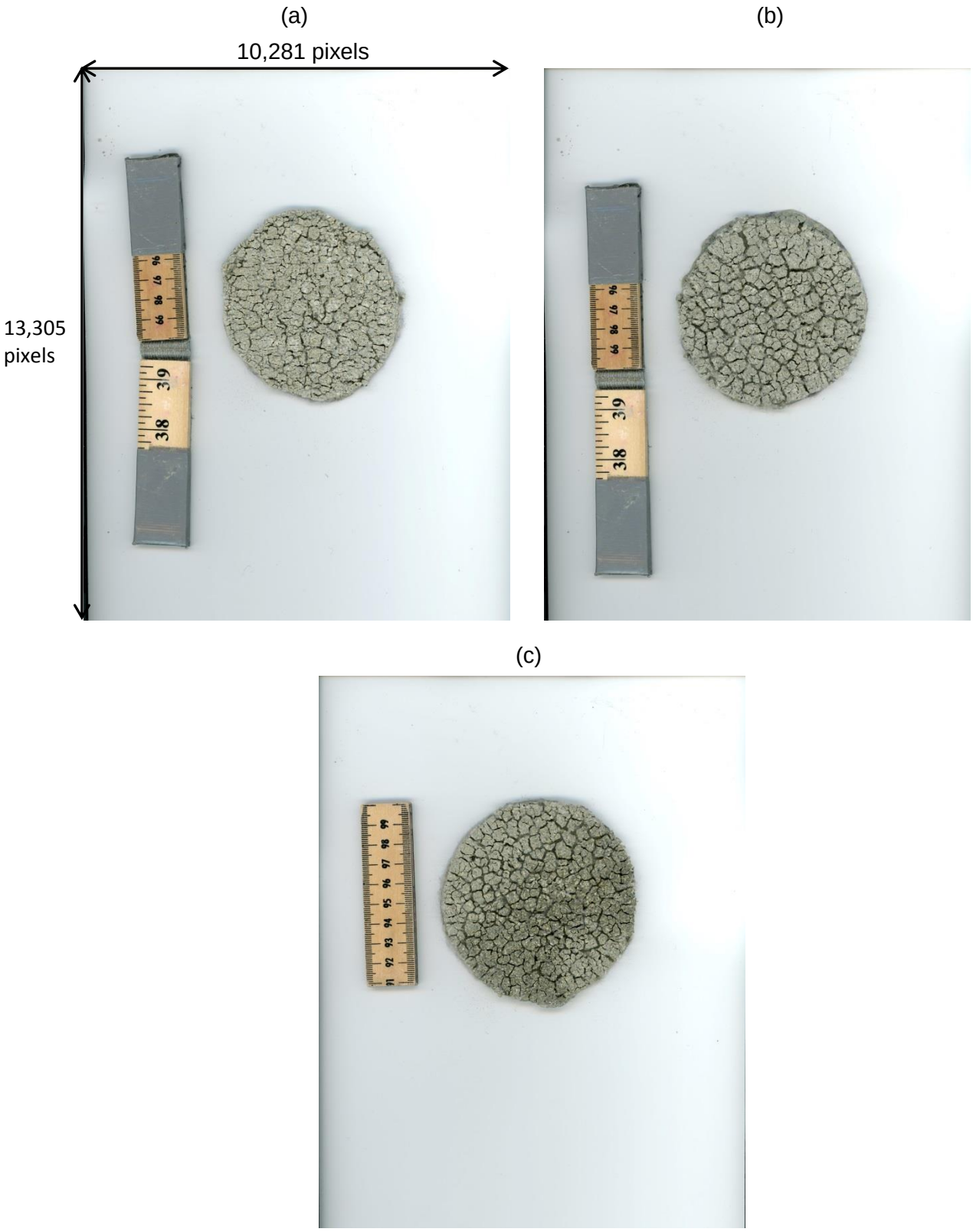

Fig. 1.4 Original full-color GCL images after desiccation (a) unconfined desiccation; (b) perforated plate desiccation; (c) in-permeameter desiccation.

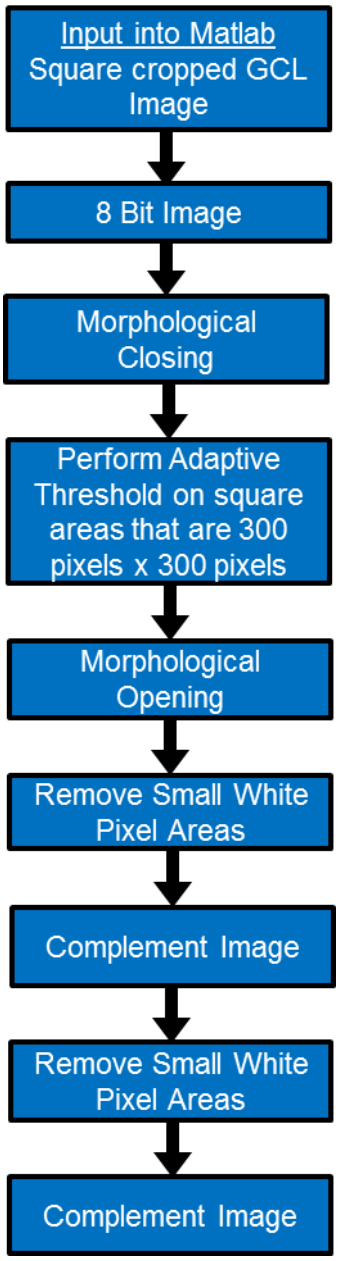

Fig. 1.5. Flowchart of image processing.

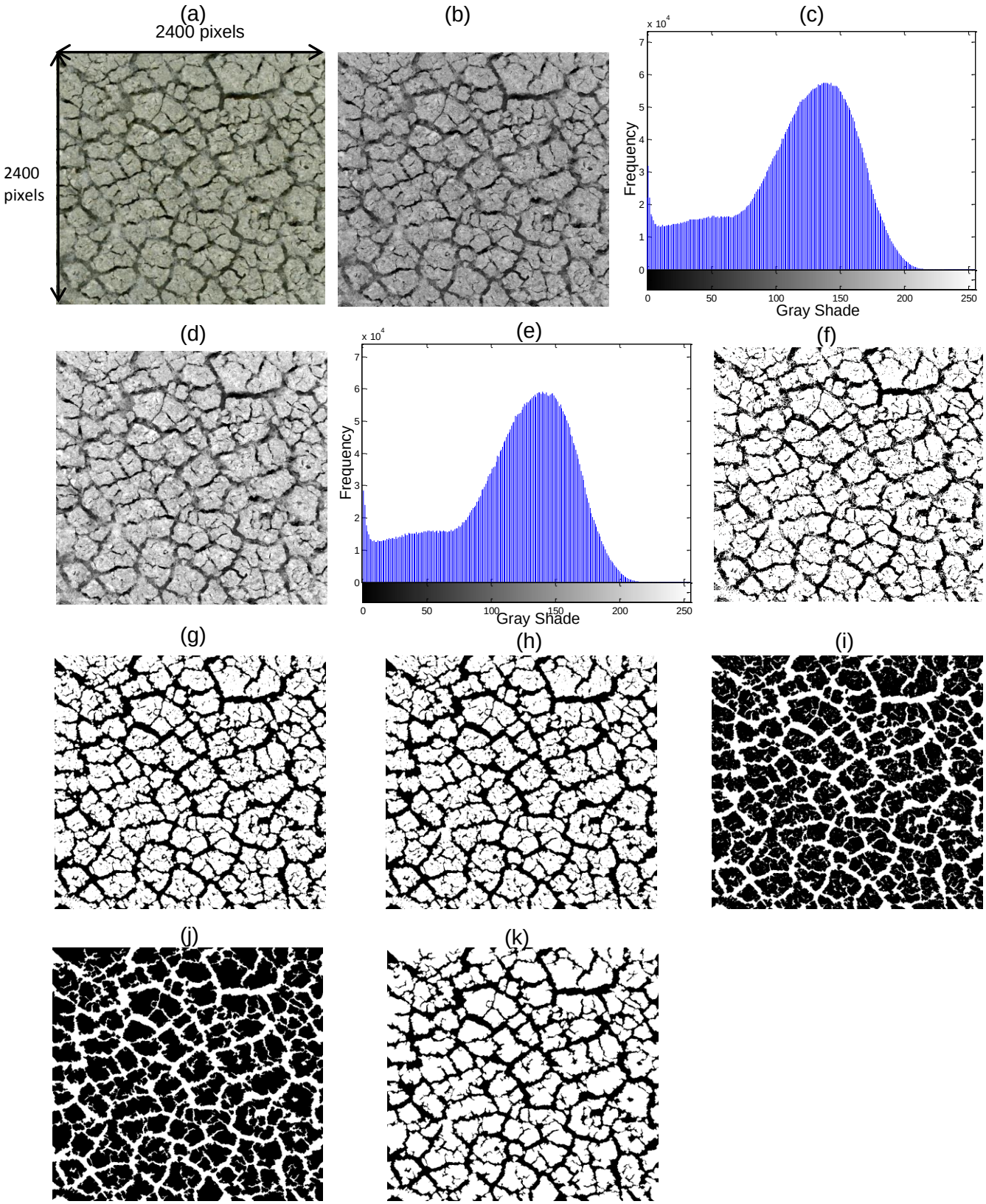

Fig. 1.6. Progression of specimen photo through processing (a) input into Matlab; (b) grayscale image; (c) grayscale histogram of (b); (d) image after morphological closing; (e) grayscale histogram of (d); (f) binary image; (g) image after morphological opening; (h) white areas under 1000 pixels removed; (i) image complement; (j) white areas under 1000 pixels removed; (k) image complement.

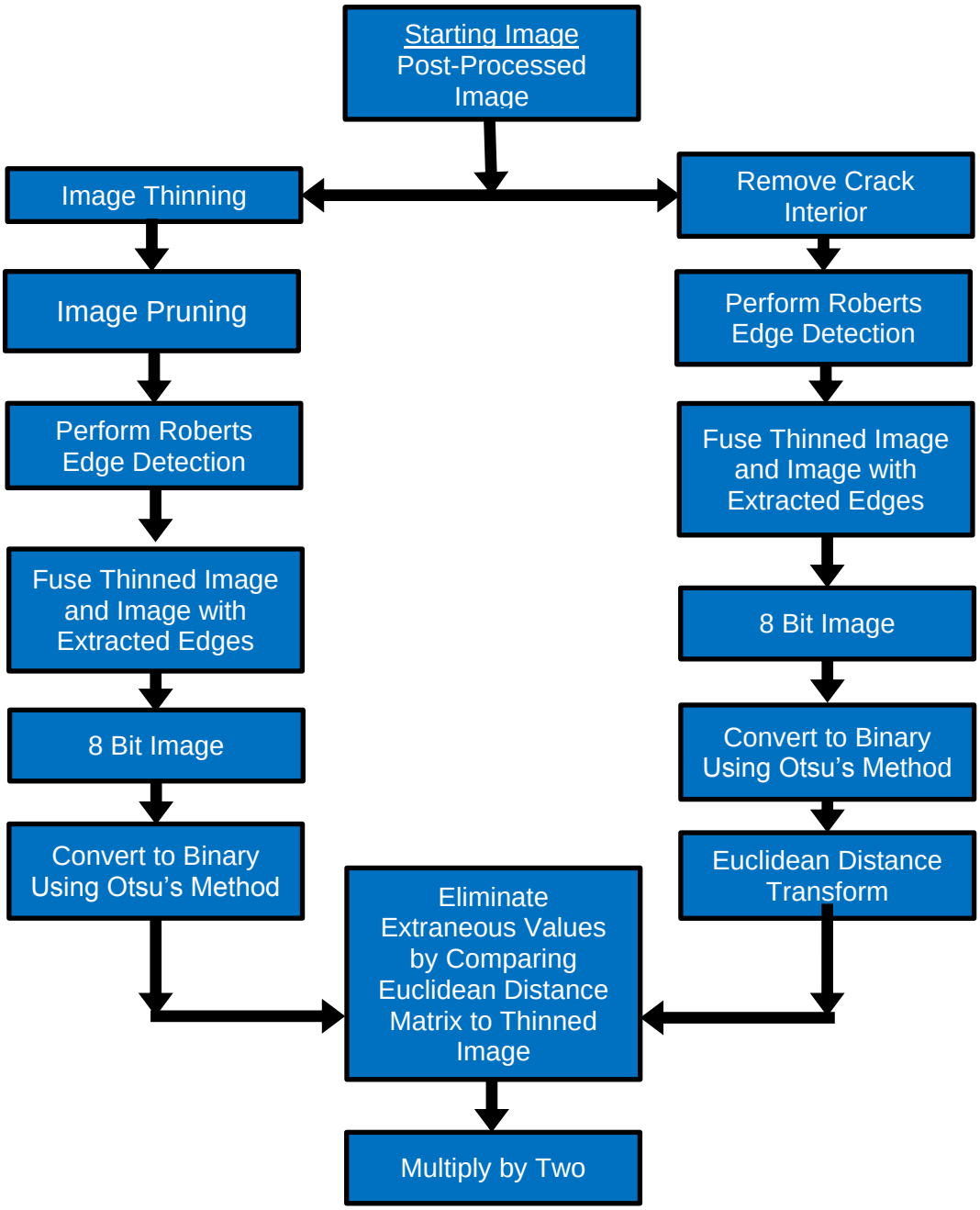

Fig. 1.7. Flowchart of the technique to determine crack thickness.

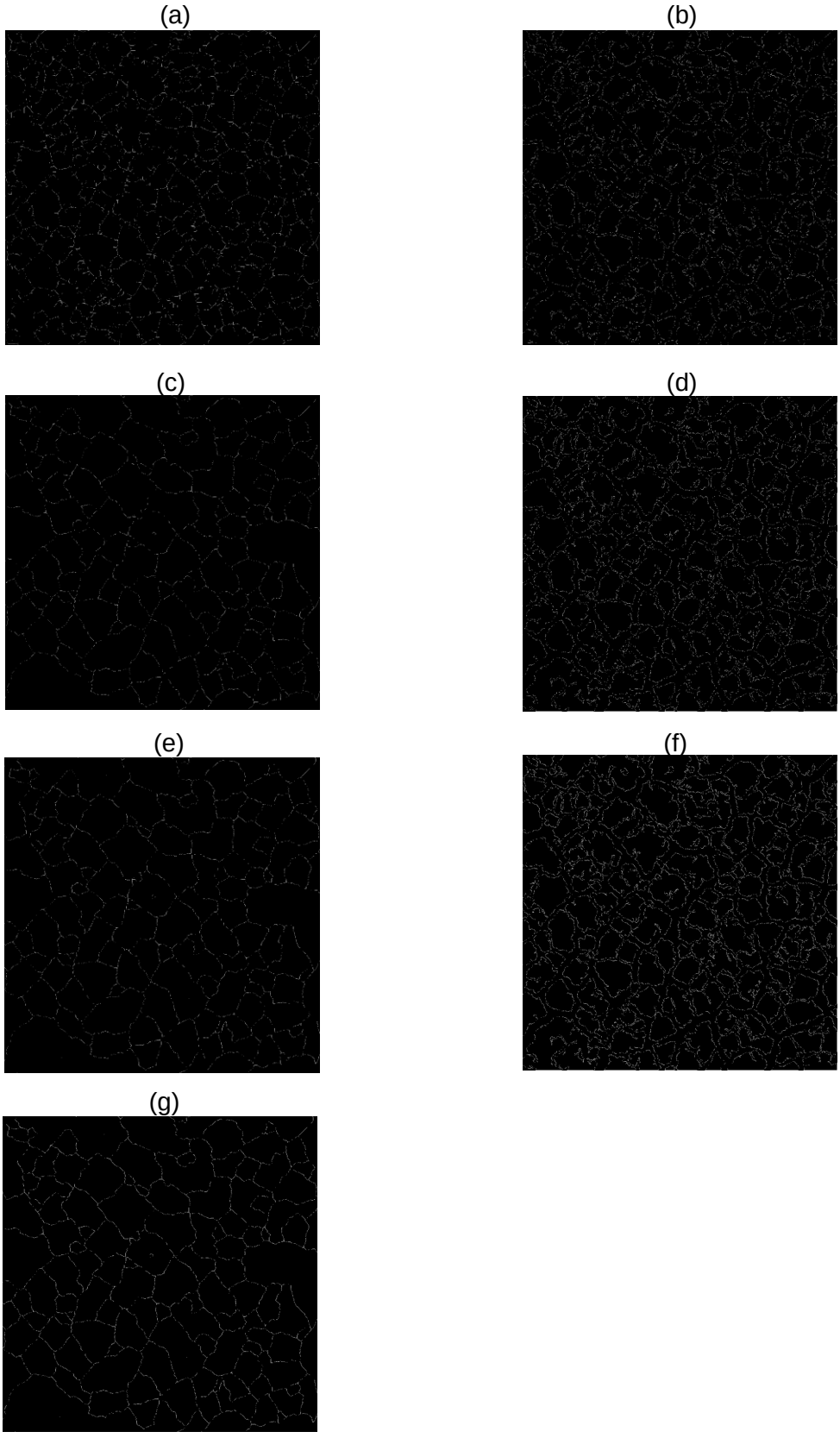

Fig. 1.8 Input into crack thickness determination (a) cracks from Fig. 1.6k are thinned to one pixel width; (b) interior pixels from Fig. 1.6k are removed; (c) pruning of (a); (d) Roberts edge extraction of (b); (e) Roberts edge extraction of (c); (f) resultant fused image of (b) and (d), used for Euclidean distance transform; (g) resultant fused image of (c) and (e), used to eliminate extraneous values from Euclidean distance transform matrix.

(a)

(b)

Fig. 1.9 The GCL subjected to unconfined desiccation became distorted from a circular shape to an oval shape after desiccation (a) plan view; (b) cross-section view.

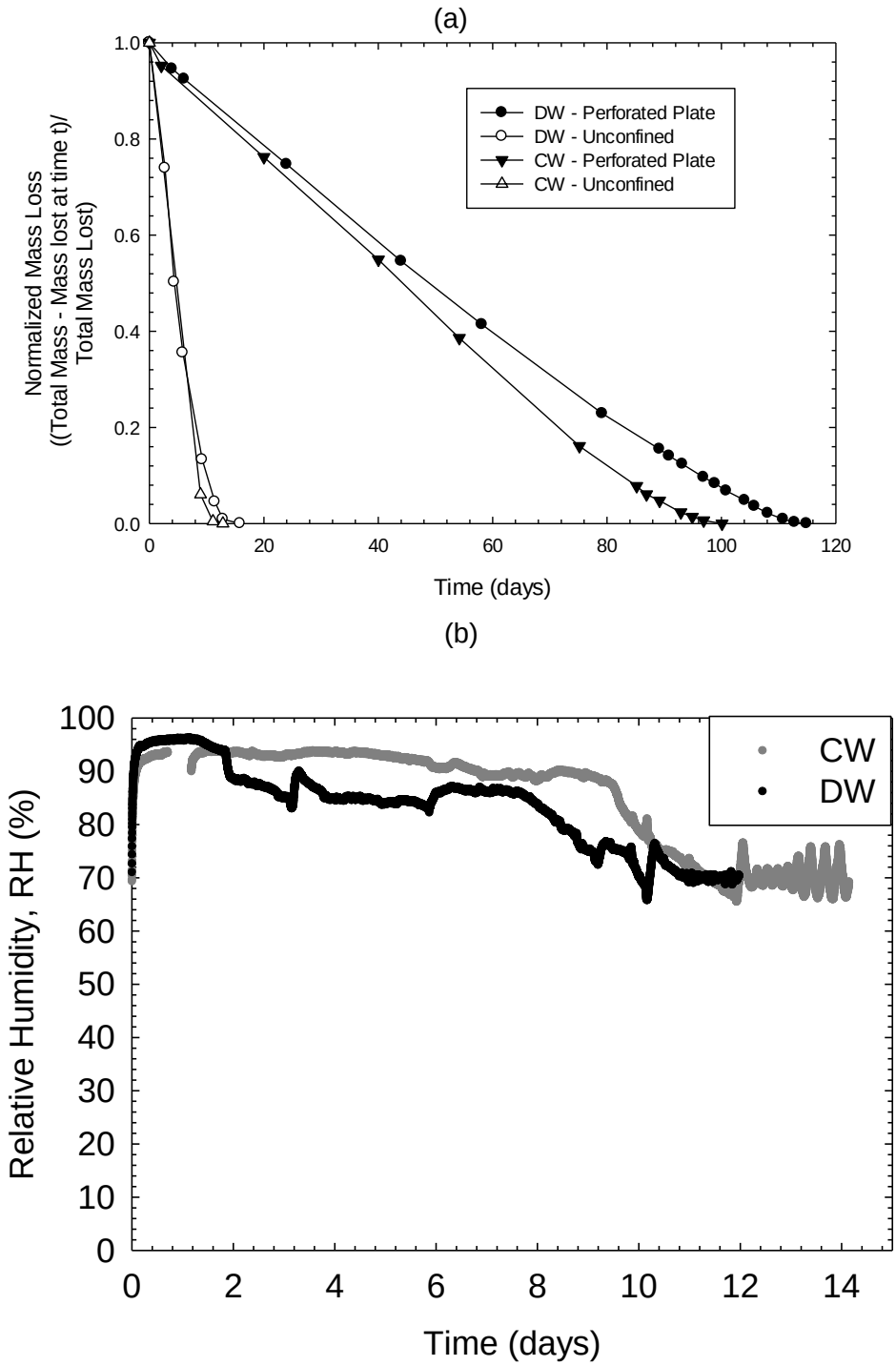

Fig. 1.10 Desiccation as a function of time for GCLs permeated with deionized water (DW) and conservative water (CW; I = 0.004 M, RMD = 0.006 $M^{0.5}$) and desiccated using (a) the unconfined and perforated plate desiccation methods; or (b) the in-permeameter technique.

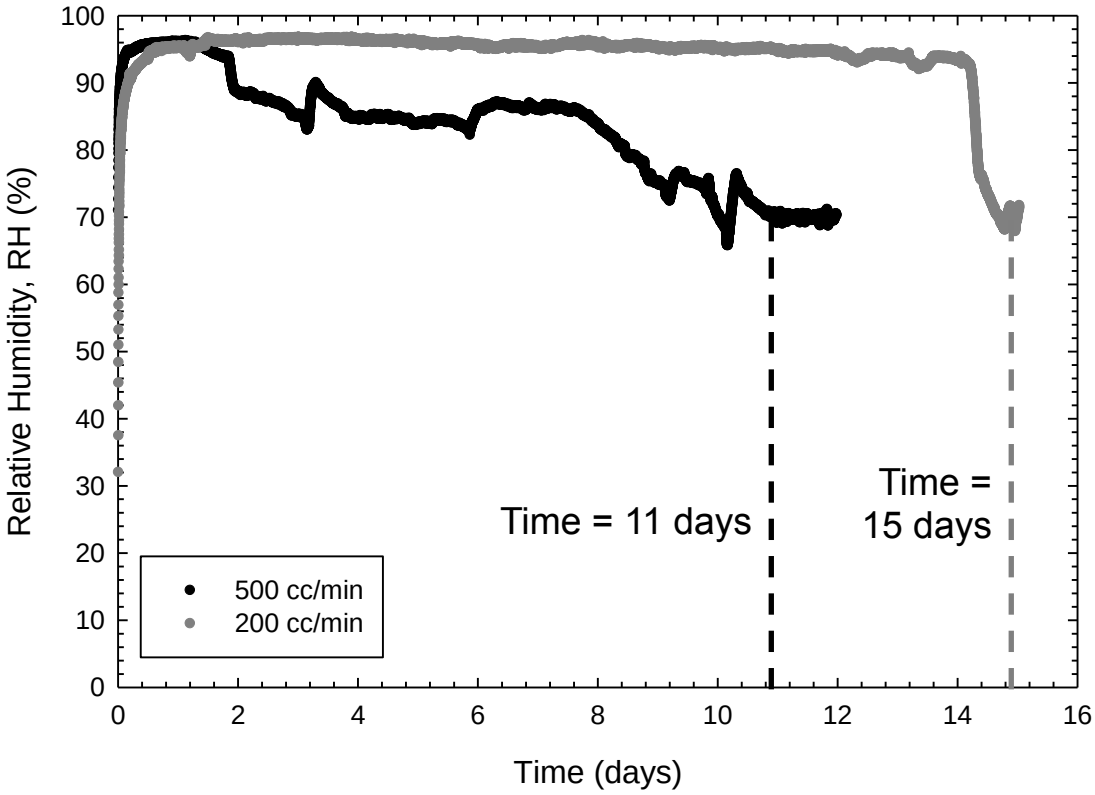

Fig. 1.11 Comparison of different dry air flow rates to the drying time by the in-permeameter desiccation method.

(a)

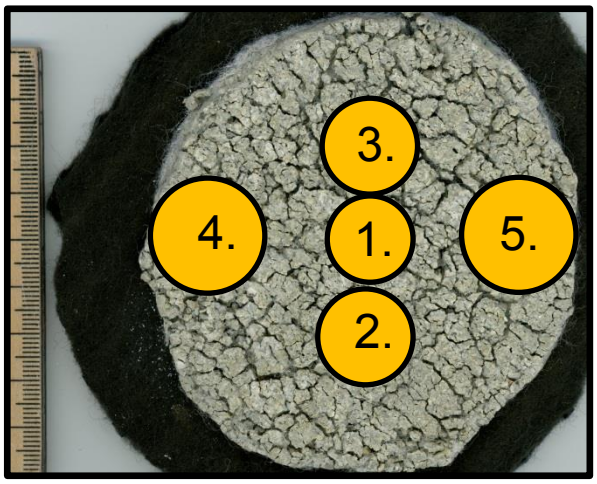

Sample Location	w
1	0.145
2	0.143
3	0.160
4	0.144
5	0.153
Remainder	0.150
μ	0.149
σ^2	0.006
CV	3.86%

(b)

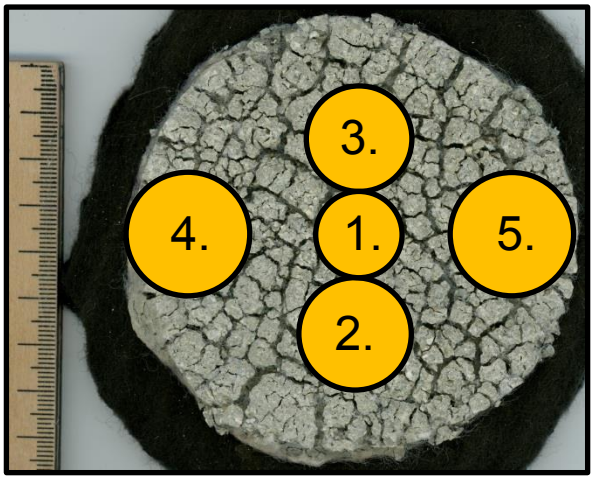

Sample Location	w
1	0.126
2	0.122
3	0.124
4	0.12
5	0.118
Remainder	0.121
μ	0.122
σ^2	0.003
CV	2.39%

(c)

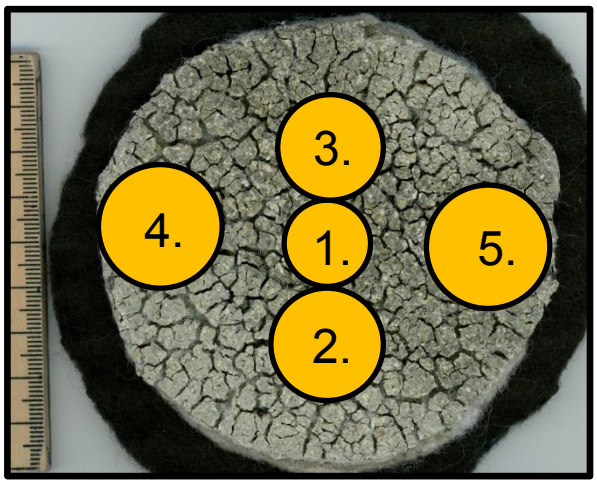

Sample Location	w
1	0.105
2	0.108
3	0.109
4	0.112
5	0.105
Remainder	0.103
μ	0.107
σ^2	0.003
CV	2.83%

Fig. 1.12 Locations of water content samples and corresponding measured water content values, mean, standard deviation, and coefficient of variation (CV) for (a) unconfined desiccation; (b) perforated plate desiccation; and (c) in-permeameter desiccation. The perforated plate method has the lowest CV; therefore, the perforated plate desiccation method results in the most uniform desiccation.

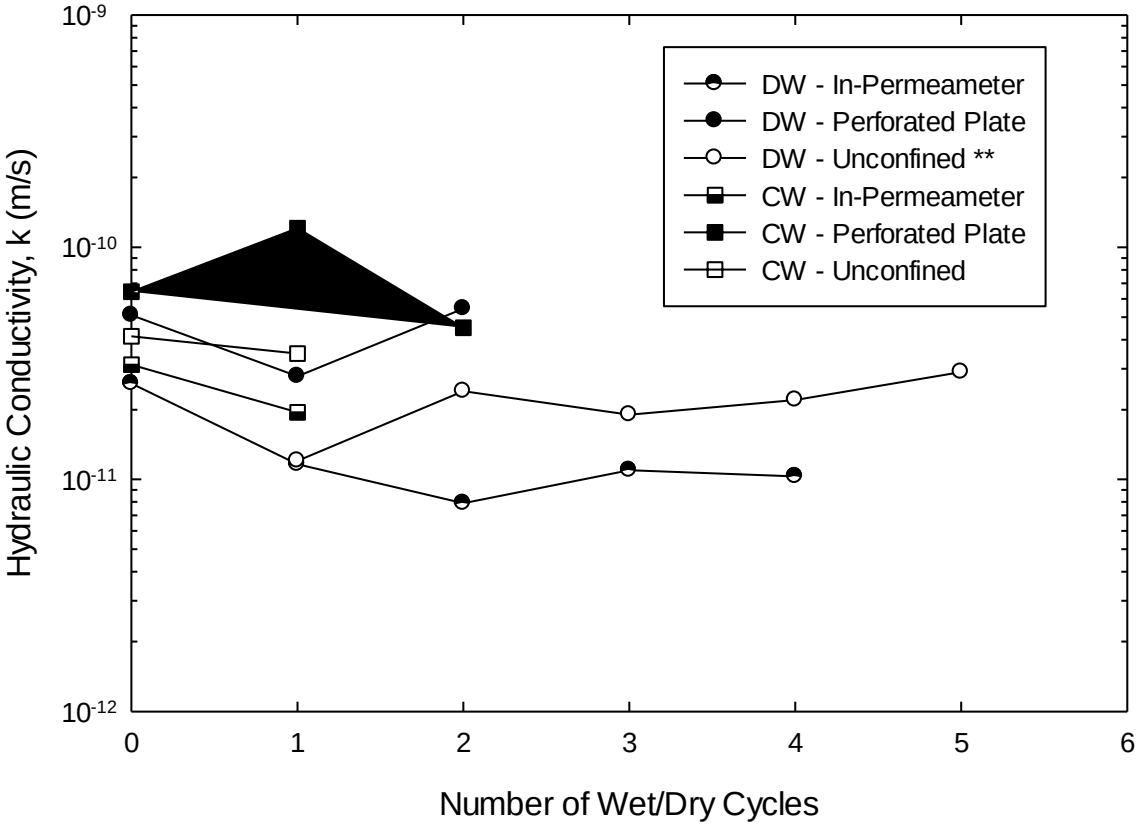

Fig. 1.13 Hydraulic conductivity of Na-bentonite GCLs permeated with deionized water (DW) and conservative water method (CW; I = 0.004 M, RMD = 0.006 $M^{0.5}$) and desiccated using the unconfined, perforated plate, or in-permeameter as a function of the number of wet-dry cycles. Note: ** indicates results taken from Lin and Benson (2000).

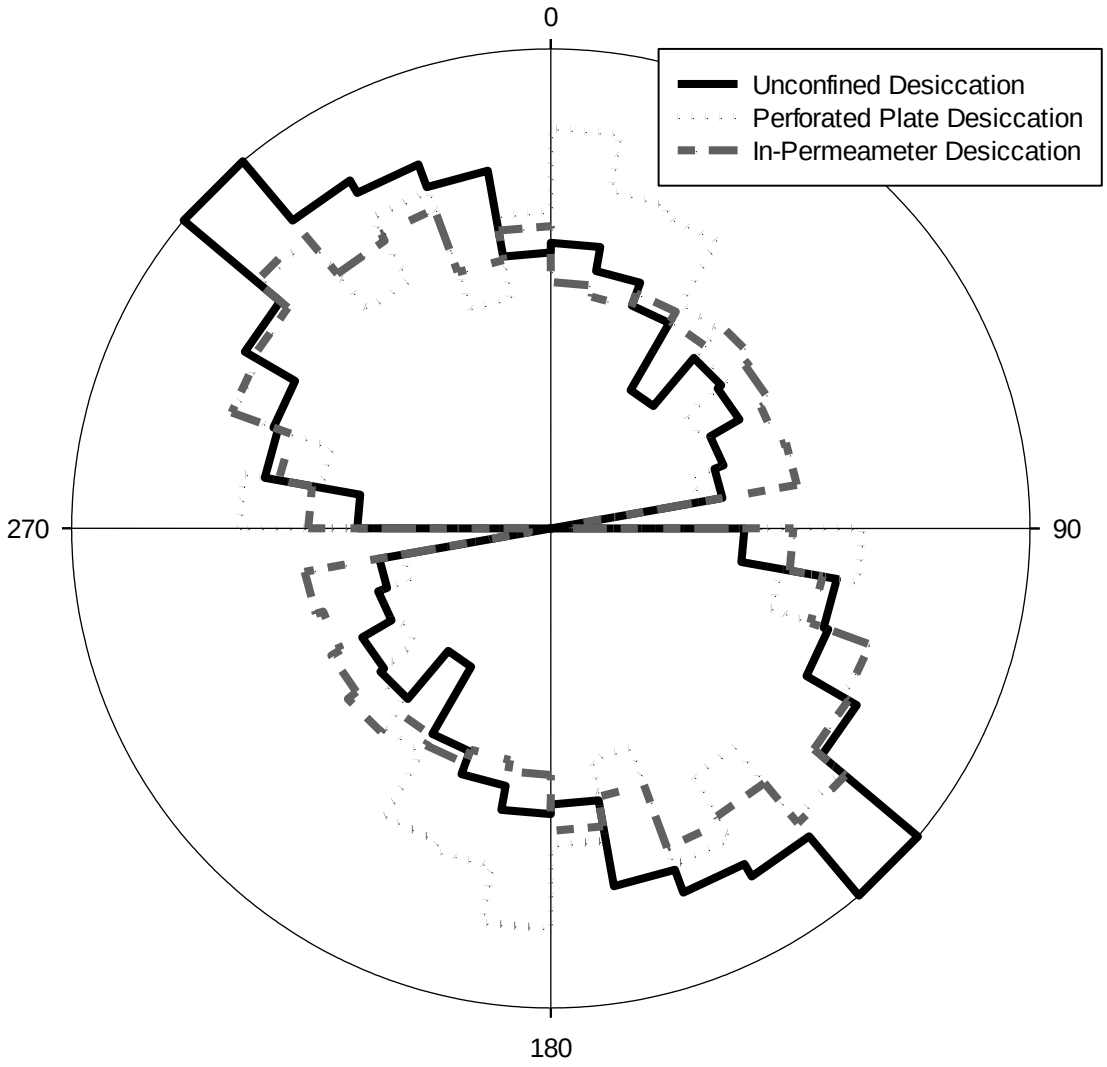

Fig. 1.14 The desiccation crack orientation with respect to horizontal obtained from image analysis. The desiccation cracks as formed by the unconfined method appeared to have a preferred orientation. The preferred orientation of the cracks is likely due to the flattening of the GCL for image acquisition. Neither the perforated plate nor the in-permeameter desiccation methods appear to have a preferred orientation.

Chapter 2

MEASUREMENT AND ANALYSIS OF DESICCATION CRACKING PATTERNS OF GEOSYNTHETIC CLAY LINERS USING IMAGE ANALYSIS

2.1 ABSTRACT

Experiments conducted in this study have been designed to validate image analysis methods developed to examine three different laboratory methods of GCL desiccation during wet-dry cycling. Recent landfill cover field studies have confirmed that osmotic swelling is inhibited and hydraulic conductivity can be three to four orders of magnitude higher than desired if the bentonite in a GCL is subjected to wet-dry cycles. Previous laboratory wet-dry cycling studies focused predominantly on the degree of cation exchange within the bentonite and not on the desiccation method used. Conventional Na-bentonite specimens were initially permeated for one month using deionized water. GCLs were then subjected to one of three cyclic desiccation techniques: (i) unconfined desiccation; (ii) perforated plate desiccation; or (iii) in-permeameter drying. After one wet-dry cycle, the GCLs were disassembled and the desiccation crack patterns were photographed. The captured images required processing before analysis. Quantitative image analysis includes crack intensity factor (CIF), average bentonite cell area (A_A), maximum bentonite cell area (A_M), average crack width (W_A), maximum crack thickness (W_M), and the frequency histogram of bentonite cell area, crack thickness, and crack orientation. The image processing and analysis methods are valid and provide a valuable tool to measure GCL crack pattern differences. Validation of the image analysis method is provided by observation of small

error values in comparisons made between simulated crack geometries of known dimensions and those quantified using the analysis.

2.2 INTRODUCTION

The formation of desiccation cracks in soil is a natural phenomenon that can significantly affect soil mechanical and hydraulic performance. When compared to an intact soil at similar water content, cracked soil is more compressible and has decreased mechanical strength (Morris et al. 1992). Hydraulic properties of unsaturated clayey soils are controlled to a large extent by the geometries of their crack networks. Previous studies have indicated that the hydraulic conductivity (k) of cracked soils is several orders of magnitude greater than that of intact soils (Boynton and Daniel 1985; Albrecht and Benson 2001). The loss of mechanical strength and high k of a cracked soil is therefore a major concern in the long term performance of structures such as landfill covers and liners required to maintain low k under changing environmental conditions.

Geosynthetic clay liners (GCLs) are factory-manufactured hydraulic barriers that contain a thin layer of bentonite clay sandwiched between two geotextiles. The most significant component of the Na-bentonite in GCLs is sodium montmorillonite, a member of the smectite family. When exposed to deionized water (DW), sodium montmorillonite is capable of a high degree of osmotic interlayer swelling and correspondingly low k (i.e. 10^{-11} m/s) during hydration and permeation. However, recent landfill cover field studies have confirmed that osmotic swelling is inhibited and k can be three to four orders of magnitude higher than desired if the bentonite in a GCL is not fully hydrated and if cation exchange has resulted in a predominantly polyvalent cation exchange complex (Egloffstein 2001; Melchior 2002; Benson et al. 2007; Meer and Benson 2007). In situ soil is subject to seasonal rainy and sunny weather, leading to periodic wet-dry cycles (Henken-Mellies et al. 2002).

2.3 BACKGROUND

2.3.1 Field Observations of GCL Cracking

Over the past decades, a number of field experiments have observed desiccation cracks in the bentonite contained within GCLs. When coupled with cation exchange, the k of exhumed GCLs with cracks is higher than anticipated (James et al. 1997; Melchior 1997, 2002; Egloffstein 2002; Benson et al. 2007; Meer and Benson 2007). James et al. (1997) exhumed an adhesive-bonded GCL containing Na-bentonite to determine why a cover with a GCL was leaking excessively. The exhumed GCL contained finely cracked zones, had an average gravimetric water content of 116%, and Na in the bentonite was extensively replaced by Ca. Hydraulic conductivity tests were not conducted on the exhumed GCL. Melchior (1997, 2002) studied five GCLs containing Na-bentonite that were installed in a landfill cover near Hamburg, Germany. Root penetration of the GCL occurred within 5 months of installation, and extensive cracking (cracks as wide as 2 mm) of the bentonite was observed in slightly more than 1 year. Moreover, complete exchange of Ca for Na occurred. Hydraulic conductivities ranged between 1×10^{-7} and 3×10^{-6} m/s and water contents ranged between 55 and 100% (average = 60%). Egloffstein (2002) reported full exchange of Ca for Na and a k of approximately 10^{-9} m/s. In addition, crack networks were observed in the bentonite. Hydraulic conductivities of the exhumed GCLs from Benson et al. (2007) and Meer and Benson (2007) fell in a broad range (5.2×10^{-11} – 1.6×10^{-6} m/s), but most were greater than 10^{-8} m/s. These high hydraulic conductivities were theorized to be caused by polyvalent for monovalent cation exchange coupled with desiccation. The exhumed GCLs also exhibited well-defined cracking networks. However, most of these investigations are limited to qualitative descriptions of desiccation cracking phenomena and quantitative measurements of k.

2.3.2 Previous Image Analysis Studies to Quantify Soil Cracking Patterns

Techniques for quantifying the main features of the crack patterns have recently evolved from direct field measurement to more sophisticated analysis by image processing (Miller et al. 1998; Velde 1999; Vogel et al. 2005; Prat et al. 2006; Costa et al. 2008; Tang et al. 2008; Lakshmikantha et al. 2009; Baer et al. 2009; Tang et al. 2011; Atique and Sanchez 2011; Trabelsi et al. 2011; Costa et al. 2013). The quantification of crack patterns in the field is typically limited to cases where the soil surface is easily accessible. A representative clay cracking pattern is separated into clay cells and cracks (Fig. 2.1). A bentonite or clay "cell" is differentiated here as a region or nodule of intact clay (often polygonal in shape) bounded by cracks on all sides. The size and area of such cells for desiccated GCL specimens are parameters quantified and discussed subsequently.

Miller et al. (1998) investigated the cracking behavior of compacted clay liners. The crack intensity factor (CIF) was introduced as a descriptor of the extent of surficial cracking (Eqn. 1). CIF is defined as

$$CIF = \frac{A_C}{A_T} \qquad (1)$$

where A_c = the surface area of the cracks (white area); and A_T = the total surface area of the image.

To compare the naturally-forming crack patterns of cultivated soils, Velde (1999) obtained photographs, applied a global threshold over the images, and performed morphological opening and skeletelization routines. After thresholding, binary images were obtained where white regions were assigned a value of one and black regions were assigned a value of zero. Opening is a morphological operation that removes small dark pixels from the foreground and places them in the image background. The result of image skeletelization was

cracks that were of single pixel thickness. Images were compared through the number of crack intersections, number of crack segments, crack width, and total crack area.

Vogel et al. (2005) investigated the effect of soil composition on cracking behavior in an attempt to determine geometric measures that can be used for the numerical simulation of soil cracking. Mixtures of sand and bentonite clay were used. The images were processed by applying an adaptive threshold over 20 x 20 pixel squares. The crack geometry was characterized by measuring the crack surface area, length, and spatial orientation.

Prat et al. (2006) recorded the initiation and propagation of cracks and in low plasticity clay. The images were processed in Image J, an image analysis software (Rasband 2005). The cracking patterns were compared by measuring the total crack length and width, CIF, and surface shrinkage.

Costa et al. (2008) qualitatively investigated the effect of desiccation rate and specimen thickness on the desiccation crack pattern. The soil used, Merri-Creek Clay, had a liquid limit of 74% and a plasticity index of 41%. That study indicated that a higher desiccation rate resulted in smaller clay cells. It was postulated that tensile stress and strain energy rose due to increased soil suction as the material desiccated and shrank. If the tensile stress exceeded the bonding strength of grains, cracks occurred. At a higher desiccation rate, more cracks were needed to release the rapid tensile stress increase in the specimen, which subsequently reduced the crack spacing and size of the clay cells. Thinner clay specimens also resulted in smaller clay cells.

Tang et al. (2008) investigated the effect of clay thickness, desiccation temperature, and soil type on the evolution of cracks in a clayey soil using image analysis. In order to measure the crack geometric characteristics, the CIF, the number of intersections and crack segments per unit area, and the mean and frequency histograms of the crack length, crack width, and clod (cell) area were measured. The images were processed by applying a global threshold and

performing skeletelization. The mean clay cell area increased with increasing temperature, which is indicative of a faster desiccation rate.

Lakshmikantha et al. (2009) evaluated the evolution of cracks in silty clay. The images were captured, then processed in Image J. Processing was performed by applying filters, a global threshold, and morphological opening. The total crack length, area of cracks, average crack width, number of cells, and crack intersection angle were measured. The researchers concluded that the crack area is an indirect measure of the increased porosity of the soil due to the presence of cracks and that intersection angles can provide insight into the mechanisms of crack formation. Image analysis is a powerful tool for the qualitative and quantitative description of surface crack patterns.

Baer et al. (2009) obtained photographs of an in situ silt loam soil. The photos were hand-edited, then analyzed for the crack area.

Tang et al. (2011) investigated the effect of the number of wet-dry cycles on the evolution of cracks in a clayey soil using image analysis. In order to measure the crack geometric characteristics, the CIF, the number of intersections per unit area, number of crack segments per unit area, mean crack length, mean crack width, and mean clod area were measured. The images were processed using previously developed software (Tang et al. 2008). The geometric characteristics of cracks changed significantly with increasing wet-dry cycles, with the changes becoming less pronounced after the third cycle. They concluded that image processing and analysis can be used for quantitatively analyzing the wet-dry cycle dependence on clay desiccation cracking behavior.

Atique and Sanchez (2011) investigated the effect of clay thickness on clay cracking behavior by using image analysis. The images were processed by imposing a global threshold on the images, then performing skeletelization. To measure the cracking geometry, the

researchers measured the number of cracks per unit area, the number of crack intersections per unit area, the total crack length, the average crack width, and the CIF. Although the clay cell size was not measured, Atique and Sanchez (2011) qualitatively found that a clay plate with smaller thickness demonstrated both a higher desiccation rate and smaller clay cells.

In order to develop models to simulate desiccation cracking behavior, Trabelsi et al. (2011) captured the time-dependent initiation and propagation of cracks for desiccated clayey soils. Grayscale images were converted to binary. The crack characterization was performed by measuring the CIF, number of cracks per unit area, mean surface area of the cells, crack width, and crack depth of the binary images.

Costa et al. (2013) compared the desiccation cracking patterns while changing the desiccation rate, material, and thickness. The desiccation tests were conducted on clay, potato starch and milled quartz sand, all featuring similar fracture energy. The cell size was compared between the various tests. They discovered quantitatively that the cell size increases as the desiccation rate decreases. The distribution of tensile stresses will depend on the boundary conditions and the material stiffness. The exact positions of crack initiation will be controlled by the flaws or pores within the material. However, not all of the flaws were observed to be activated. This was because the activation of one flaw would generate a zone of low stress, and the nearby flaws may not receive sufficient stress or strain energy to initiate or propagate.

Previous laboratory wet-dry cycling studies focused predominantly on the degree of cation exchange within the bentonite (Shan and Daniel 1991; Daniel et al. 1993; Boardman and Daniel 1996; Lin and Benson 2000; Benson and Meer 2009; Mazzieri 2011).

Experiments conducted in this study have been designed to validate the image analysis methods used to examine three different laboratory methods of GCL desiccation during wet-dry cycling (Chapter 1). Conventional Na-bentonite specimens were initially permeated for one

month using deionized water. GCLs were then subjected to one of three cyclic desiccation techniques: (i) unconfined desiccation, where the GCL was subject to ambient air-drying with no overburden stress applied; (ii) perforated plate desiccation, where the GCL was subject to ambient air-drying under a vertical total stress simulating ~1 m of overlying cover soil; or (iii) in-permeameter drying, where the GCL was flushed with controlled-humidity gas while maintained under isotropic stress conditions. After one wet-dry cycle, the desiccated GCLs were disassembled and the crack patterns were photographed. The captured images required processing before analysis. Quantitative image analysis includes crack intensity factor (CIF, Eqn. 1), average bentonite cell area (A_A), maximum cell area (A_M), average crack width (W_A), maximum crack width (W_M), and the frequency histogram of bentonite cell area, crack thickness, and crack orientation.

2.4 MATERIALS

The GCL product used in this study is a conventional Na-bentonite (Na-B) GCL, provided by Colloid Environmental Technologies Company (CETCO) under the name Bentomat ST (Hoffman Estates, IL). The free swell index (SI) of the bentonite deionized (DI) water was 26.0 mL/2 g (per ASTM D5890) and the cation exchange capacity (CEC) was determined to be 81.0 cmol+/kg (per ASTM D7503). The liquid limit was determined to be 481% and the plasticity index was determined to be 451% (per ASTM D4318). X-ray diffraction indicated that the bentonite contains 84% montmorillonite, 9% quartz, 3% plagioclase, and ≤ 2% of clinoptilolite, illite, mica, orthoclase, and calcite. The mineralogy, cation exchange capacity, and swell index for this bentonite are provided in Table 2.1. The GCL was permeated with DW.

2.5 METHODS

GCL specimens were subjected to one wet-dry cycle, which consisted of permeation with DW followed by desiccation. GCLs were then disassembled for image analysis.

2.5.1 Permeation

GCL specimens were tested for k in flexible-wall permeameters according to ASTM D 5084 Method B (falling headwater-constant tail water) to simulate a wet spring scenario for a near-surface GCL application (e.g., landfill cover). An average hydraulic gradient of 30 was chosen to simulate conditions experienced by GCLs in typical landfill cover applications (Lin and Benson 2000). The effective stress, 20 kPa, was chosen to simulate approximately one meter of cover soil. Hydraulic conductivity tests were continued until at least the following criteria were met: no systematic trend in k over time, (per ASTM D5084); at least four consecutive k readings within ± 25% of the mean (per ASTM D5084); at least four consecutive outflow-to-inflow ratios within 1.0 ± 0.25 (per ASTM D 5084); and the tests were permeated for four weeks.

2.5.2 Desiccation

Three desiccation techniques were used to assess the effects of wet-dry cycling on GCL k. The methods consisted of (i) ambient air drying under no applied confining stress which will be termed “unconfined desiccation” (Fig. 2.2a), (ii) ambient air-drying under applied vertical stress simulating ~1 m of overlying cover soil (Fig. 2.2b), or (iii) an in-permeameter drying technique where gas of known humidity is circulated over the GCL (Fig. 2.2c). Specimens were desiccated to extreme gravimetric water contents (w = 12.5%). The soil water characteristic curve (SWCC) (via Likos 2004) was determined for the Na-bentonite contained within the GCL. The wetting and drying curves represent the maximum and minimum water contents experienced by soil at each relative humidity value. Based on the SWCC, an equilibrium RH of 70% was determined to correspond to the average relative humidity between the wetting and drying curves at a gravimetric water content of 12.5%. All specimens were desiccated in an environment where the RH was kept constant at 70%. The relative humidity of the environment was continuously monitored with a capacitance-film humidity/temperature probe. The probe measured humidity between 0% RH and 99% RH at 0.01% RH resolution.

2.5.3 Disassembly and Image Acquisition

After one wet-dry cycle, the permeameter was disassembled and the woven geotextile of the GCL was removed by cutting the needle punching fibers with a sharp scalpel.

The level of success in any image processing work is dependent on the quality of captured images. Images of GCLs sans woven geotextiles were taken by an Epson B11B198011 Perfection V600 Photo Scanner 1200 dots per inch (dpi) image scanner (Long Beach, California, USA). The scanner was placed on the GCL at the center of the 8.5" x 11.7" scanning board. Images were taken at a measurement angle of 90° from the GCL.

The resultant full-color images were 10,281 by 13,305 pixels. Each image was 215.9 by 279.4 mm in size, which resulted in a pixel size of 0.021 mm (Fig. 2.4).

2.5.4 Image Processing

The full-color GCL images were imported into Adobe Photoshop (San Jose, California, USA). A square image of 2400 by 2400 pixels was cropped from the center of the GCL image to eliminate edge effects (Fig. 2.6a).

The cropped images were then imported into Matlab (Matrix Laboratory) where a small code was written for processing (Mathworks, Natick, Massachusetts, USA). A flow chart of this process is shown in Fig. 2.5. The full-color images were converted to 8 bit images (Fig. 2.6b).

An example of a gray-scale histogram is shown in Fig. 2.6c. The two ends of a gray-scale histogram vary between 0 (pure black) and 255 (pure white). Because the cracks were darker than the bentonite cells, the cracks were assigned a lower value. There are two distinct peaks of gray (the first being the bentonite frequency and the other being the cracks) with very little occurrence of gray in between. Next, the images were morphologically closed using a diamond-shaped structuring element (Fig 2.6d). Closing is an operation that reduces dark features while not affecting the background and consists of dilation followed by erosion using

the same structuring element. Dilation expands the light colors in a grayscale image while erosion expands the dark colors in a grayscale image. A structuring element is a shape used to probe or interact with a given image, with the purpose of drawing conclusions on how the shape fits or misses the objects or parts of objects in the image according to their shape or spatial orientation.

Both global thresholding using Otsu's Method (Otsu 1979) and adaptive thresholding were explored to determine which would be more effective (Fig. 2.7). The image was ultimately subjected to an adaptive mean threshold on 300 pixel by 300 pixel squares. After thresholding, binary images were obtained in which white regions (bentonite) were assigned a value of one and black regions (cracks) zero (Fig 2.7b).

The basic idea in binary morphology is to probe an image with a simple, pre-defined binary structuring element, drawing conclusions on how this shape fits or misses the shapes in the image. The binary image was morphologically opened, an operation that removes small dark pixels from the foreground and places them in the image background, using a diamond-shaped structuring element (Fig 2.8a). Opening consists of erosion followed by dilation using the same binary structuring element.

Next, all white pixel areas smaller than 1000 square pixels were removed from within the crack area (Fig 2.8b). The complement, or inverse, of the image was obtained (Fig 2.8c). Again, all white pixel areas smaller than 1000 square pixels were removed from within the bentonite cells (Fig 2.8d). The image complement was obtained (Fig. 2.8e).

The image was thinned, where selected black pixels were removed until lines of single pixel thickness remained (Fig 2.8f). Pixels were removed such that an object without holes shrunk to a minimally connected stroke located equidistant from the nearest previous outer boundaries (Pratt 2001). A string of pixels is said to be minimally connected if elimination of any

pixel results in a loss of connectivity of the remaining pixels. The thinned image was then pruned, a binary subtractive operation that erases black pixels surrounded by eight white pixel neighbors (Fig. 2.8g). The resultant image was a skeletonized version of the cracks.

2.5.5 Image Analysis

Several parameters were obtained to characterize the geometrical properties of the crack pattern. These include the crack intensity factor (CIF, Eqn. 1), average bentonite cell area (A_A), maximum cell area (A_M), average crack width (W_A), maximum crack width (W_M), and the frequency histogram of bentonite cell area, crack thickness, and crack orientation.

The CIF (Eqn. 1) is defined as the ratio of the surface area of the cracks (white area, A_c) to the total surface area of the image (A_T) (Miller et al 1998). The image before morphological thinning was used to obtain the CIF (Fig. 2.8e). The CIF was used to quantify the relative degree of cracking between the different desiccation methods.

The Sobel (Duda and Hart 1973), Prewitt (Prewitt 1970), Roberts (Roberts 1963), and Canny (Canny 1986) morphological operators were tested to determine which would extract the most cracks relative to the original image (Fig. 2.9). The Sobel, Prewitt, and Roberts operators were heuristically developed and use altered matrices with the intensity gradient analysis to extract cracks of different preferred orientations. The intensity gradient analysis uses the specified morphological operator to move through the image and detect edges based on the rate of pixel value change. The direction of smallest change will give the orientation of cracks whereas the direction of largest change will give the edge of the crack. The Canny operator convolves a one-dimensional continuous domain noisy edge signal *f(x)* with an antisymmetric impulse response function *h(x)* (Pratt 2001). An edge is marked at the local maximum of the convolved gradient *f(x)*h(x)*.

The Roberts Operator was ultimately used to detect crack boundaries using an intensity gradient analysis of the pruned image (Fig. 2.9c).

The image subjected to edge detection was fused with the pruned image to form a new image (Fig. 2.10a). The full color fused image was then converted to binary using Otsu's method (Otsu 1979). Small holes were removed from within the black pixels (Fig. 2.10b). The Cartesian coordinates of the fused image were converted to polar coordinates using the Hough Transform (Sklansky 1978). The line length and orientation with respect to horizontal were extracted from the polar coordinates to form the frequency histograms of crack orientation.

A flow chart of the crack width determination technique is shown in Fig. 2.10. The process of determining crack width began by removing the crack interior of the image before morphological thinning (Fig. 2.11a). The edges of the crack exterior were extracted using the Roberts Operator (Roberts 1963) (Fig. 2.11b). The image subjected to edge detection was fused with the crack exterior image to form a new image (Fig. 2.11c). The full color fused image was then converted to binary using Otsu's method (Otsu 1979). Small holes were removed from within the black pixels. As a result of crack interior removal, all pixels surrounded by four white pixels were black, distinguishing the boundary pixels as white. An Euclidean distance transform was performed on the resultant image. The Euclidean distance formula is defined as

$$distance = \sqrt{(x_2 - x_1)^2 + (y_2 - y_1)^2} \qquad (2)$$

where (x_1, y_1) and (x_2, y_2) are the Cartesian coordinates of two points. The distance transform assigned a number for each image pixel that is the distance between that pixel and the nearest white pixel in the image.

The resultant distance matrix was the same size as the original image. The value corresponding to each point in the distance matrix lists the shortest distance between each point

and the nearest white border. However, the matrix also included the distance from within the bentonite cells to the nearest crack border. To eliminate the effects of the bentonite cells, the distance matrix was compared to a skeletonized version of the cracks (Fig. 2.11d). In this final crack thickness matrix, all values in the distance matrix that did not correspond to the crack skeleton were assigned a value of zero. The crack skeleton was assumed to be located in the exact middle of the crack and the cracks were assumed to be symmetrical, meaning that the crack width is two times the value given in the distance matrix. The crack thickness matrix was compared to the original image. The mean crack thickness, maximum crack thickness, and frequency histogram of crack thickness were extracted from the crack thickness matrix.

The number and size of bentonite cells were measured while analyzing the binary images. The fused binary image was used to extract the quantity, size, and centroid of the clay cells. A bentonite cell was defined as a black region bounded by white cracks on all sides. The frequency histogram of bentonite cell area was also obtained.

2.6 VERIFICATION OF TECHNIQUE

In order to determine whether the image processing procedure affects measured cell area, images were created that featured a single triangular, square, rectangular, and circular shape with a size varying between 10 mm^2 and 20 mm^2 were imported into Matlab. The shape area and error were determined for all line thicknesses and morphological operator combinations. Error is defined in this case as

$$error = \frac{\text{actual} - \text{approximation}}{actual} * 100\% \quad (3)$$

where actual = the known shape area; and approximation = the shape area as determined via Matlab. The error of each shape was plotted against the known shape area (Fig. 2.12). The error for all shapes and areas was very small, often below 1%. The area was almost always

underestimated with the only exceptions being slight overestimations of the circular shape. Therefore, the image processing procedure does not affect the measured cell area.

In order to determine the edge detection technique that would most accurately determine crack thickness, lines of thickness varying between 0.1 and 2.1 mm were imported into Matlab. The edges of the crack exterior and center were extracted using the Sobel, Prewitt, Roberts, or Canny morphological operators. The average line width, frequency histogram, and error were determined for all line thicknesses and morphological operators combinations. The error of each edge detection technique was plotted against the known thickness (Fig. 2.13). Regardless of the edge detection technique, the analysis tends to underestimate the line thickness. However, the underestimation is larger when determining small (i.e. less than 0.6 mm) line thicknesses. This is likely because the comparison crack skeleton image used to eliminate extraneous numbers from the distance matrix is greater than one pixel in thickness. The resolution of the image is 0.021 mm/pixel. For a line that is five pixels thick (i.e. 0.21 mm), a crack skeleton that is two pixels thick will result in an underestimation of 0.021 mm, or an error of 20%.

The Roberts morphological operator resulted in the smallest error for all line thicknesses; therefore, the Roberts Operator was chosen for all subsequent edge extraction analyses.

To further verify the crack thickness technique, lines of thickness varying between 0.2 mm and 2.1 mm were imported into Matlab (Fig. 2.14a). The average line width and frequency histogram was determined for the image (Fig. 2.14b). There are distinct peaks that correspond to the approximate width of each line, although the location of each peak is slightly lower than the known thickness. This is consistent with the single-line thickness analysis.

In reality, a GCL crack pattern will contain irregularly shaped cracks of varying thickness. In an attempt to capture a degree of crack thickness heterogeneity, several synthetic crack images were created featuring a single triangle (Fig. 2.15a), multiple triangles (Fig. 2.15b), a single ellipse (Fig. 2.16a), and multiple ellipses (Fig. 2.16b), each with a widest base of 2.1 mm.

The average line width and frequency histograms were determined for each image (Figs. 2.15c, 2.15d, 2.16c, and 2.16d).

The frequency histogram of the single triangle does not correspond entirely with the expected result (Fig. 2.15c). There is an equal frequency of each thickness until approximately 1.8 mm although the widest base is 2.1 mm. The underestimation phenomenon can be attributed to the thinning and pruning operations. The thinning operation will remove pixels such that an object shrinks to a minimally connected stroke located equidistant from the nearest previous outer boundaries. A triangle will be thinned to a line ending with a ‘v’ shape. The pruning operation removes the ‘v’ shape, isolating the triangle middle to be analyzed by the thickness algorithm.

The frequency histogram of multiple triangles is as expected (Fig. 2.15d). There is a greater frequency of thickness in the range between 0.4 mm and 1.5 mm. There is a reduced frequency of the triangle base and tip due to overlap when intersecting multiple triangles.

The frequency histogram of the single ellipse shows an increased thickness frequency around 2.0 mm (Fig. 2.16c). This reflects the greater frequency of thicknesses at the widest portion of the ellipse.

The frequency histogram of multiple ellipses is very similar to the single ellipse frequency histogram, also reflecting an increased thickness frequency around 2.0 mm (Fig. 2.16d). The multiple ellipse frequency histogram shows thicknesses greater than 2.0 mm due to the interaction and overlap of multiple ellipses.

2.7 SUMMARY AND CONCLUSION

Experiments conducted in this study were designed to validate the image analysis methods used to examine three different laboratory methods of GCL desiccation during wet-dry cycling. Conventional Na-bentonite specimens were initially permeated, subjected to one of three cyclic

desiccation techniques: (i) unconfined desiccation; (ii) perforated plate desiccation; or (iii) in-permeameter drying, disassembled, and photographed. The captured images required processing before analysis. In order to determine whether the image processing procedure affects measured cell size, images were created that featured a single triangular, square, rectangular, and circular shape with a size varying between 10 mm^2 and 20 mm^2 were subject to Matlab analysis. The error for all shapes and sizes was very small, often below 1%. The size was almost always underestimated with the only exceptions being slight overestimations of the circular shape. The image processing procedure was concluded to not affect the measured cell size. In order to determine whether the image processing procedure would accurately determine crack thickness, lines of known thickness varying between 0.1 and 2.1 mm were subject to Matlab analysis. Regardless of the edge detection technique, Matlab underestimated the line thickness. However, the underestimation is larger when determining small (i.e. less than 0.6 mm) line thicknesses. The image processing methods were concluded to not alter the overall quality of the image. The image analysis methods are valid and provide a valuable tool to measure the differences between GCL crack patterns.

2.8 REFERENCES

Albrecht, B., and Benson, C., 2001, “Effect of desiccation on compacted natural clays,” *J. Geotech. Geoenvironmental Eng.*, Vol.127(1), pp.67-75.

ASTM D4318, 2010, "Standard Test Methods for Liquid Limit, Plastic Limit, and Plasticity Index of Soils," *Annual Book of ASTM Standards*, ASTM International, West Conshohocken, PA.

ASTM D4373, 2007, “Standard Test Method for Rapid Determination of Carbonate Content of Soils,” *Annual Book of ASTM Standards*, ASTM International, West Conshohocken, PA.

ASTM D5084, 2003, “Standard Test Method for Measurement of Hydraulic Conductivity of Saturated Porous Materials Using a Flexible Wall Permeameter,” *Annual Book of ASTM Standards*, ASTM International, West Conshohocken, PA.

ASTM D5890, 2006, “Standard Test Method for Swell Index of Clay Mineral Component of Geosynthetic Clay Liner,” *Annual Book of ASTM Standards*, ASTM International, West Conshohocken, PA.

ASTM D7503, 2010, “Standard Test Method for Measuring Exchange Complex and Cation Exchange Capacity of Inorganic Fine-Grained Soils”, *Annual Book of ASTM Standards*, ASTM International, West Conshohocken, PA.

Atique, A., and Sanchez, M., 2011, “Analysis of cracking behavior of drying soil,” *2nd International Conference on Environmental Science and Technology*, Vol.6, Singapore, pp. VI66-VI70.

Baer, J., Kent, T., and Anderson, S., 2009, “Image analysis and fractal geometry to characterize soil desiccation cracks,” *Geoderma*, Vol.154(1-2), pp.153-163.

Benson, C. and Meer, S., 2009, “Relative Abundance of Monovalent and Divalent Cations and the Impact of Desiccation on Geosynthetic Clay Liner,” *J. Geotech. Geoenviron. Eng.*, Vol. 135(3), pp. 349–358.

Benson, C., Thorstad, P., Jo, H., and Rock, S., 2007, "Hydraulic performance of geosynthetic clay liners in a landfill final cover," *Journal of Geotech. and Geoenviron. Engineering*, Vol.133(7), pp.814-827.

Boardman, T., and Daniel, D., 1996, "Hydraulic conductivity of desiccated geosynthetic clay liners," *Journal of Geotech. Engineering*, Vol.122(3), pp.204-208.

Boynton, S., Daniel, D., 1985, “Hydraulic conductivity tests on compacted clay,” *J. Geotech. Eng.*, Vol.111(4), pp.465-478.

Canny, J., 1986, “A computational approach to edge detection,” *IEEE Transactions on Pattern Analysis and Machine Intelligence*, Vol.PAMI-8(6), pp.679-698.

Costa, S., Kodikara, J., and Shannon, B., 2013, “Salient factors controlling desiccation cracking of clay in laboratory experiments,” *Géotechnique*, Vol.63(1), pp.18-29.

Costa, S., Kodikara, J., and Thusyanthan, N., 2008, “Study of desiccation crack evolution using image analysis,” *Unsaturated Soils Advances in Geo-Engineering Proc. of the 1st European Conference*, Durham, United Kingdom.

Daniel D., Shan., H., and Anderson, J., 1993, "Effects of partial wetting on the performance of the bentonite component of a geosynthetic clay liner," *Geosynthetics '93*, Vol. 1, Vancouver, Canada, pp. 1483-1496.

Duda, R., and Hart, P., 1973, *Pattern recognition and scene analysis*, Wiley, New York

Egloffstein, T., 2001, “Natural bentonites – Influence of the ion exchange and partial desiccation on permeability and self-healing capacity of bentonites used in GCLs,” *Geotextiles and Geomembranes*, Vol.19(7), pp.427-444.

Egloffstein, T., 2002, “Bentonite as sealing material in geosynthetic clay liners – Influence of the electrolytic concentration, the ion exchange and exchange with simultaneous partial desiccation on permeability,” *Clay Geosynthetic Barriers*, H. Zanzinger,R. M. Koerner, and E. Gartung, (eds.), pp. 141-153.

Henken-Mellies, W., Zanzinger, H., and Gartung, E., 2002, "Long-term field test of a geosyntheticl barrier in a landfill cover system," *Clay Geosynthetic Barriers*, H. Zanzinger, R. Koerner, and E. Gartung, eds., pp.303-309.

James, A., Fullerton, D., and Drake, R., 1997, "Field performance of GCL under ion exchange conditions," *Journal of Geotech. and Geoenviron. Engineering*, Vol.123(10), pp.897-901.

Lakshmikantha, M., Prat, P,. and Ledesma, A., 2009, “Image analysis for the quantification of a developing crack network on a drying soil,” *Geotechnical Testing Journal*, Vol.32(6), pp.505-515.

Likos, W., 2004, “Measurement of Crystalline Swelling in Expansive Clay,” *Geotech. Testing Journal*, Vol. 27(6), pp. 540–546.

Lin, L. and Benson, C., 2000, “Effect of Wet-Dry Cycling on Swelling and Hydraulic Conductivity of GCLs,” *J. Geotech. Geoenviron. Eng.*, Vol. 126(1), pp. 40–49.

Mazzieri, F., 2011, “Impact of desiccation and cation exchange on the hydraulic conductivity of factory-prehydrated GCLs,” *Geo-Frontiers*, pp. 976-985.

Meer, S., and Benson, C., 2007, "Hydraulic conductivity of geosynthetic clay liners exhumed from landfill final covers," *Journal of Geotech. and Geoenviron. Engineering*, Vol.133(5), pp.550-563.

Melchior, S., 1997, "In situ studies on the performance of landfill caps," *Proc., Int. Containment Technology Conf.*, Florida State University, Tallahassee, Florida, pp. 365-373.

Melchior, S., 2002, "Field studies and excavations of geosynthetic clay barriers in landfill covers," *Proc., Int. Geosynthetic Clay Barriers Symp.*, H. Zanzinger, R. M. Koerner, and E. Gartung, Eds., Swets and Zeitlinger, Lisse, Netherlands, pp.321-330.

Miller, C., Mi, H., and Yesiller, N., 1998, “Experimental analysis of desiccation crack propagation in clay layers,” *Journal Of The American Water Resources Association*, Vol.34(3), pp.677-686.

Morris, P., Graham, J., and Williams, D., 1992, “Cracking in drying soils,” *Canadian Geotechnical Journal*, Vol.29(2), pp.263-277.

Otsu, N., 1979, "A threshold selection method from gray-level histograms," *EEE Transactions on Systems, Man, and Cybernetics*, Vol. SMC-9(1), pp. 62-66.

Prat, P., and Lakshmikantha, M., 2006, “Size effect in the cracking of drying soil,” *Proceedings of the 16th European Conference of Fracture, Alexandroupolis, Greece,* pp. 1373-1374.

Pratt, W., 2001, *Digital Image Processing*, 3rd Ed., Wiley, New York.

Prewitt, J., 1970, “Object enhancement and extraction”, *Picture Processing and Psychopictorics*, B.S. Lipkin and A. Rosenfield, Eds., Academic Press, New York.

Roberts, L., “Machine perception of three dimensional solids”, PhD Dissertation, Massachusetts Institute of Technology, Cambridge, Massachusetts, 1963.

Scalia, J., and Benson, C., 2010, “Effect of Permeant Water on the Hydraulic Conductivity of Exhumed GCLs. *Geotechnical Testing Journal*, 1-11.

Shan, H., and Daniel, D., 1991, "Results of laboratory tests on a geotextile/bentonite liner material," *Geosynthetics '91*, Vol. 1, Atlanta, USA, pp.517-535.

Sklansky, J., 1978, "On the hough technique for curve detection," *IEEE Transactions on Computers*, Vol. 27(10), pp.923-926.

Tang, C., Cui, Y., Shi, B., Tang, A., and Liu, C., 2011, “desiccation and cracking behaviour of clay layer from slurry state under wetting-drying cycles,” *Geoderma*, Vol.166(1), pp.111-118.

Tang, C., Shi, B., Liu, C., Zhao, L., and Wang, B., 2008, “Influencing factors of geometrical structure of surface shrinkage cracks in clayey soils,” *Engineering Geology*, Vol.101(3-4), pp.204-217.

Trabelsi, H., Jamei, M., Zenzri, H., and Olivella, S., 2012, “Crack patterns in clayey soils: Experiments and modeling,” *International Journal For Numerical And Analytical Methods In Geomechanics*, Vol.36(11), pp.1410-1433.

Velde, B., 1999, “Structure of surface cracks in soil and muds,” *Geoderma*, Vol.93(1-2), pp.101-124.

Vogel, H., Hoffman, H., and Roth, K., 2005, “Studies of crack dynamics in clay soil I. Experimental methods, results, and morphological quantification,” *Geoderma*, Vol.125(3-4), pp.203-211.

2.9 TABLES

Table 2.1. Mineralogy, cation exchange capacity, swell index, mass per unit area, water content, loss on ignition, and bound cations in the exchange complex of fresh bentonite from the GCL used in this study.

	Properties	Na-B GCL	Determination Method
Index Properties	Swell Index (mL/2 g)	29.5	ASTM D5890
	Mass per Unit Area (kg/m^2)	5.7	
	Water Content (%)	4.7	ASTM D2216
	Loss on Ignition (%)	2.06	Scalia 2012
	Liquid Limit (%)	481	ASTM D4318
	Plastic Limit (%)	451	
Mineralogy	Montmorillonite (%)	84	X-Ray Diffraction
	Quartz(%)	9	
	Plagioclase(%)	3	
	Clinoptilolite (%)	2	
	Illite, Mica, Orthoclase (%)	1	
	Average calcite by mass (%)	1.03	ASTM D4373
Bound Cations (cmol+/kg)	Na	30.5	ASTM D7503
	Ca	28.8	
	Mg	8.4	
	K	2.2	
	CEC (cmol$^+$/kg)	81.0	

2.10 FIGURES

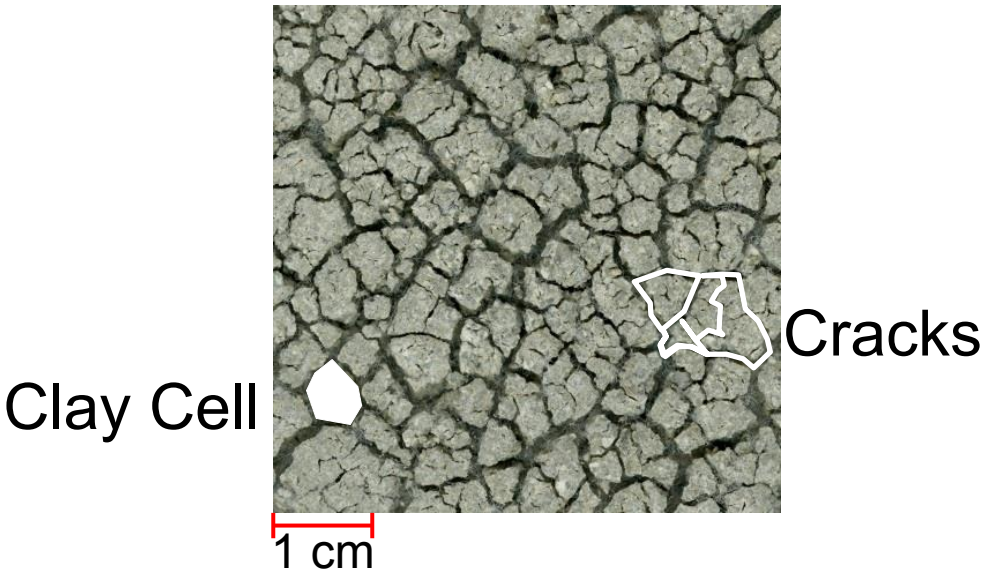

Fig. 2.1. A representative clay cracking pattern that is separated into clay cells and cracks. A clay cell is defined as a gray region bounded by dark cracks on all sides.

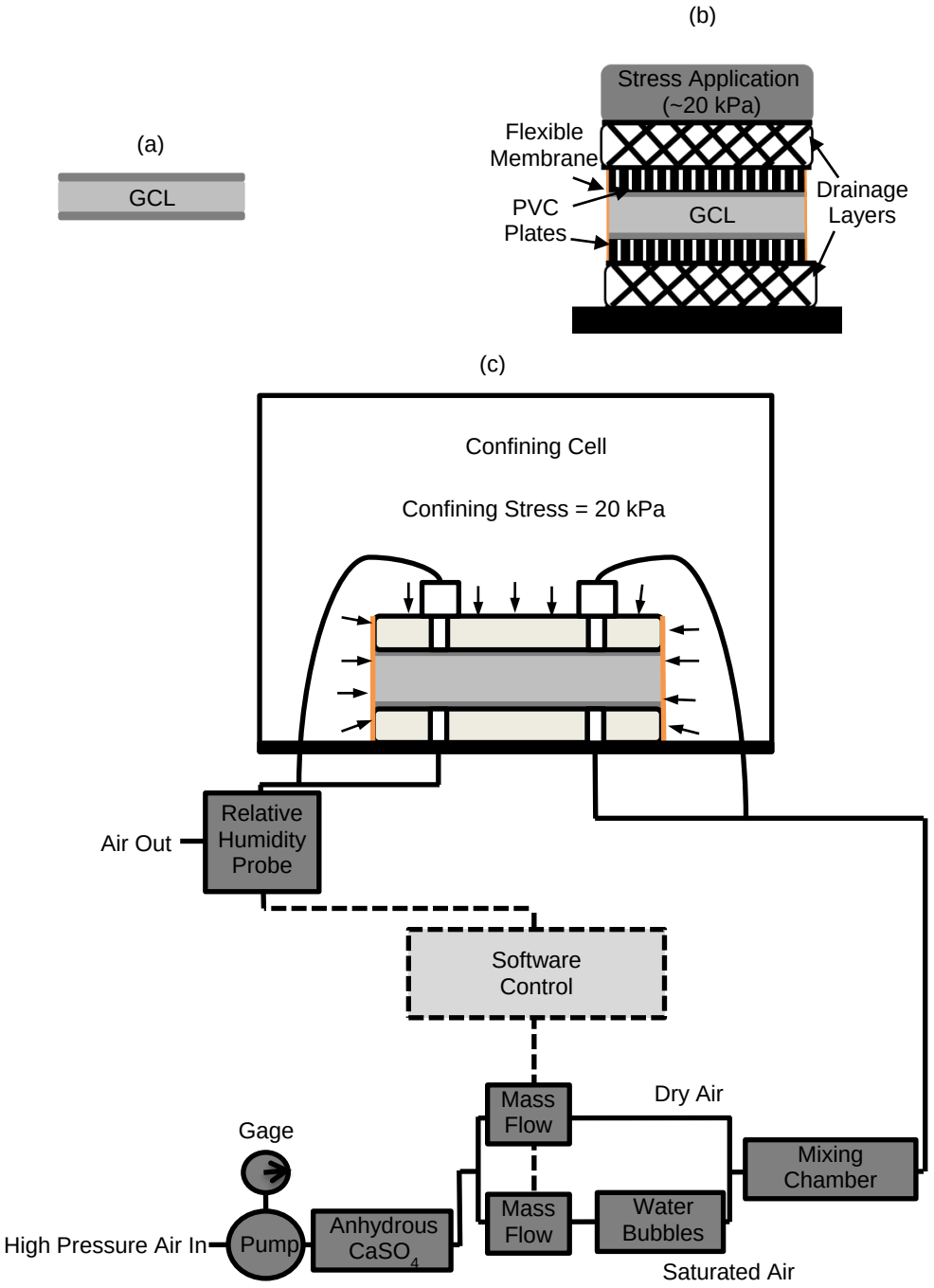

Fig. 2.2. Schematic drawings of the experimental GCL desiccation systems (a) unconfined desiccation (b) perforated plate desiccation employs rigid perforated PVC plates placed above and below the GCL to limit physical disturbance (c) in-permeameter drying eliminates both stress changes and the potential for physical disturbance.

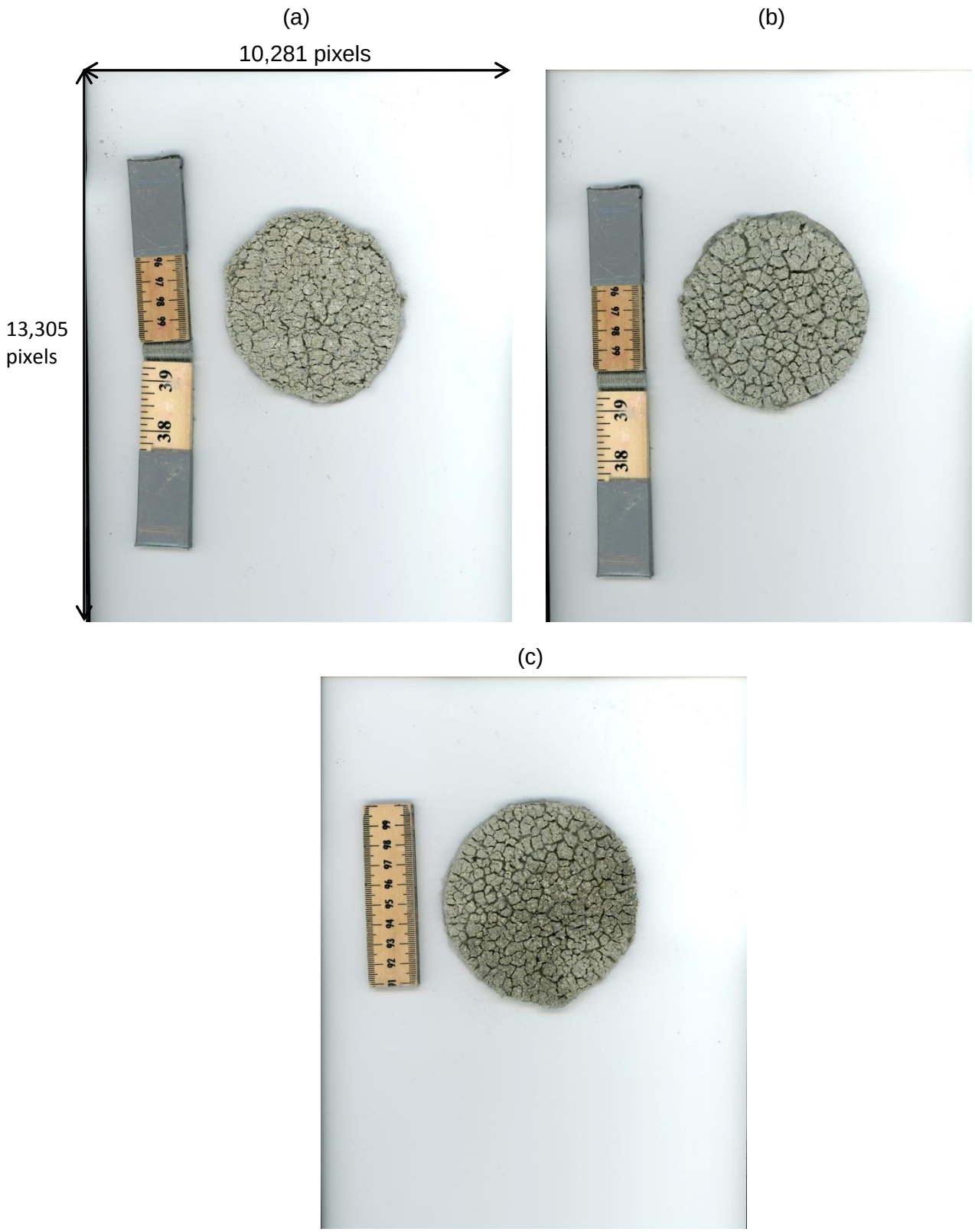

Fig. 2.3 Original full-color GCL images after desiccation (a) unconfined desiccation; (b) perforated plate desiccation; (c) in-permeameter desiccation.

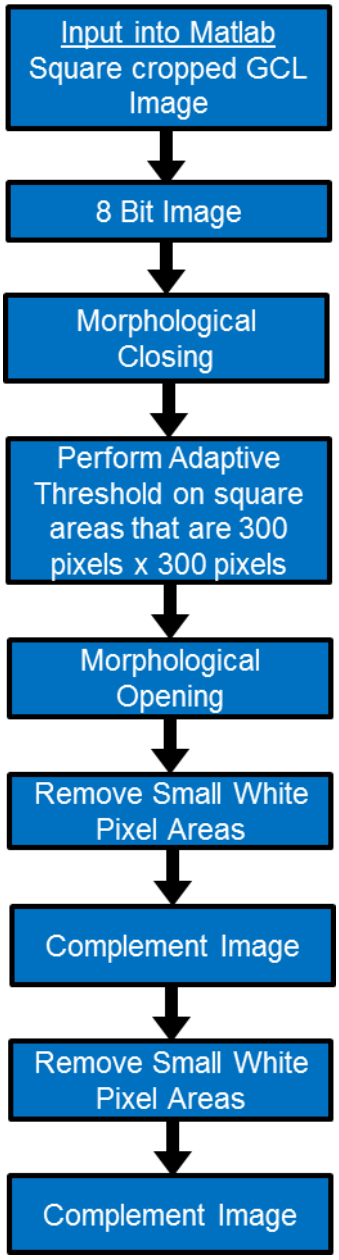

Fig. 2.4. Flowchart of image processing.

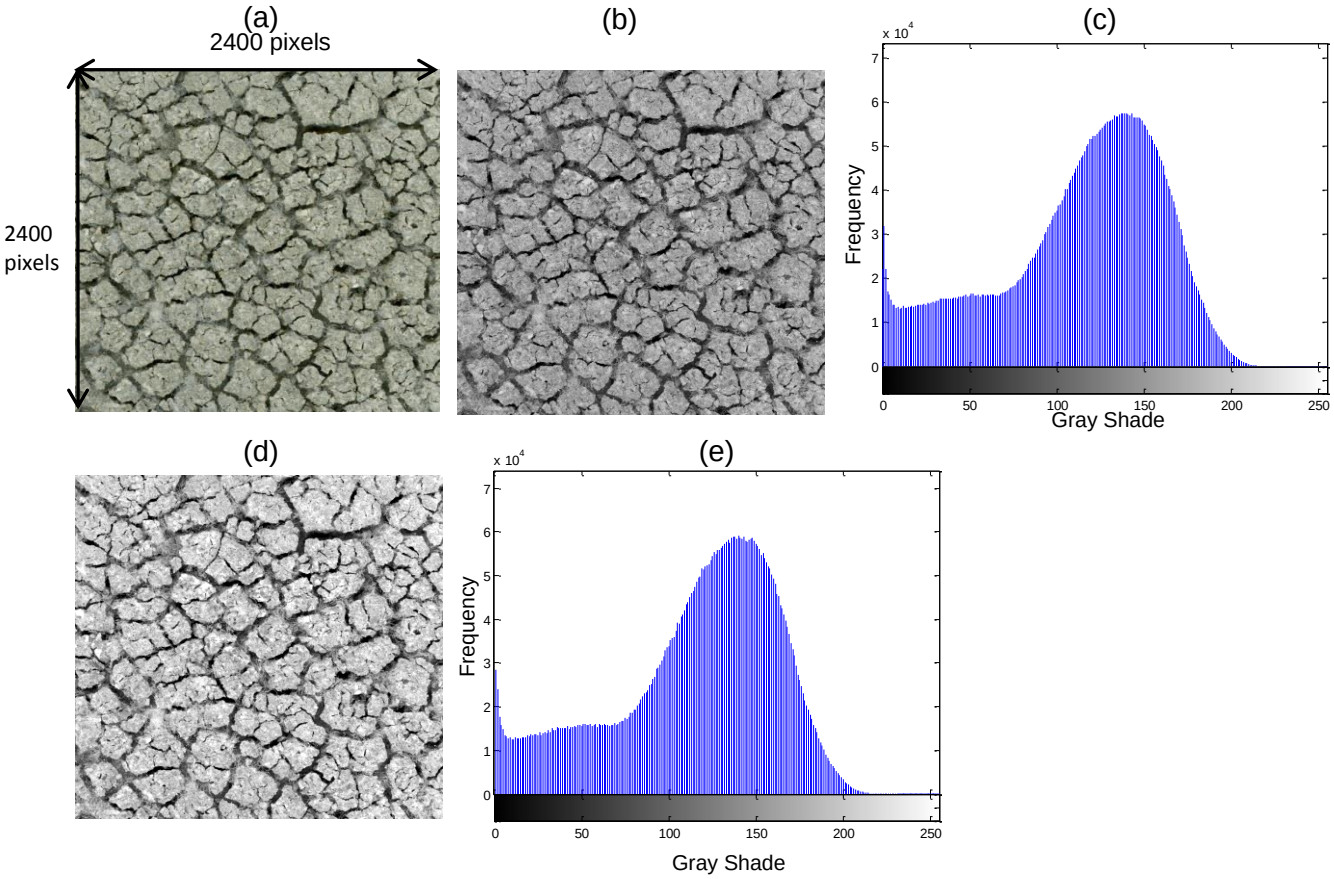

Fig. 2.5 Progression of specimen photo through grayscale processing (a) input into Matlab; (b) grayscale image; (c) grayscale histogram of (b); (d) image after morphological closing; (e) grayscale histogram of (d).

(a) (b)

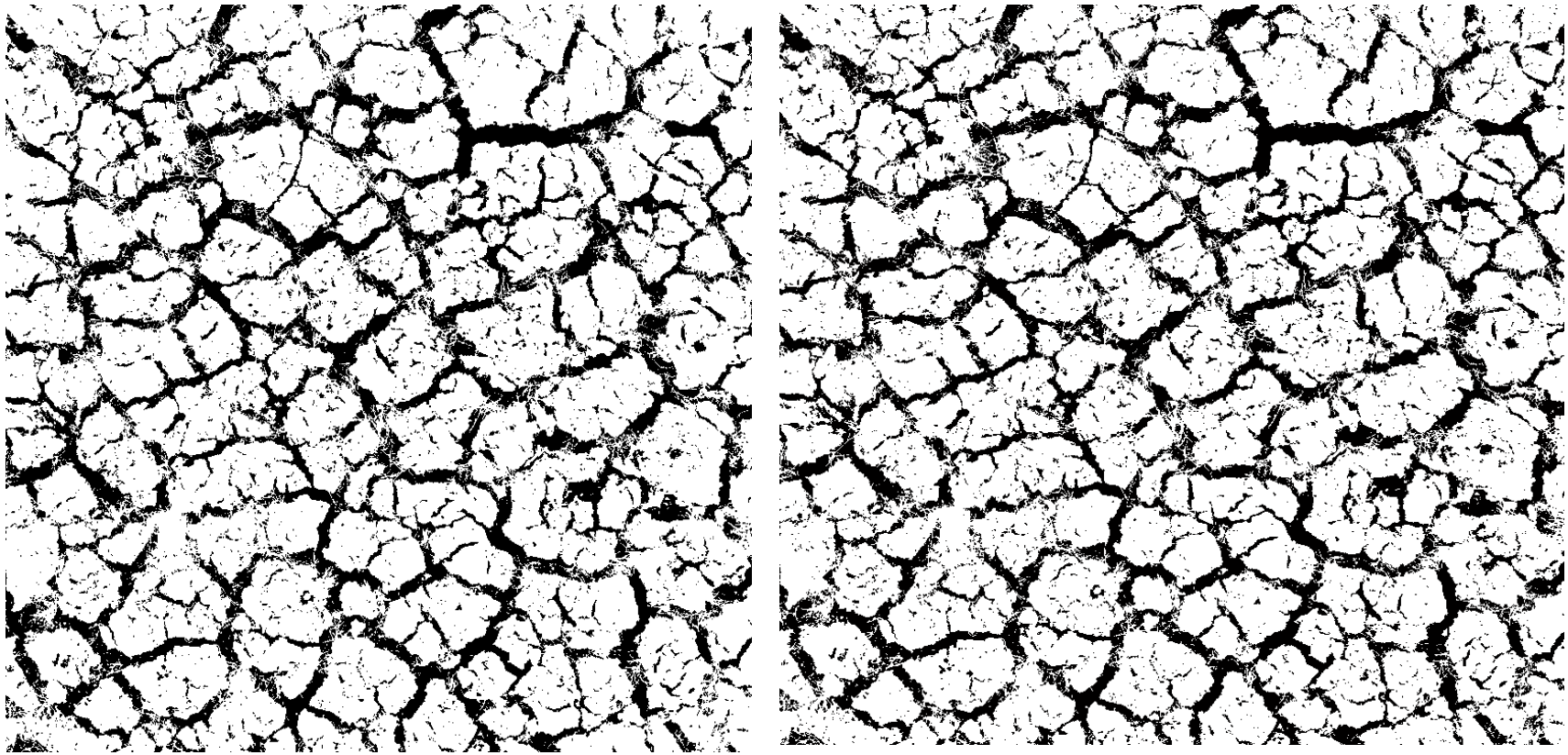

Fig. 2.6 Comparison of thresholding techniques (a) Otsu's Global Thresholding Method; (b) adaptive mean threshold, ultimately chosen.

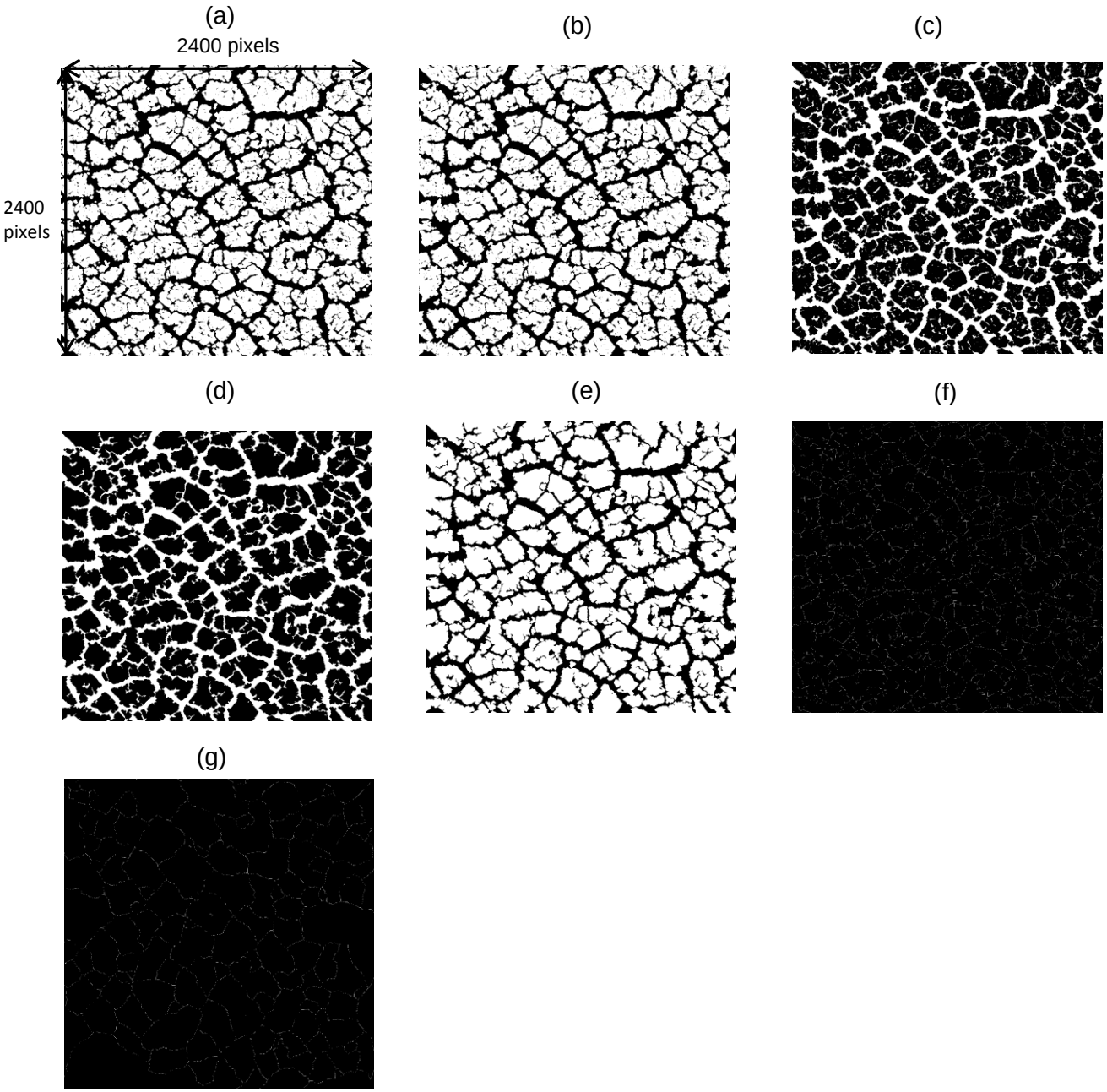

Fig. 2.7. Progression of specimen photo through processing (a) image after morphological opening; (b) white areas under 1000 pixels removed; (c) image complement; (d) white areas under 1000 pixels removed; (e) image complement; (f) image after morphological thinning; (g) pruned image.

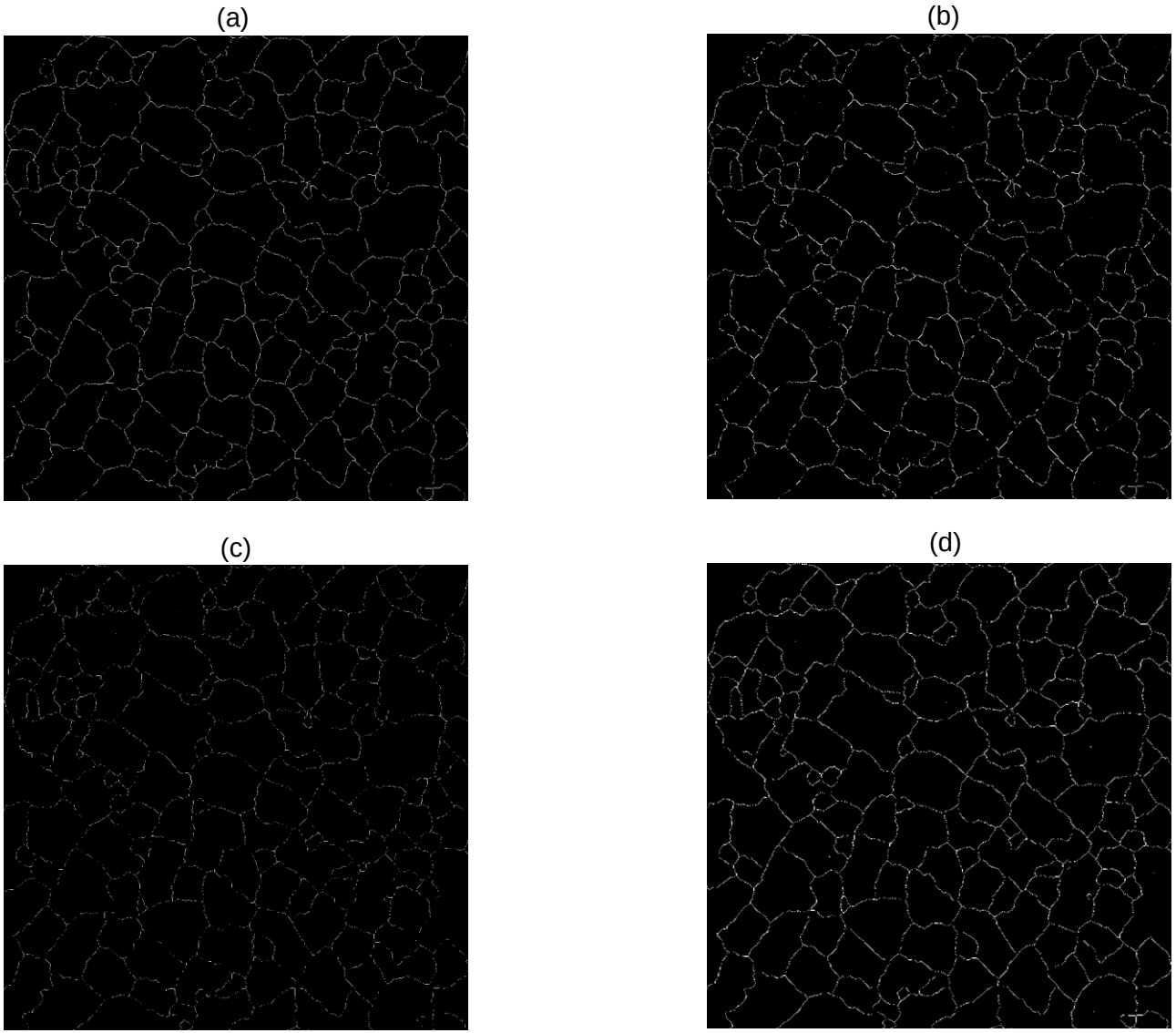

Fig. 2.8 Comparison of edge detection operators (a) Sobel; (b) Prewitt; (c) Roberts, ultimately chosen; (d) Canny.

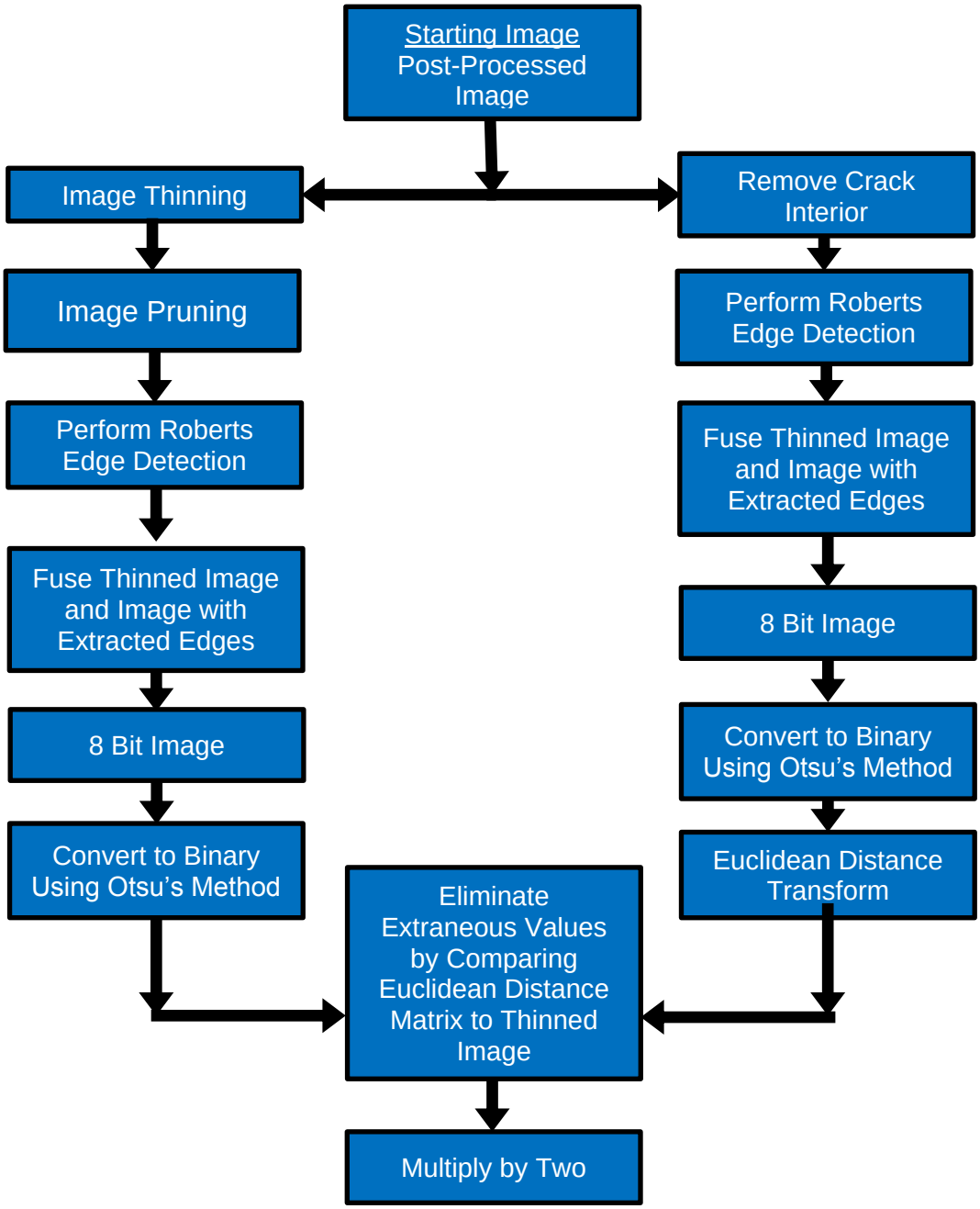

Fig. 2.9 Flowchart of the technique to determine crack thickness.

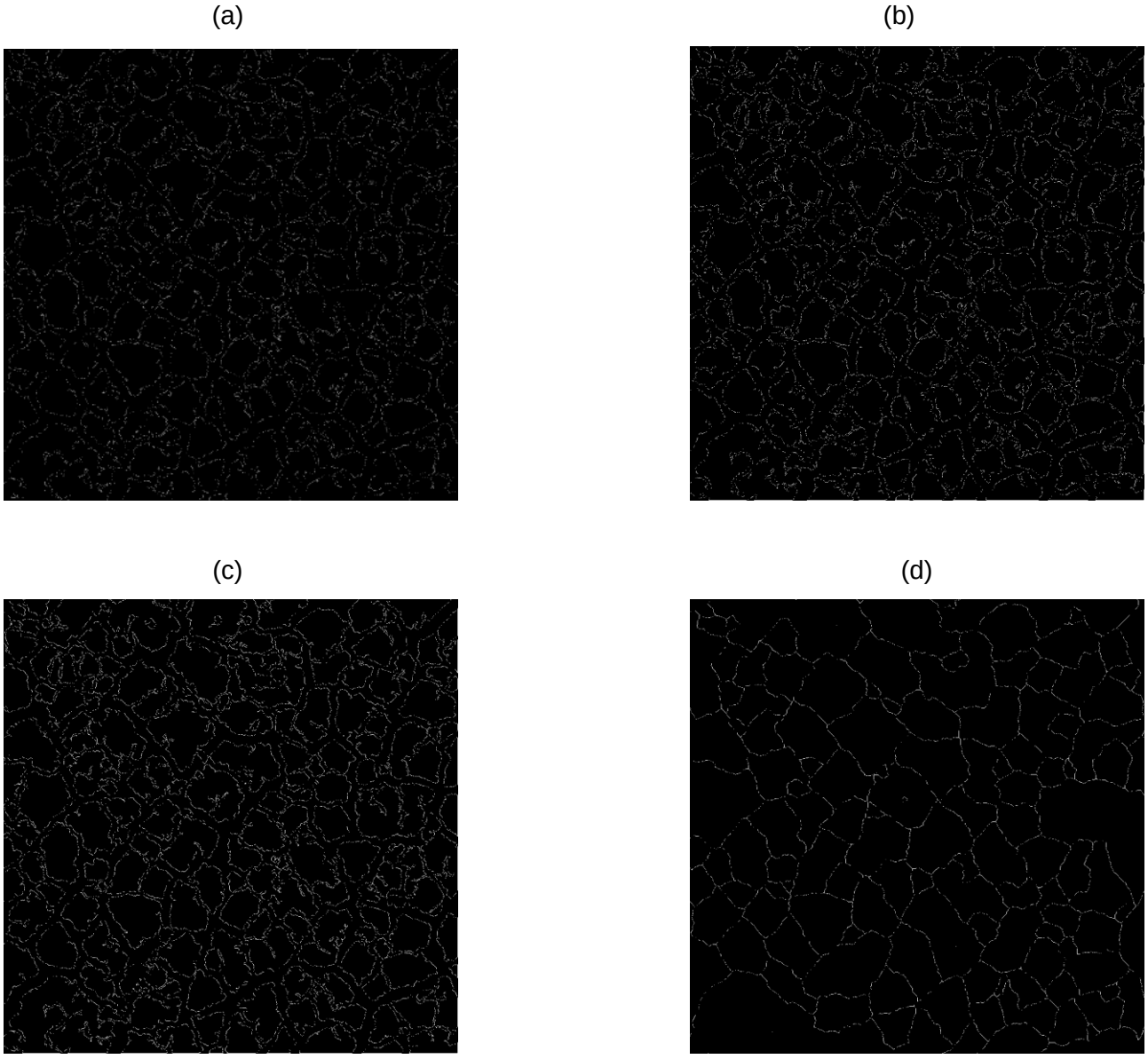

Fig. 2.10 Input into crack thickness determination (a) interior pixels from Fig. 2.8e are removed; (b) Roberts edge extraction of (a); (c) resultant fused image of (a) and (b), image used for Euclidean distance transform (d) skeletonized cracks used to eliminate extraneous values from Euclidean distance transform matrix.

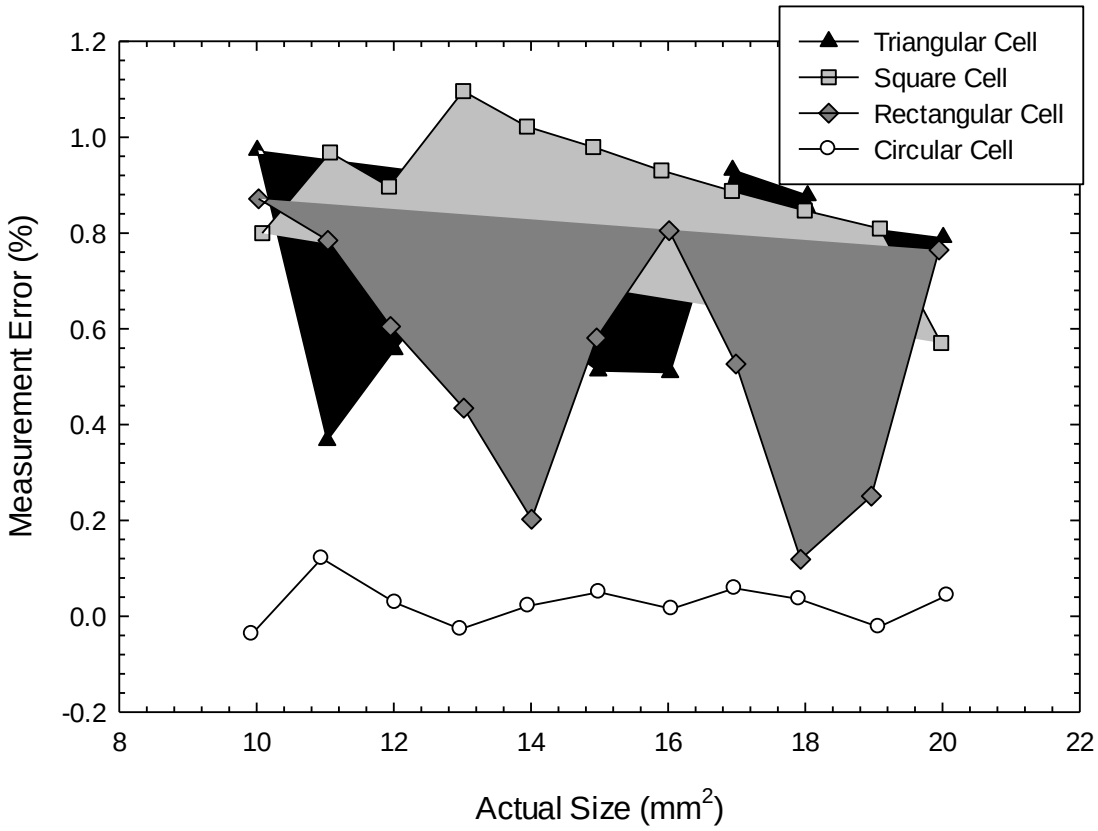

Fig. 2.11 Verification study of cell area determination technique. The error for all shapes and sizes were consistently below 2%. The image processing procedure does not affect the measured cell area.

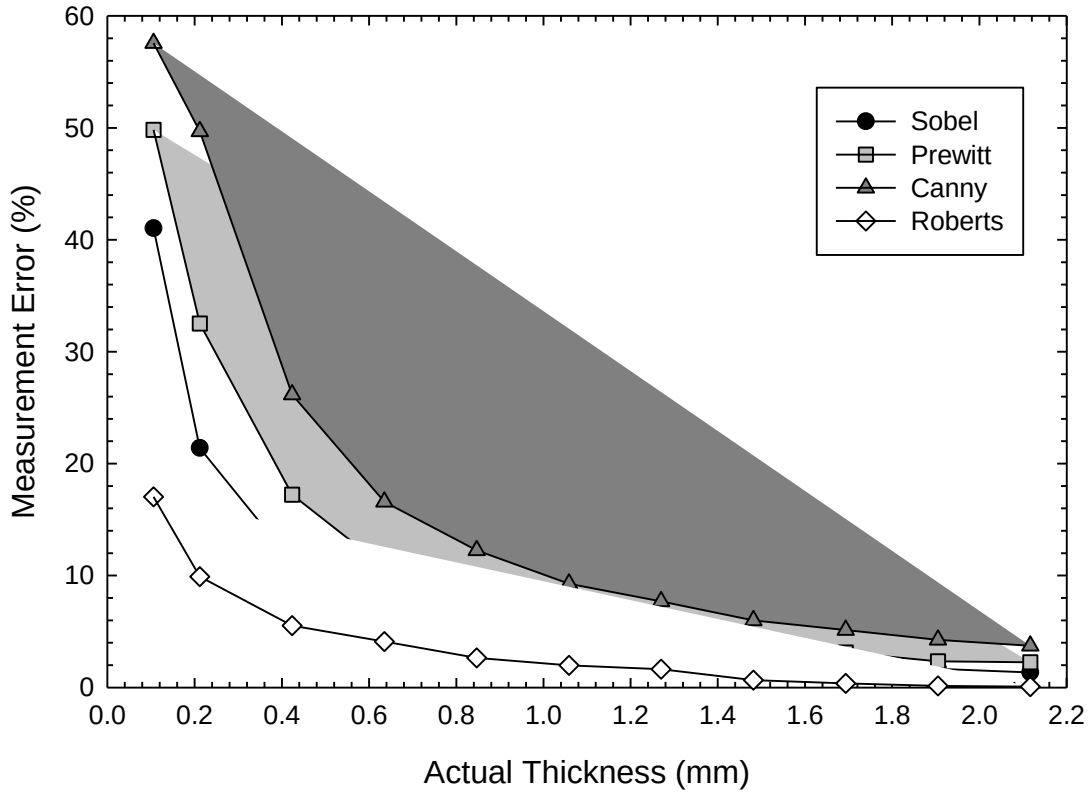

Fig. 2.12 How the Sobel, Prewitt, Canny, and Roberts (chosen) edge detection techniques affect the measured width in Matlab. Regardless of the edge detection technique, Matlab will underestimate the line width. However, the underestimation is larger when determining small (i.e. greater than 0.6 mm) line widths. This is likely because the comparison crack skeleton image used to eliminate extraneous numbers from the distance matrix is greater than one pixel thick. The Roberts morphological operator resulted in the smallest error for all line thicknesses; therefore, the Roberts Operator was chosen for edge extraction.

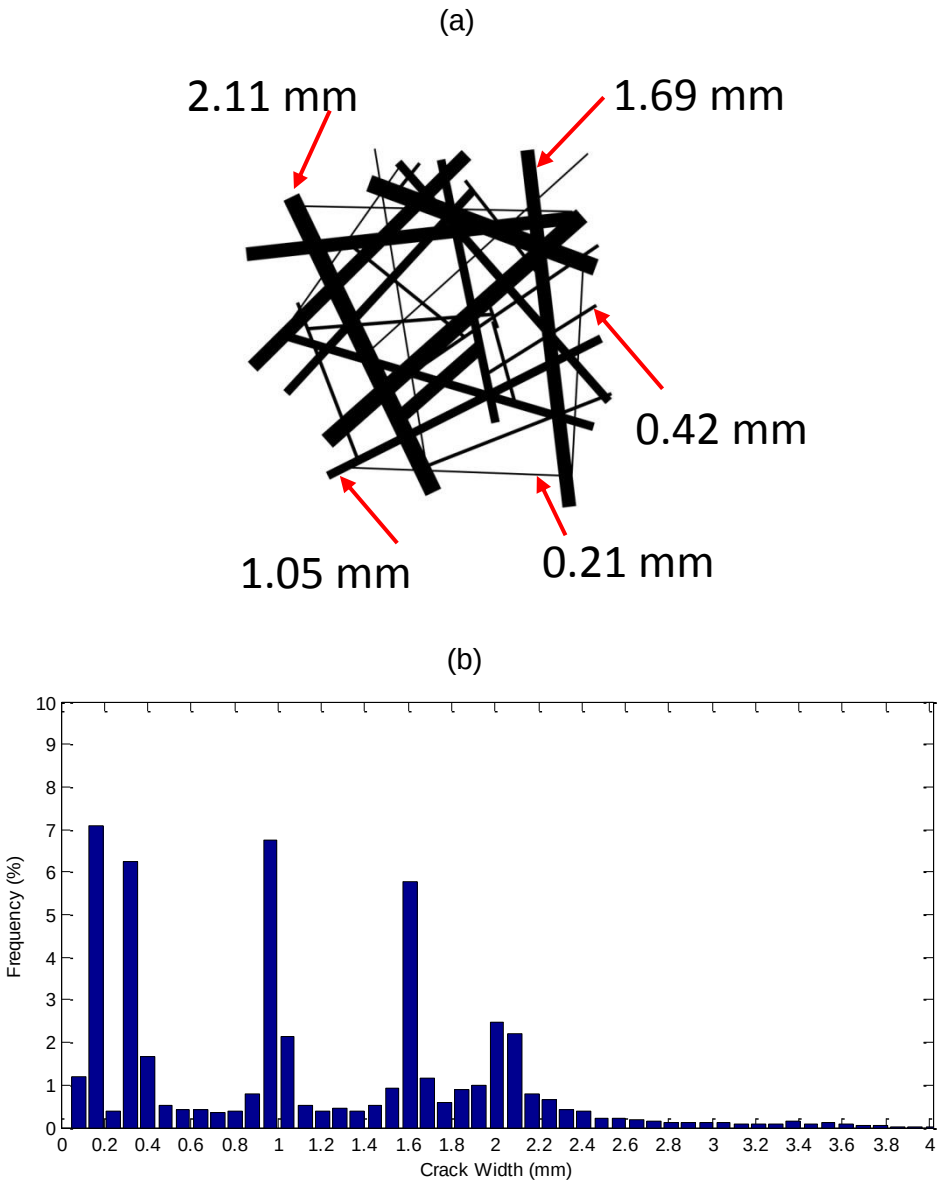

Fig. 2.13 Verification study of crack thickness determination technique (a) photo imported to Matlab line thickness determination; (b) crack width frequency histogram. Although Matlab underestimates the line thickness, peaks correspond to the approximate true line thickness. Note that the average thickness as measured by Matlab was 1.16 mm.

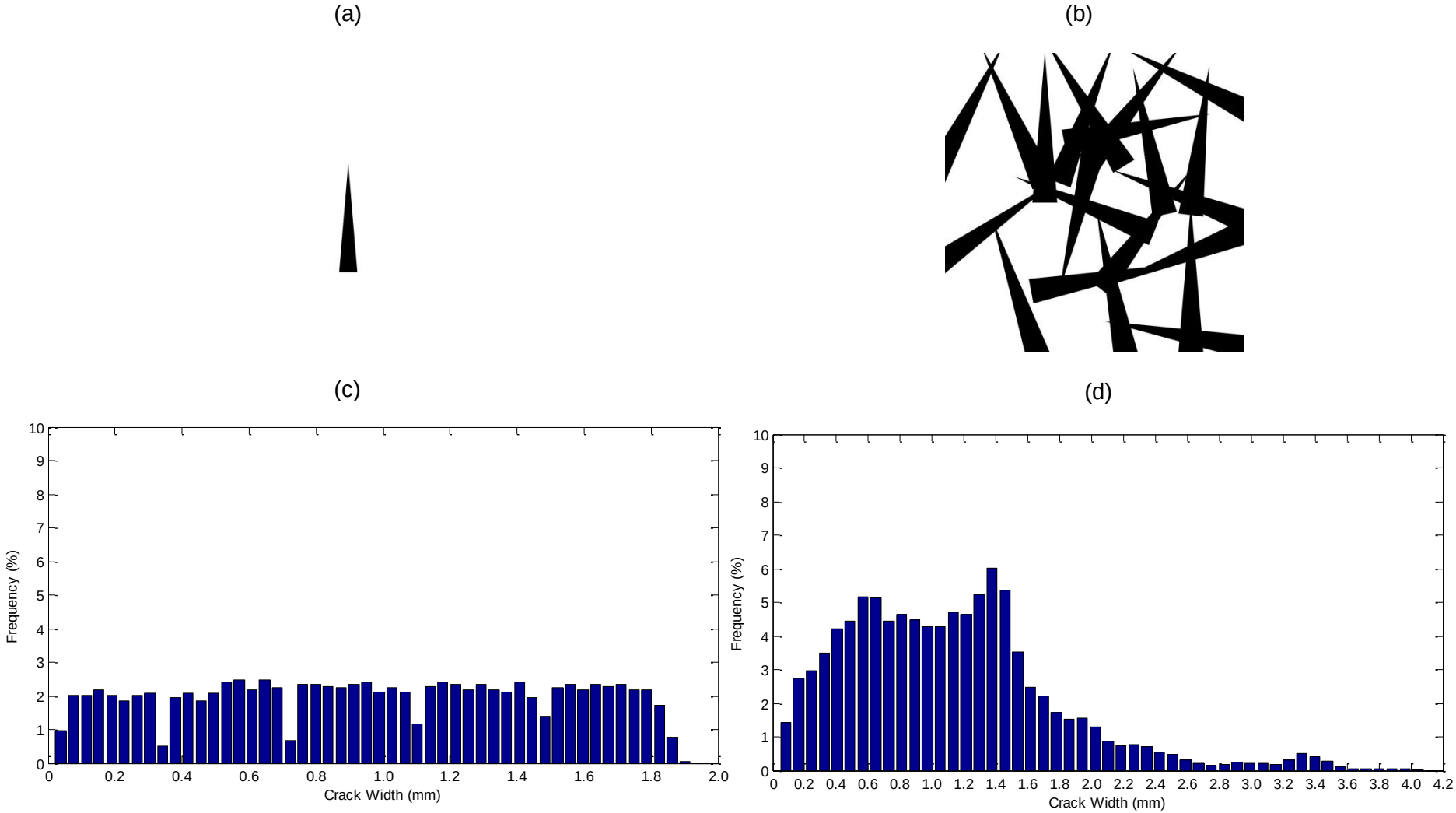

Fig. 2.14 Study to determine the effect of crack heterogeneity on measured crack thickness. The base of all triangles was 2.11 mm (a) single triangle photo submitted to Matlab to determine thickness; (b) multiple triangle photo submitted to Matlab to determine thickness; (c) crack width frequency histogram for single triangle. Average thickness as measured by Matlab was 1.02 mm. (d) crack width frequency histogram for multiple triangles. Average thickness as measured by Matlab was 1.14 mm.

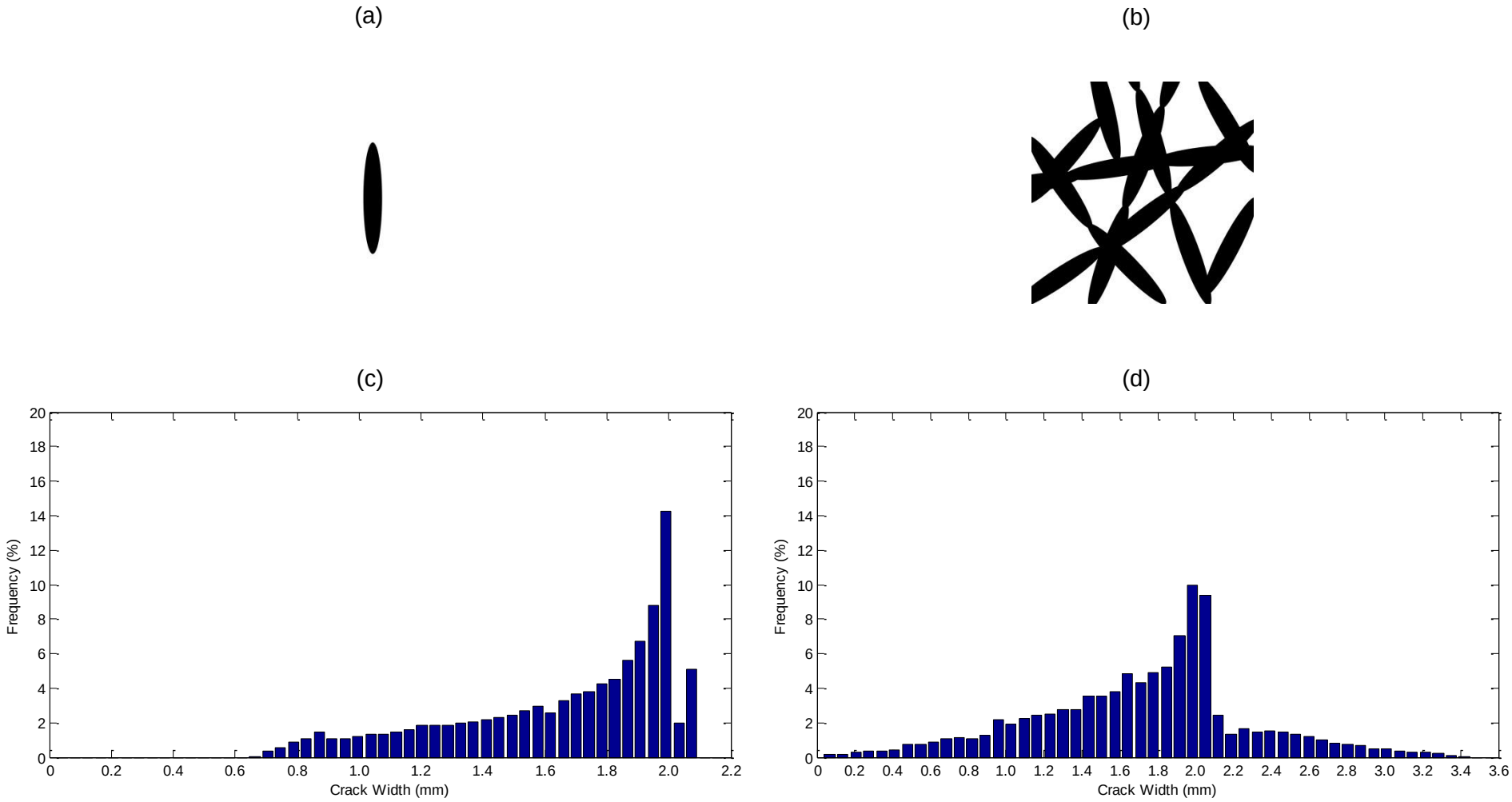

Fig. 2.15 Study to determine the effect of crack heterogeneity on measured crack thickness. The widest portion of all ellipses was 2.11 mm. (a) single ellipse photo submitted to Matlab to determine thickness; (b) multiple ellipse photo submitted to Matlab to determine thickness; (c) crack width frequency histogram for single ellipse. Average thickness as measured by Matlab was 1.92 mm. (d) crack width frequency histogram for multiple ellipses. Average thickness as measured by Matlab was 1.80 mm.

Appendix A

EFFECT OF WET-DRY CYCLING ON GEOSYNTHETIC CLAY LINERS WITH POLYMER-MODIFIED BENTONITE

A.1 INTRODUCTION

Polymer modifications of bentonite focus on activating and maintaining osmotic swell such that low hydraulic conductivity would be maintained under adverse conditions such as high ionic strength and extreme pH (Onikata et al. 1996; Trauger and Darlington 2000; Katsumi et al. 2001; Ashmawy et al. 2002; Kolstad et al. 2004; Katsumi et al. 2008; Mazzieri 2011; Scalia 2012, Scalia et al. 2014). Trauger and Darlington (2000) developed and tested BPA, a bentonite-superabsorbent-polymer composite formed by amending bentonite by in-situ polymerization of an organic monomer within Na-bentonite slurry. Trauger and Darlington (2000) did not provide the formulation of BPA, nor the specific superabsorbent polymer used. The hydraulic conductivity of the BPA GCL to seawater was 4,000-times lower than a Na-bentonite GCL (5×10^{-12} m/s versus 2×10^{-8} m/s). The addition of superabsorbent polymer was hypothesized by Trauger and Darlington (2000) to improve contaminant resistance by structural reinforcement of the interlayer by intercalated polymer, to lock native Na^+ ions satisfying the cation exchange capacity by polyelectrolyte adsorption, and to supplement swell via the absorption of water by superabsorbent polymer.

Scalia et al. (2014) tested the second generation BPA material, termed bentonite polymer composite (BPC). Na-bentonite was modified by intercalation and in-situ polymerization of acrylic acid to form Na-polyacrylate within and outside the montmorillonite interlayer. The material maintained a low (i.e. less than 9×10^{-11} m/s) hydraulic conductivity when permeated with aggressive solutions. However, the swell of BPC decreased with increased solution

concentration, and exhibited swells typical of Ca-bentonite in aggressive solutions. Thus, the mechanism underlying the low hydraulic conductivity of BPC in aggressive solutions was decoupled from swell. Scalia (2012) completed further studies to investigate the mechanisms behind the decoupled hydraulic conductivity and swell behavior. Low BPC hydraulic conductivity was ultimately attributed to several mechanisms. Intercalated polymer in the montmorillonite layer activated osmotic swelling. Hydraulically active porosity was clogged by precipitated carbonate minerals, in situ polymerized polyacrylate chains, and mobile low molecular weight polyacrylate. Absorbed polymer prevented the exchange of native Na^+ cations. In addition, the addition of BPC to Na-bentonite in portions as low as 1% (by-mass) resulted in a lower equilibrium hydraulic conductivity than pure BPC.

Wet-dry cycling studies have been performed to determine the hydraulic compatibility of polymer-modified bentonites in cover systems, albeit not with the BPC material. Mazzieri (2011) performed wet-dry cycling testing on a dense-prehydrated (DPH) GCL using deionized water (DW) and a 0.0125 M $CaCl_2$ solution. DPH-GCLs are polymer-modified GCLs produced through the uniform prehydration of a dilute aqueous solution containing Na-carboxylmethyl cellulose and methanol to a water content of approximately 43%, then densification by calendaring (first described in Kolstad et al. 2004). Hydration was performed in an oedometer cell at vertical stress of 12.5 kPa. Severe desiccation was achieved in a thermostatic chamber at a constant temperature of 35 °C, RH ranging between 20% and 40%, and under a vertical stress of 6 kPa. The drying phase was considered complete when mass loss of the GCL ceased. The water content, after dehydration, w_{dry}, was estimated gravimetrically by assuming that the initial solid mass (soils, adsorbed polymers and geotextiles) had remained constant. After rehydration, the specimens were transferred to a permeameter for hydraulic conductivity testing. An average effective stress of 12.5 kPa was applied during permeation. The impact of wet-dry cycles on k was found to be limited when DW was used as hydrating liquid. Conversely, the k permanently

increased to 5.5 x 10^{-7} m/s after the third cycle of severe desiccation using the $CaCl_2$ solution. Mazzieri (2011) concluded that the additives to a DPH-GCL were removed as a result of desiccation-permeation cycling.

Experiments conducted in this study have been designed to examine the effect of GCL wet-dry cycling on polymer-modified GCLs. Results were compared between three GCLs with varying degrees of polymer modification and included a Na-bentonite GCL (control), a GCL dry-blended with a proprietary polymer for added chemical resistance, and a GCL that contains a Na-bentonite and BPC blend. Specimens were initially permeated for one month using DW (control) or pore waters representing landfill cover soils. GCLs were then exposed to perforated plate desiccation, where the GCL was subject to ambient air-drying under a vertical total stress simulating ~1 m of overlying cover soil. The cycle was repeated up to ten times to represent ten years of time. The hydraulic conductivity, swell index, cation exchange capacity, water content, and polymer content (as determined by loss on ignition) were compared as a function of wet-dry cycles.

A.2 MATERIALS

A.2.1 GCLs

Three GCLs with varying degrees of polymer modification were used in this study. All GCLs were manufactured by the Colloid Environmental Technologies Company (CETCO, Hoffman Estates, Illinois, USA) and consisted of a silt-woven geotextile and a non-woven staple filter geotextile encasing the bentonite material. The GCLs were held together through needle punching fibers. The initial thickness for all GCLs ranged from between 5 to 7 mm. The material properties for each GCL are described below. The mineralogy and physical characteristics for all bentonites are presented in Table A.1.

A.2.1.1 Na-Bentonite GCL

The GCL containing conventional Na-bentonite (termed CS-GCL) is sold under the name Bentomat ST, had a mass per unit area of 5.7 kg/m^2, and the initial bentonite water content was 4.7%. The swell index of CS-GCL to DW was 26.0 mL/2 g (per ASTM D5890) and the cation exchange capacity was determined to be 81.0 cmol+/kg (per ASTM D7503). The liquid limit was determined to be 481% and the plasticity index was determined to be 451% (per ASTM D4318). X-ray diffraction indicated that the bentonite contains 84% montmorillonite, 9% quartz, 3% plagioclase, and ≤ 2% of clinoptilolite, illite, mica, orthoclase, and calcite.

A.2.1.2 Na-Bentonite and Polymer Dry Blend

The GCL containing Na-bentonite and polymer dry blend (termed CR-GCL) is sold under the name Resistex ST, had a mass per unit area of 6.5 kg/m^2, and the initial bentonite water content was 5.3%. The swell index of CR-GCL to DW was 27.0 mL/2 g and the cation exchange capacity was determined to be 78.2 cmol+/kg. The liquid limit was determined to be 478% and the plasticity index was determined to be 450%. X-ray diffraction showed that the bentonite contained 86% montmorillonite, 8% quartz, 3% plagioclase, 1% clinoptilolite, 1% illite and mica, 1% orthoclase, and trace amounts of kaolinite.

A.2.1.3 BPC and Na-Bentonite Blend

The GCL containing a blend of BPC and Na-bentonite (termed CT-GCL) is sold under the name Continuum ST, has a mass per unit area of 6.1 kg/m^2, and the initial water content was determined to be 7.2%. The liquid limit was determined to be 554% and the plasticity index was 526%. X-ray diffraction showed that the bentonite contained 78% montmorillonite, 8% quartz, 5% plagioclase, 1% clinoptilolite, 7% illite and mica and trace amounts of orthoclase and kaolinite. The swell index of CT-GCL to DW was determined to be 85.5 mL/2g. The average cation exchange capacity of the CT-GCL was 142.7 cmol$^+$/kg after 6 replicate tests.

A.2.2 Permeant Liquids

Scalia and Benson (2010) collected soil cover layers from various landfills around the country, performed column elution tests (via Benson and Meer 2009) to collect soil pore water, analyzed the resultant eluate, and compiled this data in addition to data from similar studies (Meer and Benson 2007; Bradshaw 2008) (Fig. A.1). Based on this data, three permeant solutions were chosen: (i) DW, used as the control, (ii) a synthetic dilute water solution representing an average pore water chemistry, termed Average Water (AW), and (iii) a predominantly divalent synthetic solution considered to yield a conservative estimate of GCL hydraulic conductivity for MSW landfill cover applications, termed Conservative Water (CW). Refer to Table A.2 for chemical properties of the permeant solutions.

A.3 METHODS

GCL specimens were subjected to several wet-dry cycles, which consisted of permeation followed by desiccation. GCLs were disassembled after one, three, and five wet-dry cycles for solids analysis.

A.3.1 Permeation

GCL specimens were tested for k in flexible-wall permeameters according to ASTM D 5084 Method B (falling headwater-constant tail water) to simulate a wet spring scenario for a near-surface GCL application (e.g., landfill cover). In-cell hydration with the permeant solution of interest was conducted for 48 hours prior to flow. After the permeameter was assembled and connected to the falling headwater apparatus, cell pressure was applied and all tubing was saturated with the permeant liquid. The inflow line of the permeameter was left open to allow the specimen to hydrate while the effluent line remained closed. An average hydraulic gradient of 30 was chosen to simulate conditions experienced by GCLs in typical landfill cover applications (Lin and Benson 2000). The effective stress, 20 kPa, was chosen to simulate approximately one meter of cover soil. Hydraulic conductivity tests were continued until at least the following

criteria were met: no systematic trend in k over time, (per ASTM D5084); at least four consecutive k readings within ± 25% of the mean (per ASTM D5084); at least four consecutive outflow-to-inflow ratios within 1.0 ± 0.25 (per ASTM D 5084); and the tests were permeated for four weeks.

A.3.2 Desiccation

After hydration and permeation, the GCL was removed from the permeameter for desiccation (Fig. A.2). Rigid perforated PVC plates were placed above and below the GCL to limit disturbance due to physical movement of the GCL. Specimens were desiccated in a controlled RH environment (RH = 70%) under an applied vertical stress of 20 kPa, simulating approximately one meter of overlying cover soil. The RH of a small room was controlled using a residential room humidifier system (Honeywell model HCM-6009, Palatine, Illinois, USA) and monitored using a humidity probe. If the RH deviated from the target of 70% RH by 5%, the humidifier controls were manually adjusted. In general, the RH was maintained at 73.7% +/- 4.3% with a maximum RH of 86.5% and a minimum RH of 57.4% using this approach. Specimens were periodically weighed and desiccation was considered complete when the specimen mass ceased changing.

A.3.3 Liquid Limit and Plastic Limit

The liquid limit and plastic limit were determined for all GCL materials in accordance with ASTM D4318. Materials were ground to 100% passing a standard No.-40 woven wire sieve (ASTM E11). In addition to baseline tests in DW, AW and CW were used as hydrating solutions. The liquid limits and plastic limits of all materials and all solutions are summarized in Table A.1.

A.3.4 Swell Index

Swell index (SI) tests were performed on the CS-GCL, CR-GCL, and CT-GCL in accordance with ASTM D5890. Materials were ground to 100% passing a standard No.-200 woven wire

sieve (ASTM E11) with a mortar and pestle. In addition to baseline tests in DW, AW and CW were used as hydrating solutions. Swell indices are summarized in Table A.1. Swell index using DW was performed on GCL materials that have experienced one, three, and five wet-dry cycles.

A.3.5 Polymer Content

Polymer content via loss on ignition was conducted as described by Scalia et al. (2014) for the CS-GCL, CR-GCL, and CT-GCL prior to hydraulic conductivity testing. The material was ground to pass a No. 20 woven wire sieve (ASTM E11) and was oven dried at 105°C for 12 to 16 hr. Oven-dried material was placed in a pre-ignited crucible and the mass was recorded. The crucible was then placed in a 550°C furnace for 4 h to ignite volatile substances. After 4 h, the crucible was removed from the furnace and allowed to cool in a water-free atmosphere. The mass of the crucible and material and the mass loss on ignition were then determined. Polymer content was calculated by assuming that base Na-bentonite lost 1.6% mass and that Na-polyacrylate lost 74.7% mass (Scalia et al. 2014). Na-bentonite lost mass due to the removal of strongly bound water from the montmorillonite interlayer (Grim 1968). The results of loss on ignition testing are presented in Table A.1. Bentonite from the CT-GCL was determined to have initially contained 12.0-13.0% polymer by mass. The loss on ignition test was performed on GCL materials that have experienced one, three, and five wet-dry cycles.

A.3.6 Soluble Cations, Bound Cations, and Cation Exchange Capacity

Soluble cations, bound cations, and cation exchange capacity were determined for the CS-GCL, CR-GCL, and CT-GCL prior to and post hydraulic conductivity testing in accordance with ASTM D7503. Chemical analysis of soluble cation and bound cation extracts was conducted by ICP-OES following USEPA Method 6010 B (USEPA 2007). The eluate used to calculate cation exchange capacity was measured via the salicylate method (EPA Method 350.1) using high range (0 – 50 mg/L) $N\text{-}NH_3$ “Test ‘N Tube” vials (Hach Company: Method 10031) with a Spectronic 20 Gensys spectrophotometer (ThermoFisher Scientific, Waltham, Massachusetts).

Calculation methods for soluble cation concentrations, bound cation concentrations, and cation exchange capacity are presented in ASTM D 7503. The soluble cation, bound cation, and cation exchange information is presented in Table A.1. The concentrations of soluble and bound cations in addition to cation exchange capacity was performed on GCL materials that have experienced one, three, and five wet-dry cycles.

A.4 RESULTS

Hydraulic conductivities of GCL specimens subjected to repeated wet-dry cycling consisting of permeation followed by desiccation are shown in Fig. A.3. All hydraulic conductivity values represent the mean hydraulic equilibrium value of several replicates. Hydraulic conductivity testing will continue for the three GCL products until the testing matrix is completed and results will be analyzed by a subsequent researcher.

A.5 REFERENCES

Ashmawy, A., El-Hajji, D, Sotelo, N., and Muhammad, N., 2002, “Hydraulic performance of untreated and polymer-treated bentonite in inorganic landfill leachates,” *Clays and Clay Minerals*, Vol.50(5), pp.546-552.

ASTM D4318, 2010, "Standard Test Methods for Liquid Limit, Plastic Limit, and Plasticity Index of Soils," *Annual Book of ASTM Standards*, ASTM International, West Conshohocken, PA.

ASTM D4373, 2007, “Standard Test Method for Rapid Determination of Carbonate Content of Soils,” *Annual Book of ASTM Standards*, ASTM International, West Conshohocken, PA.

ASTM D5084, 2003, “Standard Test Method for Measurement of Hydraulic Conductivity of Saturated Porous Materials Using a Flexible Wall Permeameter,” *Annual Book of ASTM Standards*, ASTM International, West Conshohocken, PA.

ASTM D5890, 2006, “Standard Test Method for Swell Index of Clay Mineral Component of Geosynthetic Clay Liner,” *Annual Book of ASTM Standards*, ASTM International, West Conshohocken, PA.

ASTM D7503, 2010, “Standard Test Method for Measuring Exchange Complex and Cation Exchange Capacity of Inorganic Fine-Grained Soils”, *Annual Book of ASTM Standards*, ASTM International, West Conshohocken, PA.

ASTM E11, 2013, "Standard Specification for Woven Wire Test Sieve Cloth and Test Sieves," *Annual Book of ASTM Standards*, ASTM International, West Conshohocken, PA.

Benson, C. and Meer, S., 2009, “Relative Abundance of Monovalent and Divalent Cations and the Impact of Desiccation on Geosynthetic Clay Liner,” *J. Geotech. Geoenviron. Eng.*, Vol. 135(3), pp. 349–358.

Benson, C., Thorstad, P., Jo, H., and Rock, S., 2007, "Hydraulic performance of geosynthetic clay liners in a landfill final cover," *Journal of Geotech. and Geoenviron. Engineering*, Vol.133(7), pp.814-827.

Bradshaw, S., 2008, “Effect of Cation Exchange During Subgrade Hydration and Leachate Permeation,” M.S. thesis, University of Wisconsin—Madison, WI, USA.

Buckley, J., Gates, W., and Gibbs, D., 2012, "Forensic examination of field GCL performance in landfill capping and mining containment applications", *Geotextiles and Geomembranes*, Vol.33, pp.7-14.

Egloffstein, T., 2001, “Natural bentonites – Influence of the ion exchange and partial desiccation on permeability and self-healing capacity of bentonites used in GCLs,” *Geotextiles and Geomembranes*, Vol.19(7), pp.427-444.

Egloffstein, T., 2002, “Bentonite as sealing material in geosynthetic clay liners – Influence of the electrolytic concentration, the ion exchange and exchange with simultaneous partial desiccation on permeability,” *Clay Geosynthetic Barriers*, H. Zanzinger,R. M. Koerner, and E. Gartung, (eds.), pp. 141-153.

Grim, R. 1968, *Clay Mineralogy*, 2nd Ed., McGraw-Hall, New York.

Hach Company: Method 10031, 2003, Method 10031: “Salicylate Method, Test `N Tube(TM) Vials, HR, 0 to 50.0 mg/L NH3-N.” Retrieved February 8, 2013 from Web site: https://www.hach.com/fmmimghach?/CODE%3ANITROGENAMM_TNT_HIGH2071%7C1

James, A., Fullerton, D., and Drake, R., 1997, "Field performance of GCL under ion exchange conditions," *Journal of Geotech. and Geoenviron. Engineering*, Vol.123(10), pp.897-901.

Katsumi, T., Ishimori, H., Onikata, M., and Fukagawa, R., 2008, “Long-term barrier performance of modified bentonite materials against sodium and calcium permeant solutions,” *Geotextiles and Geomembranes*, Vol.26(1), pp.14-30

Katsumi, T., Onikata, M., Hasegawa, S., Lin, L., Kondo, M., and Kamon, M., 2001, “Chemical Compatibility of Modified Bentonite Permeated with Inorganic Chemical Solutions.” *Geoenvironmental Impact Management*, Thomas Telford, London, 419-424.

Kolstad, D., Benson, C., and Edil, T., 2004, “Hydraulic Conductivity and Swell of Nonprehydrated GCLs Permeated with Multi- Species Inorganic Solutions,” *J. Geotech. Geoenviron. Eng.*, Vol. 130(12), pp. 1236–1249.

Mansour, R., 2001, "GCL perforance in semi-arid climate conditions," *Proc., Sardinia 2001, 8th Int. Waste Management and Landfill Symp.*, T. Christensen, R. Cossu, and R. Stegmann, eds., CISA, Cagliari, Italy, pp.219-226.

Mazzieri, F., 2011, “Impact of desiccation and cation exchange on the hydraulic conductivity of factory-prehydrated GCLs,” *Geo-Frontiers*, pp. 976-985.

Meer, S., and Benson, C., 2007, "Hydraulic conductivity of geosynthetic clay liners exhumed from landfill final covers," *Journal of Geotech. and Geoenviron. Engineering*, Vol.133(5), pp.550-563.

Melchior, S., 1997, "In situ studies on the performance of landfill caps," *Proc., Int. Containment Technology Conf*., Florida State University, Tallahassee, Florida, pp. 365-373.

Melchior, S., 2002, "Field studies and excavations of geosynthetic clay barriers in landfill covers," *Proc., Int. Geosynthetic Clay Barriers Symp.*, H. Zanzinger, R. M. Koerner, and E. Gartung, Eds., Swets and Zeitlinger, Lisse, Netherlands, pp.321-330.

Onikata, M., Kondo, M., and Kamon, M., 1996, “Development and Characterization of a Multiswellable Bentonite.” *Environmental Geotechnics*. Taylor and Francis, Rotterdam, 587-590.

Scalia, J., 2012, Bentonite-polymer composites for containment applications. PhD Dissertation, University of Wisconsin, Madison, Wisconsin, 2012.

Scalia, J., and Benson, C., 2010, “Effect of Permeant Water on the Hydraulic Conductivity of Exhumed GCLs. *Geotechnical Testing Journal*, 1-11.

Scalia, J., Benson, C., Bohnhoff, G,. Edil, T., and Shackelford, C., 2014, “Long-term hydraulic conductivity of a bentonite-polymer composite permeated with aggressive inorganic solutions,” *Journal of Geotech. and Geoenviron. Engineering*, Vol.140(3), p.04013025(1).

Trauger, R., and Darlington, J., 2000, “Next-generation geosynthetic clay liners for improved durability and performance,” *TR-220*. Colloid Environmental Technologies Company, Arlington Heights, 2-14.

USEPA, 1993, *Method 350.1: Determination of Ammonia Nitrogen by Semi-Automated Colorimetry*. US Environmental Protection Agency, Office of Solid Waste and Emergency Response, Washington, DC.

A.6 TABLES

Table A.1. Mineralogy, cation exchange capacity, swell index, mass per unit area, water content, loss on ignition, and bound cations in the exchange complex of fresh bentonite from the GCLs used in this study.

	Properties	CS-GCL	CR-GCL	CT-GCL	Determination Method
Index Properties	Swell Index (mL/2 g)	29.5	27	85.5	ASTM D5890
	Mass per Unit Area (kg/m^2)	5.7	6.5	6.1	
	Water Content (%)	4.7	5.3	7.2	ASTM D2216
	Loss on Ignition (%)	2.06	2.18	13.7	Scalia 2012
	Liquid Limit (%)	481	478	554	ASTM D4318
	Plastic Limit (%)	451	450	526	
Mineralogy	Montmorillonite (%)	84	86	78	X-Ray Diffraction
	Quartz(%)	9	8	8	
	Plagioclase(%)	3	3	5	
	Clinoptilolite (%)	2	1	1	
	Illite, Mica, Orthoclase (%)	1	2	7	
	Average calcite by mass (%)	1.03	trc	1.02	ASTM D4373
Bound Cations (cmol+/kg)	Na	30.5	38.4	94.5	ASTM D7503
	Ca	28.8	27.7	14.2	
	Mg	8.4	7.4	5.4	
	K	2.2	1.7	1.5	
	Sum	69.9	75.2	115.6	
	CEC ($cmol^+/kg$)	81	78.2	142.7	

Table A.2. Chemical properties of permeant waters used in GCL testing.

Permeant Solution	**Abbreviation**	**[NaCl] (M)**	**[$CaCl_2$] (M)**	**I (M)**	**RMD ($M^{1/2}$)**	**pH**	**Electrical Conductivity (µS/cm)**
Deionized Water	DW	<0.005	<0.005	$<1.3x10^{-7}$	undefined	6.50	18.9
Average Water	AW	0.0008	0.0013	0.002	0.045	6.35	290
Conservative Water	CW	0.0003	0.0019	0.004	0.006	6.24	419

A.7 FIGURES

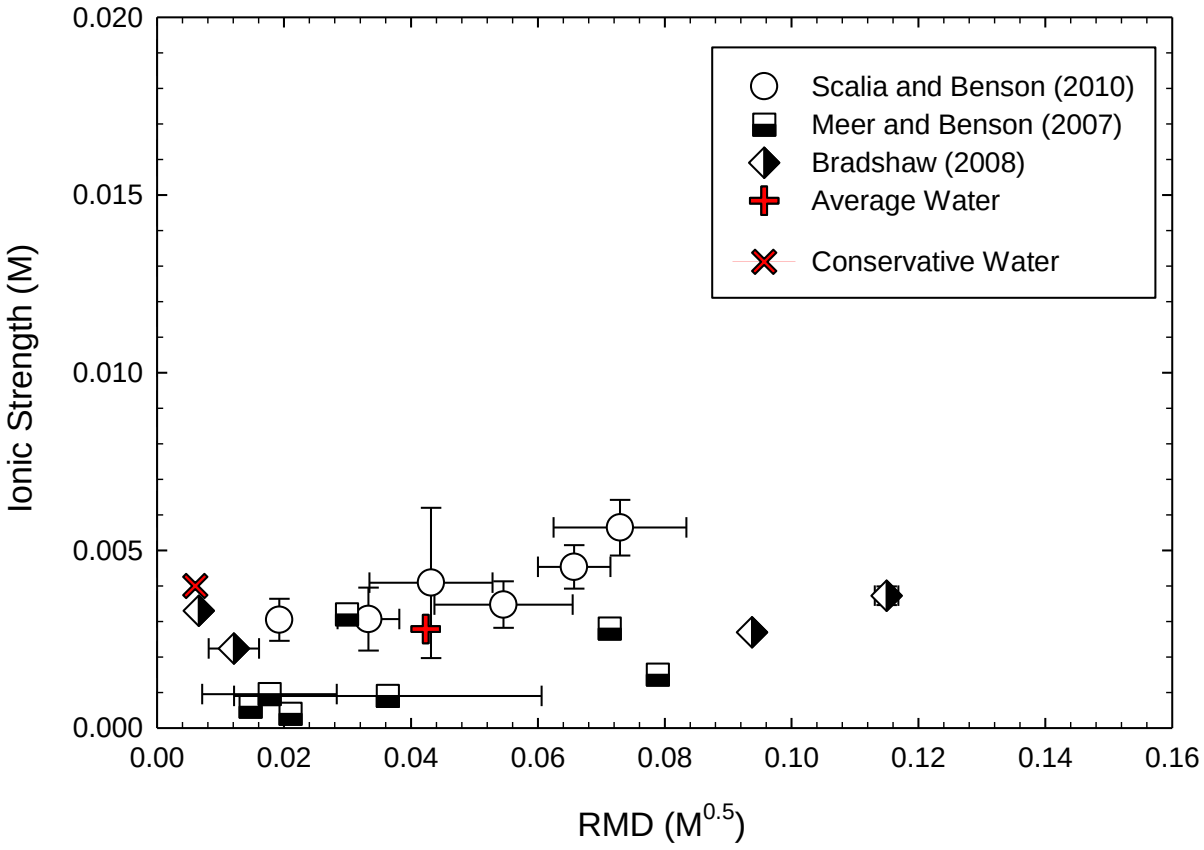

Fig. A.1. Ionic strength versus RMD of pore water eluent solutions from batch test procedure ASTM D6141. Error bars correspond to one standard deviation from the mean. Average water (AW) and conservative water (CW), the permeant water used for laboratory testing, are also shown. Modified from Scalia and Benson (2010).

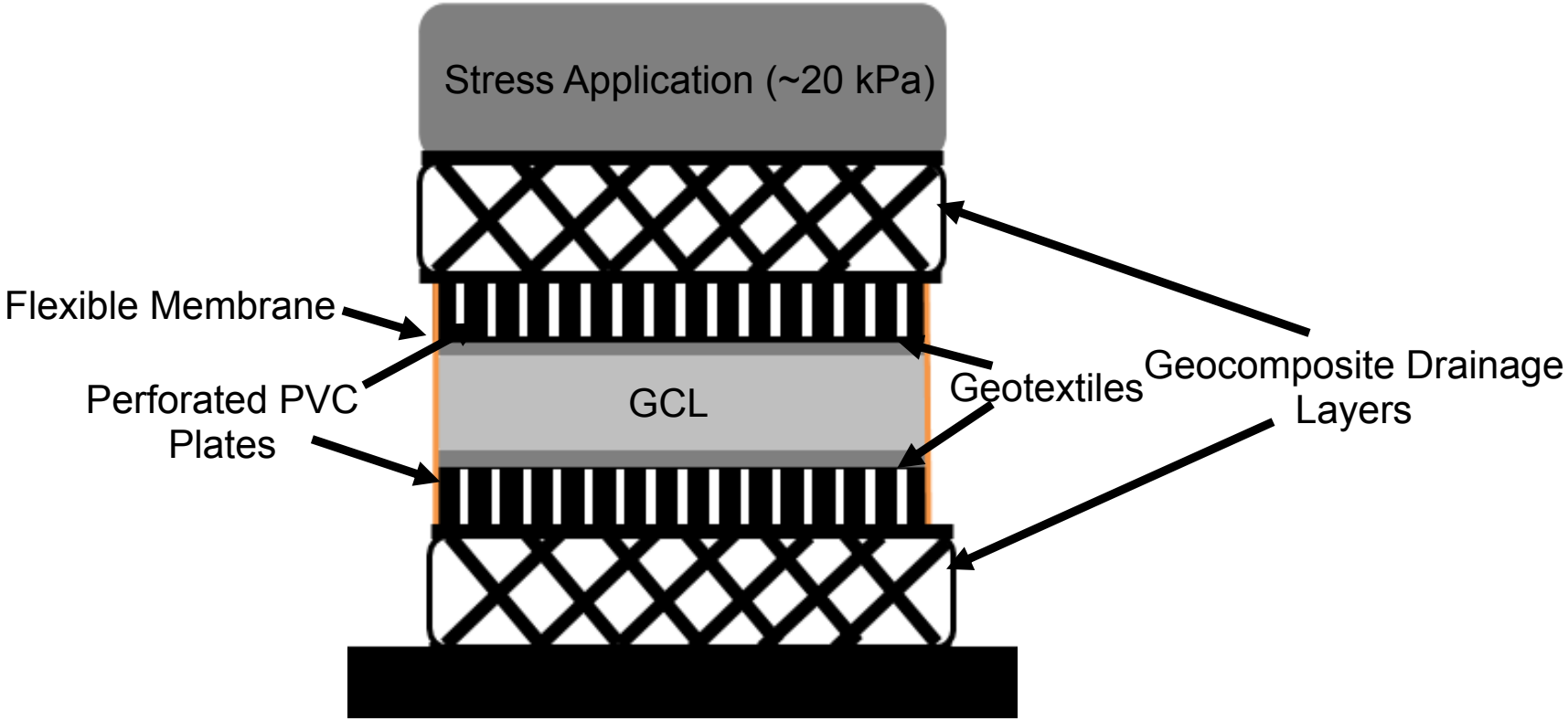

Fig. A.2 Schematic drawing of the perforated plate desiccation system which employs rigid perforated PVC plates placed above and below the GCL to limit physical disturbance.

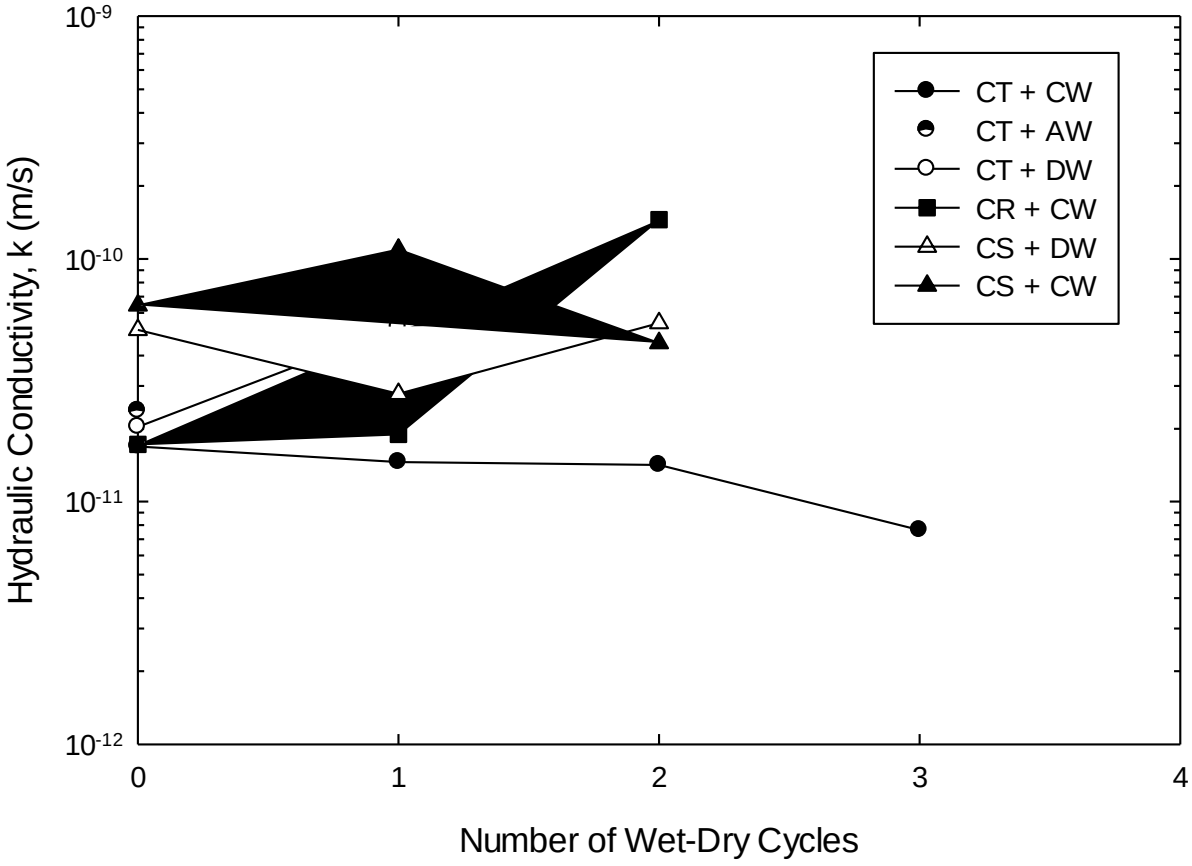

Fig. A.3. Hydraulic conductivity of conventional and polymer-modified GCLs permeated with deionized water (DW), average water (AW, I = 0.002 M, RMD = 0.045 $M^{0.5}$), and conservative water (CW; I = 0.004 M, RMD = 0.006 $M^{0.5}$) as a function of the number of wet-dry cycles.

Appendix B

THE EFFECT OF ELEVATED TEMPERATURE ACID MINE DRAINAGE ON THE HYDRAULIC CONDUCTIVITY OF GEOSYNTHETIC CLAY LINERS

B.1 INTRODUCTION

Acid mine drainage is the outflow of acidic water from mines, formed through the oxidation of sulfide minerals. Mine tailings and waste rock is more prone to sulfide oxidation due to both higher surface area and temperatures as high as 47 °C (Nordstrom et al. 2000). Since large masses of sulfide minerals are exposed quickly during the mining and milling processes, the surrounding environment often cannot attenuate the resultant low pH conditions. Exposed metals that were once part of the host rock become more soluble at higher temperatures and exacerbate the deleterious effect of low pH on terrestrial and aquatic receptors. Logarithmic increases in metal levels in waters from sulfide-rich mining environments are common where surface or groundwater pH becomes more acidic and temperature increases. Human health risks and ecological injury have been identified by the EPA. It is important to contain acid mine drainage from entering the environment.

The application of GCLs in mining generally pushes the performance beyond recommended limits typical for other environmental and engineering applications. Exposure of the GCL to high overburden and traffic stresses and excessive temperatures as well as high salinity and extreme pH of acid mine drainage may affect the integrity of the geosynthetic component and the performance of the bentonite component (Hornsley et al. 2010).

In the past, laboratory experiments have observed the hydraulic conductivity of bentonite contained within GCLs permeated with acid mine drainage solutions (Kashir and Yanful 2001;

Lange et al. 2007; Shackelford et al. 2010). Kashir and Yanful (2001) performed hydraulic conductivity testing on bentonite paste permeated with acid mine drainage from New Brunswick, Canada. The hydraulic conductivity of the bentonite paste was 5 times higher relative to the bentonite paste permeated with DW. Lange et al. (2007) permeated a needle-punched GCL with acidic drainage and process waters from gold tailings. The hydraulic conductivity of the GCL permeated with acidic drainage was 6.5 times higher relative to DW while the hydraulic conductivity of the GCL permeated with process water was 1.8 times higher relative to DW. Shackelford et al. (2010) permeated conventional and contaminant-resistant GCLs with process water and a synthetic leachate from a proposed zinc and copper mine. The hydraulic conductivity of both GCLs was 2.3 to 3.9 orders of magnitude higher when permeated with the synthetic leachate than when permeated with DW. These tests were conducted at room temperature (i.e. between 20 °C and 25 °C), but acid mining leachate temperatures could be as high as 47 °C (Nordstrom et al. 2000). Testing soil specimens in the laboratory at temperatures different from those in the field may lead to erroneous predictions of hydraulic conductivity.

Bouazza et al. (2008) investigated the effect of increased temperature on the hydraulic conductivity of a needle-punched GCL. Elevated temperatures increased the hydraulic conductivity of GCLs due to the evolution of the permeant viscosity with temperature.

The proposed study will evaluate examine the effect of elevated temperature acid mine drainage on the hydraulic conductivity of GCLs.

B.2 PROPOSED TESTING

In order to perform elevated temperature hydraulic conductivity testing, the permeameter should be fully immersed in a covered and insulated elevated temperature water bath (Fig. B.1). Temperature probes will be placed in the elevated temperature water tank, the pressure cell, and the influent line to ensure uniform heating. Insulated lines will be required between the heated water tank and the GCL to prevent heat loss. Tubing should be long enough to ensure a

long enough residence time to heat influent water. All plastic permeameter components will be checked to ensure that the elevated temperature will not degrade or destroy the material. The permeameter may need to be altered to ensure that the permeameter fits inside the water bath. Extra care should be taken to not harm oneself when handling the permeameter.

A pilot study should be performed with DW to address any unexpected complications that arise from elevated temperature testing.

Elevated hydraulic conductivity testing should be performed in a large fume hood in anticipation of chemical volatilization. The water bath would also warm the surrounding air, so a smaller space would be ideal to limit the radius of warmed air.

B.3 REFERENCES

Bouazza, A., Abuel-Naga, H., Gates, W., and Laloui, L., 2008, “Temperature effects on volume change and hydraulic properties of geosynthetic clay liners,” *The First Pan American Geosynthetics Conference and Exhibition*, Cancun, Mexico, Vol. 1, pp. 102-109.

Hornsley, W., Schiers, J., Gates, W., and Bouazza, A., 2010, “The impact of mining solutions/liquors on geosynthetics,” *Geotextiles and Geomembranes*, Vol.28(2), pp.191-198.

Jo, H., Benson, C., Lee, J., Shackelford, C., and Edil, T., 2005, “Long-Term Hydraulic Conductivity of a Non-Prehydrated Geosynthetic Clay Liner Permeated with Inorganic Salt Solutions,” *J. Geotech. Geoenviron. Eng.*, Vol. 131(4), pp. 405–417.

Jo, H., Katsumi, T., Benson, C., and Edil, T., 2001, Hydraulic conductivity and swelling of non-prehydrated GCLs permeated with single species salt solutions, *J. Geotech. Geoenvironmental Eng.*, 127(7), 557-567.

Kashir, M., and Yanful, E., 2001, “Hydraulic conductivity of bentonite permeated with acid mine drainage,” *Canadian Geotech. Journal*, Vol.38(5), pp.1034-1048.

Katsumi, T., Ishimori, H., Onikata, M., and Fukagawa, R., 2008, “Long-term barrier performance of modified bentonite materials against sodium and calcium permeant solutions,” *Geotextiles and Geomembranes*, Vol.26(1), pp.14-30

Kolstad, D., Benson, C., Edil, T., and Jo. H., 2004, “Hydraulic conductivity of a dense prehydrated GCL permeated with aggressive inorganic solutions,” *Geosynthetics International*, Vol.11(3), 233-241.

Lange, K., Rowe, R., and Jamieson, H., 2007, "Metal retention in geosynthetic clay liners following permeation by different mining solutions," *Geosynthetics International*, Vol.14(3), pp.178-187.

Nordstrom, D., Alpers, C., Ptacek, C., and Blowes, D., 2000, “Negative pH and extremely acidic mine waters in Iron Mountain, California,” *Environmental Science & Technology,* Vol.34(2), pp.254-258.

Scalia, J., and Benson, C., 2010, “Effect of Permeant Water on the Hydraulic Conductivity of Exhumed GCLs. *Geotechnical Testing Journal*, 1-11.

Schackelford, C., Sevick, G., Eykholt, G., 2010, “Hydraulic conductivity of geosynthetic clay liners to tailings impoundment solutions,” *Geotextiles and Geomembranes*, Vol.28(2), pp.149-162.

Shackelford, C., Benson, C., Katsumi, T., Edil, T., and Lin, L., 2000, “Evaluating the Hydraulic Conductivity of GCLs Permeated with Non-Standard Liquids.” *Journal of Geotextiles and Geomembranes*, 18(2-3), 133-161.

B.4 FIGURES

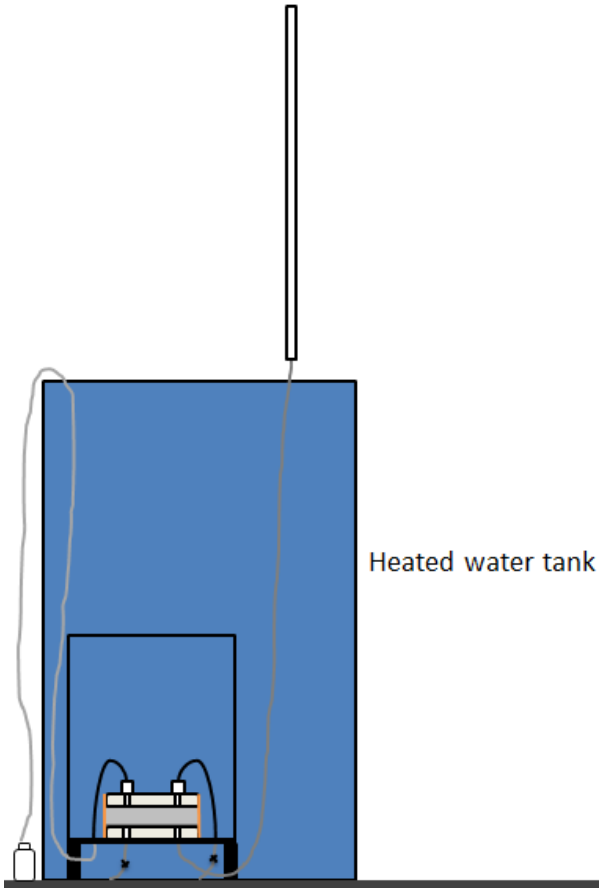

Fig. B.1. Proposed elevated temperature setup where the entire permeameter is surrounded by an elevated water bath.

Appendix C

IMAGE ANALYSIS MATLAB CODE

```
clear all; close all; clc;

% Obtain Image, input resolution
RGB = imread('BD159_7.21.14_cropped.jpg'); %input appropriate image file
Resolution = 0.02116667; %%mm/pix %input image resolution

%% Grayscale images and histograms
grayscale = rgb2gray(RGB);

% Grayscale histograms and figures
figure; imshow (RGB); title ('unaltered image');
figure; imshow (grayscale); title ('grayscale');
figure; imhist (grayscale); title ('grayscale histogram');
%% Erode and dilate image
se = strel('diamond',1);
im_close = imclose(grayscale, se);
figure; imshow(im_close); title ('closed');
figure; imhist(im_close); title ('closed');

%% %% Use adaptive thresholding to separates the foreground from the
background.
%  The local threshold mean-C or median-C is applied to the section of the
image im_close.
%  ws is the local window size.
%  tm is 0 or 1, a switch between mean and median. tm=0 mean(default); tm=1
median.
tm = 0;
C = 20;
ws = 300;
if tm==0
    mIM=imfilter(im_close,fspecial('average',ws),'replicate');
else
    mIM=medfilt2(im_close,[ws ws]);
end
sIM=mIM-im_close-C;
threshold=im2bw(sIM,0);
threshold=imcomplement(threshold);

figure; imshow(threshold); title ('image closed, adaptive threshold')
%% Open image
se_open = strel('diamond', 9);
bw2 = imopen(threshold,se_open);
figure; imshow(bw2); title ('closed, adaptive threshold, opened');

%% Remove white areas of less than 1000 pixels area
area_open = bwareaopen(bw2, 1000);
```

```
figure; imshow(area_open); title ('closed, adaptive threshold, opened, 1000
or less connected pixels removed')
%% Complement Image
Icomp = imcomplement(area_open);
figure; imshow(Icomp); title ('complemented image');
%% Remove areas of 1000 or less connected pixels
area_open2 = bwareaopen(Icomp, 1000);
figure; imshow (area_open2); title ('1000 or less connected pixels removed');
Icomp2 = imcomplement (area_open2);
figure; imshow (Icomp2); title ('ready for crack analysis');
%% Image Analysis on black cracks
% Crack area percentage, use figure Icomp2
[xmax, ymax] = size(Icomp2);
Binary1=double(Icomp2);
White_pix=0;
Black_pix=0;
for i=1:(xmax)
    for j=1:(ymax)
        if Binary1(i,j)==1
            White_pix=White_pix+1;
        else
            Black_pix=Black_pix+1;
        end
    end
end
total_area = xmax*ymax;

% Determine crack index factor (CIF)
CIF = (Black_pix/total_area)*100

%% Thin image to extract edges
Ithin = bwmorph(area_open2, 'thin', inf);
% use spur to eliminate noise
Ispur = bwmorph (Ithin, 'spur', inf);
% Check to see if images match up
C = imfuse (RGB,area_open2);
C2 = imfuse (RGB, Ithin);
C3 = imfuse (RGB, Ispur);
figure; imshow (C); title ('cracks and original');
figure; imshow(C2); title ('thinned and original');
figure; imshow (C3); title ('despurred and original');
figure; imshow(area_open2); title ('before thinning');
figure; imshow(Ithin); title ('after thinning');
figure; imshow (Ispur); title ('after despurring');

%% Extract edges. Find lines (desiccation cracks) in image.
BW = edge(Ispur,'roberts');

% compare edge extraction of crack center with original image
C5 = imfuse (RGB, BW);

% fuse original and edge extraction images
C6 = imfuse (Ispur, BW);

% convert fused image first to grayscale, then to a binary image using Otsu's
Method
```

```
gray = rgb2gray (C6);
level3 = graythresh (gray);
BW2 = im2bw(gray,level3);

% compare binary fused image to original image to determine if images match
C7 = imfuse (BW2, RGB);

% show figures
figure; imshow (BW); title ('crack center after edge extraction');
figure; imshow (C6); title ('fused thinned cracks and edge extraction');
figure; imshow (BW2); title ('ready for analysis');
figure; imshow (C7); title ('compare crack center with original image');

% Perform Hough Transform
[H,theta,rho] = hough(BW2, 'RhoResolution',10,'Theta',-90:0.5:89.5);

% Display the original image.
figure; subplot(2,1,1);
imshow(RGB);
title('Desiccation Image');

% Display the Hough matrix.
subplot(2,1,2);
imshow(imadjust(mat2gray(H)),'XData',theta,'YData',rho,'InitialMagnification'
,'fit');
title('Hough Transform of Desiccation Image');
xlabel('\theta'), ylabel('\rho');
axis on, axis normal, hold on;
colormap(hot);

% Find the peaks in the Hough transform matrix, H, using the houghpeaks
function.
P = houghpeaks(H,2000);
% Superimpose a plot on the image of the transform that identifies the peaks.
x = theta(P(:,2));
y = rho(P(:,1));
plot(x,y,'s','color','black');

% Find lines in the image using the houghlines function.
lines = houghlines(BW,theta,rho,P,'FillGap',10,'MinLength',50);

% Create a plot that superimposes the lines on the original image.
figure, imshow(RGB), hold on
max_len = 0;
for k = 1:length(lines)
    xy = [lines(k).point1; lines(k).point2];
    plot(xy(:,1),xy(:,2),'LineWidth',2,'Color','green');

    % Plot beginnings and ends of lines
    plot(xy(1,1),xy(1,2),'x','LineWidth',2,'Color','yellow');
    plot(xy(2,1),xy(2,2),'x','LineWidth',2,'Color','red');

    % Determine the endpoints of the longest line segment
    len = norm(lines(k).point1 - lines(k).point2);
    if ( len > max_len)
```

```
        max_len = len;
        xy_long = xy;
    end
end

% highlight the longest line segment
plot(xy_long(:,1),xy_long(:,2),'LineWidth',2,'Color','red');
hold off

%% Frequency histogram of Crack Orientation based on Hough Transformation
t = extractfield(lines, 'theta');

% Make histogram
orientation_binranges=linspace(-90,80,18);

histoorientation_bincounts = histc(t,orientation_binranges);

histoorientation_binpercent = zeros (1, length(orientation_binranges));
for q = 1:1:length(orientation_binranges);
    histoorientation_binpercent(q) =
histoorientation_bincounts(q)/length(t)*100;
end
figure; bar(orientation_binranges,histoorientation_binpercent)
axis ([-90 90 0 10]);
xlabel('Crack Orientation Relative to Horizontal (Deg.)');
ylabel('Frequency (%)');

%% Frequency histogram of Crack Length based on Hough transformation
length1 = extractfield(lines, 'point1');
length2 = extractfield(lines, 'point2');

% Determine length of cracks, store in array called 'truelength'
nmax = length(lines);

o1 = zeros (1, nmax);
o2 = zeros (1, nmax);
p1 = zeros (1, nmax);
p2 = zeros (1, nmax);
len = zeros (1, nmax);
truelength = zeros (1, nmax);
for n = 1:nmax;
    o1 (1, n) = length1((2*n)-1);
    p1 (1, n) = length1(2*n);
    o2 (1, n) = length2((2*n)-1);
    p2 (1, n)= length2(2*n);
    len (1, n) = sqrt(((o1(n)-o2(n))^2) + ((p1(n)-p2(n))^2));
    truelength (1, n) = len (1,n) * Resolution;
end

% Make histogram
maxlength = max(truelength);
length_max_binwidth = maxlength/100;
length_binranges=zeros(1,101);
for v = 1:101
    length_binranges(1,v)= v*length_max_binwidth;
```

```
end
histolength_bincounts = histc(truelength,length_binranges);
histolength_binpercent = zeros (1, 101);
for k = 1:1:length(length_binranges);
    histolength_binpercent(k) =
histolength_bincounts(k)/length(truelength)*100;
end
figure; bar(length_binranges,histolength_binpercent)
axis ([0 maxlength 0 100]);
xlabel('Crack Length (mm)');
ylabel('Frequency (%)');

%% Determine Centroids of clay cells, determine number of cells, frequency
histogram of cell area
% touch up binary image to remove small pixelations
Idiag = bwmorph(BW2, 'diag');
Icomp3 = imcomplement (Idiag);
area_open3 = bwareaopen(Icomp3, 1000);

% Only for manufactured pictures, need to exclude the outside boundary from
% being included in the area analysis
Icomp3 = imcomplement (Icomp2);
e = imfill (Icomp3); % choose outer border of image
figure; imshow (e);
Icomp4 = imcomplement (e);
figure; imshow (Icomp4); title ('used for shape analysis');

% extract area, centroid, and weighted centroid of bentonite nodules
% for manufactured pictures, use Icomp4
% for GCL pictures, use area_open3
s = regionprops(Icomp2, grayscale, {'Centroid','WeightedCentroid', 'Area'});

% Check to ensure that all nodules are counted by superimposing the
% centroid (blue) and weighted centroid (red) locations over the crack
% skeleton image
figure; imshow(Icomp2)
title('Weighted (red) and Unweighted (blue) Centroid Locations');
hold on
numObj = numel(s);
for k = 1 : numObj
    plot(s(k).WeightedCentroid(1), s(k).WeightedCentroid(2), 'r*');
    plot(s(k).Centroid(1), s(k).Centroid(2), 'bo');
end
hold off

% Extract area from s matrix and convert to 'true_area' array by
% multiplying by the resolution
area = extractfield (s, 'Area');
true_area = (area*(Resolution^2));

% Frequency histogram of Area
maxarea = max(true_area)
area_max_binwidth = maxarea/100;
area_binranges=zeros(1,101);
for b = 1:101
    area_binranges(1,b)= b*area_max_binwidth;
```

```
end
histoarea_bincounts = histc(true_area,area_binranges);
histoarea_binpercent = zeros (1, 101);
for u = 1:1:length(area_binranges);
    histoarea_binpercent(u) = histoarea_bincounts(u)/length(true_area)*100;
end
figure; bar(area_binranges,histoarea_binpercent)
axis ([0 maxarea 0 100]);
xlabel('Cell Area (mm^2)');
ylabel('Frequency (%)');

%% Average Bentonite Cell Area
sum_area = 0;
for l = 1:length (area);
    sum_area = area (1,l) + sum_area;
end
An = sum_area * (Resolution ^ 2); % units are mm^2
Nn = length (area);
Average_cell = An/Nn

%% Crack Thickness Determination
% create an image of just the crack boundaries
Iremove = bwmorph (Icomp2, 'remove', inf);
% perform edge extraction on crack boundaries
Edge = edge(Iremove,'roberts');

% fuse original and edge extraction images
C8 = imfuse (RGB, Edge);

% fuse edge extraction of crack boundary and crack boundary images
C9 = imfuse (Edge, Iremove);

% convert fused image first to grayscale, then to a binary image using Otsu's
Method
gray2 = rgb2gray (C9);
level4 = graythresh (gray2);
BW3 = im2bw(gray2,level4);

% compare binary fused image to original image to determine if images match
C10 = imfuse (BW3, RGB);

% show figures
figure; imshow (Iremove); title ('crack boundaries before edge extraction');
figure; imshow (Edge); title ('crack boundaries after edge extraction');
figure; imshow (C9); title ('edge extraction of crack boundary and crack
boundary');
figure; imshow (C10); title ('compare crack boundaries with original image');
figure; imshow (BW3); title ('final crack boundaries');

% touch up binary image to remove small pixelations
Idiag2 = bwmorph(BW3, 'diag');
Icomp4 = imcomplement (Idiag2);
area_open4 = bwareaopen(Icomp4, 10);
Crack_Bound = imcomplement (area_open4);
figure; imshow (Crack_Bound); title ('ready for analysis');
```

```
% distance between boundaries (with bentonite nodules)
Distance_bound_thin = bwdist(Crack_Bound);

% sort out bentonite nodules by only including the information that
% corresponds to the thinned image (crack skeleton)
cracks = zeros (xmax, ymax);
for i=1:(xmax)
    for j=1:(ymax)
        if area_open3(i,j)==1
            cracks (i,j) = 0;
        else
            cracks (i,j) = Distance_bound_thin (i,j);
        end
    end
end

%% make crack thickness isomap
crack_gray = mat2gray(cracks);
figure; subimage (crack_gray);
hold on
imcontour(cracks);
hold off

figure; subimage (RGB); hold on; imcontour (cracks); hold off;

% move measurements into an array named 'true_crack_array'
crack_array = cracks(cracks > 0);
true_crack_array = (2*crack_array*Resolution);

%% make array measurements into crack thickness frequency histogram
maxwidth = max(true_crack_array)
crackwidth_max_binwidth = maxwidth/100;
crackwidth_binranges=zeros(1,101);
for ck = 1:101
    crackwidth_binranges(1,ck)= ck*crackwidth_max_binwidth;
end
histocrack_bincounts = histc(true_crack_array,crackwidth_binranges);
histocrack_binpercent = zeros (1, 101);
for count = 1:1:length(crackwidth_binranges);
    histocrack_binpercent(count) =
histocrack_bincounts(count)/length(true_crack_array)*100;
end
figure; bar(crackwidth_binranges,histocrack_binpercent)
axis ([0 maxwidth 0 100]);
xlabel('Crack Width (mm)');
ylabel('Frequency (%)');

%% Average crack width
sum_width = 0;
for crac = 1:length (crack_array);
    sum_width = crack_array (crac,1) + sum_width;
end
Wn = 2*sum_width*Resolution;
Average_width = Wn/length(crack_array) % units are mm
```

Appendix D

VALIDATION OF LINE ORIENTATION DETERMINATION TECHNIQUE

In order to validate the line orientation determination technique, a synthetic image with lines of known thickness and various orientations was generated, imported into Matlab, and subjected to processing and analysis. The original figure, lines detected via Matlab, and line orientation frequency histogram are shown in Fig. D.1.

The lines extended in orientations varying between 0° and 360° at 10° increments. Therefore, the line orientation frequency histogram should have shown equal frequency of all orientations between 0° and 360°. The frequency histogram did not reflect this trend for several reasons. First, line intersections will affect the number of counted lines. If there is one intersection, the same line will be counted both before and after the intersection. Second, not all lines were counted. In addition, the analysis does not take the further complication of lines with varying thickness into account.

Since the line orientation determination algorithm was not validated, the quantitative results obtained for the crack frequency histogram (Section 1.5.5.3, Fig. 1.14) should be reviewed with reservations.

D.1 FIGURES

(a)

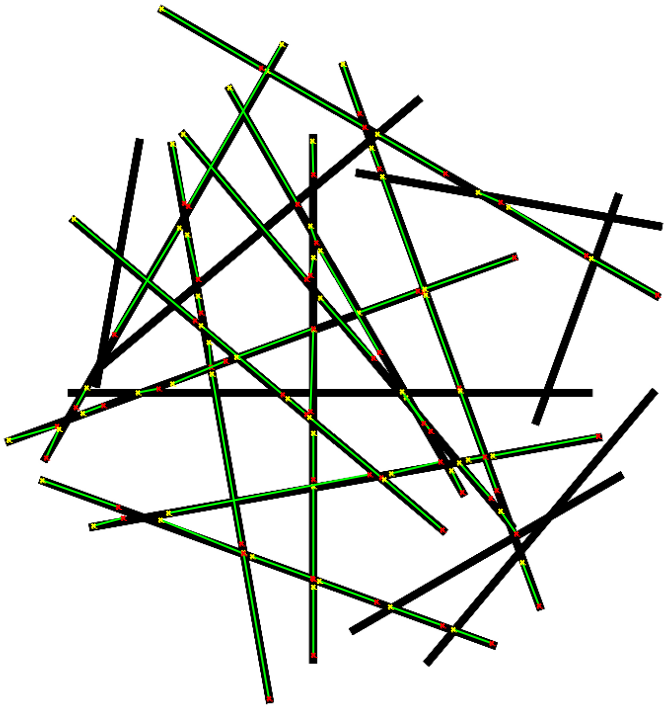

(b)

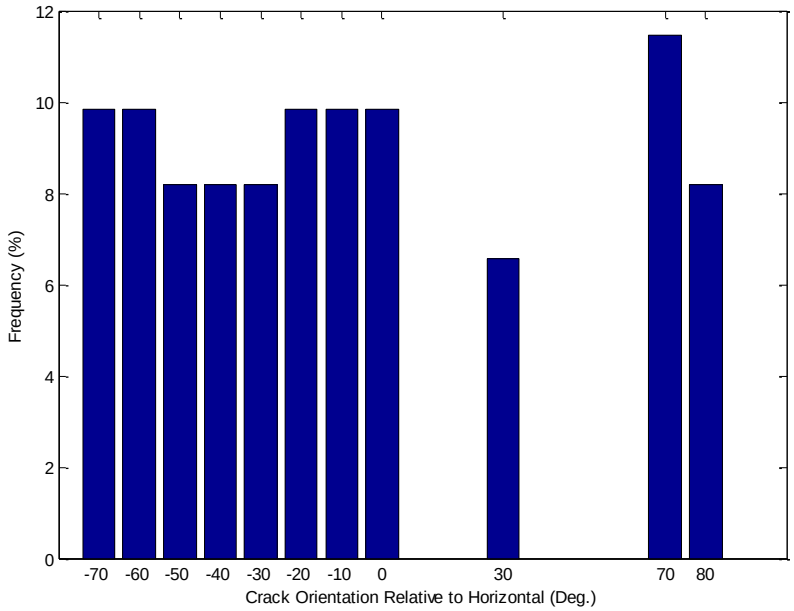

Fig. D.1. Line orientation verification (a) Image imported into Matlab; thin green lines indicate lines recognized via edge detection techniques; (b) frequency histogram.